Porphyrin-and Phthalocyanine-Sensitized Solar Cells(Dissertation_全文)

AUTHOR(S):

Eu, Seunghun

CITATION:

Eu, Seunghun. Porphyrin-and Phthalocyanine-Sensitized Solar Cells. 京都大学, 2008, 博士(工学)

ISSUE DATE:

2008-09-24

URL:

https://doi.org/10.14989/doctor.k14168

Porphyrin- and Phthalocyanine-Sensitized Solar Cells

2008

Seunghun Eu

Porphyrin- and Phthalocyanine-Sensitized Solar Cells

2008

Seunghun Eu

Contents

GENERAL INTRODUCTION

Exhaustion of fossil fuels and global energy concerns have never been recognized as seriously as in recent times. In this context, research efforts to acquire energy from the alternative, clean and renewable, sources such as wind or geothermal energy are being intensively and extensively exploited. Among them, solar energy dwarfs all others in abundance, availability, and scalability. In fact, the energy reached from the sun in one hour on the earth (4.3×10^{20} J) is larger than that is consumed by all human beings in the entire year (4.1×10^{20} J, 2004).[i]

To acquire energy from the sun is not novel idea at all. Inorganic solar cells, typified by the silicon p-n junction cell, were developed in the 1950s and have been employed for the fabrication of the some utilities. The energy of photons from the sun is used to excite the electrons from the valence band, where they are tightly bound to the atom, into the conduction band, where they can be freely moved: provided that the photon holds enough energy to push the electron over this band gap, it can generate the electrical current, otherwise it would be lost as heat. The band gap of the silicon is known to be about 1.1 eV (at 300 K) which corresponds to the wavelength of 1100 nm. Namely, the photons in the sunlight hold the energy higher than 1.1 eV can generate the electrical energy and this limits the theoretical efficiency (31 %) of the single layer solar cell made with silicon - the Shockley-Queisser limit.[ii] The best lab-based silicon solar cell is now reported to be performed with ca. 24 % of conversion efficiency, but the commercial cells in many cases display only 15 - 20 % of the efficiency.[iii] In current manufacturing schemes for silicon-based solar cells, the cost for processing and purifying the silicon occupies only about 10 % of the final cost; the remaining 90 % is engaged with other inflexible processes, albeit the price of the silicon is highly competitive.[iv] Explorations for the innovative technologies based on relatively cheap materials with different price mechanisms to substitute the present solar cell are the natural consequences. As such a

variety of unprecedented devices including bulk heterojunction solar cell or quantum dot solar cell have been explored.[v] Although their performances are still inferior compared with present silicon-based cells and thus not yet close for commercialization, one or two successes are believed to dramatically change the current status of the energy supply. Own characteristics such as flexibility and light weight are the additional fascination of the novel types of the devices.

Dye-sensitized solar cell (DSSC) with mesoporous semiconductor is regarded as one of the most promising candidates among them.[vi] In fact, the concept of the dye sensitization of semiconductors, excitation of the dye molecules and subsequent electron injection from the dyes into the semiconductors, can be traced back to the 1960s.[vii] Efficient electron injection was observed and the mechanism of the sensitization processes was well-documented.[viii] These early studies, however, were based on the single crystal semiconductor and thereby could not demonstrate ample light harvesting efficiency that is also indispensable to achieve high performance photoelectrochemical and/or photovoltaic cells. Seminal report by O'Regan and Grätzel in the early 1990s opened the new horizon in this research field.[ix] Of significance in their device is laid in the employment of mesoporous semiconductor films instead of the single crystal to immobilize the dye molecules. This approach affords several hundred-fold augment in the surface area compared with that of the planar surface, allows the increased amount of dye molecules on the surface, and accordingly guarantees the enhanced light harvesting capability of the cell. The basic working mechanism of DSSC is displayed is Figure 1. The dye molecule immobilized on the mesoporous semicondcutor (typically anatase TiO_2) gathers the incident light, and injects the electron into the conduction band of the semiconductor after the photoexcitation. The resulting dye cation is regenerated by the iodide and the following triiodide is reduced at the counter electrode, with the circuit being completed via electron movement through the external load. This process affords the photocurrent.

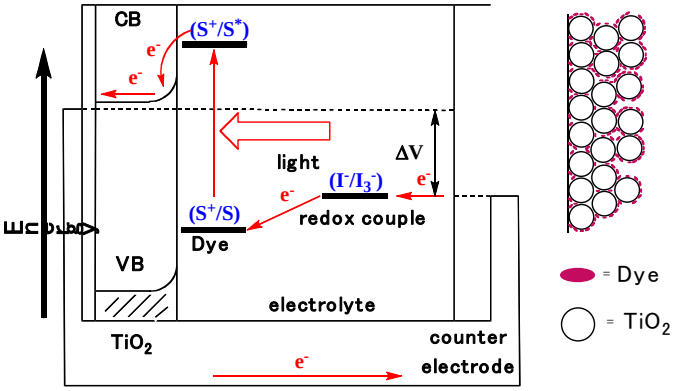

Figure1. Mechanism of the dye-sensitized solar cells

The photovoltage generated under illumination corresponds to the energy difference between the quasi Fermi level of the semiconductor and the redox potential of the iodide/triiodide redox couple.[x] Overall, the device transforms the light energy into the electrical energy without any permanent chemical transformation. Briefly, three different but closely related materials are responsible for the operation with this well-performed device: the dye that can absorb the incident light and transfer the electron to the electrode, mesoporous semiconductor that can afford the very high surface area, and redox couple that is responsible for the charge relay for the continuous operation of the device. Although the research efforts in this field have been spanning these three specific areas, of particular importance is the development of the well-performance dye.

High performance dyes are requested to display broad light absorption capability, which can cover the whole solar light spectrum, along with fast injection of electrons from photo-excited dyes to the conduction band of semiconductor electrodes, and slow recombination between the injected electrons and resulting dye cations and/or I^-/I_3^- redox couples. The majority of dyes for DSSC are immobilized onto the TiO_2 by the aid of anchoring groups such as carboxylic acid, sulfonic acid, phosphonic acid, and others.[xi] All of them are believed to make a covalent bond with the TiO_2 surface that provides good electronic communications between the dye and the TiO_2. Among them the carboxylic acid group has been most frequently used for derivatizing the TiO_2 surface

with a variety of chemical compounds after the report of Anderson et al.[xii] Namely, molecules containing carboxylic acid group are known to spontaneously adsorb onto, and form bridging, ester-like, and/or bidentate binding with the TiO_2 depending on the dye, dye coverage, pH, sensitizing time, and preparation of the TiO_2.[xiii] Anchoring groups are of central importance in the interfacial phenomena for nearly all kinds of dyes for DSSC. The number, position, and identity of anchoring groups have been reported to affect cell performances including electron injection, charge recombination, light absorption capability, and stability.[xiv] Variations of bridge between the dye and the anchoring group afford another control of cell performances. Separation distance between the dye and the anchoring group is known to have an influence on the electron injection rate by managing the electronic coupling.[xv] Photophysical properties can be tailored by manipulating the length of bridge.[xvi] Open circuit potential (V_{OC}) can also be raised by lengthening the separation distance between the center of the dye and the anchoring group.[xvii]

In this first part of this dissertation, three porphyrins with *meso* 5-membered heteroaromatic spacers, 5-(5-carboxy-2-thienyl)-10,15,20-tris(2,4,6-trimethylphenyl)-porphyrinatozinc(II) (Zn5S), 5-(5-carboxy-2-furyl)-10,15,20-tris(2,4,6-trimethylphenyl) porphyrinatozinc(II) (Zn5O), and 5-(4-carboxy-2-thienyl)-10,15,20-tris(2,4,6-trimethyl-phenyl)porphyrinatozinc(II) (Zn4S), have been designed and synthesized to evaluate the effects of the spacers on the structures of the porphyrin films on the TiO_2 and photovoltaic properties of porphyrin-sensitized TiO_2 cells. Modifications in spacers including switching one element (i.e., sulfur vs oxygen) in the bridge or changing the position of the anchoring group (i.e., carboxylic acid) were found to have significant effects on the dye coverage and the structures of the porphyrin monolayers on the TiO_2 surface, and photovoltaic properties of the porphyrin-sensitized TiO_2 cells. The high photovoltaic properties of Zn5S-sensitized cell can be rationalized by the additional electron transfer pathway through specific interaction between the sulfur atom inherent in the bridge and the TiO_2 surface.

In the second part of this dissertation, two β, β'-quinoxalino porphyrins containing different numbers of carboxylic acid binding groups, monocarboxyquinoxalino[2,3-β]porphyrin (ZnQMA) and dicarboxyquinoxalino[2,3-β]-porphyrin (ZnQDA), have been synthesized and evaluated as photosensitizers for porphyrin-sensitized TiO_2 cells. Both of the compounds showed broadened, red-shifted, and amplified light absorption with the aid of π-extensions. Electrochemistry along with DFT calculations revealed that the low-lying LUMO by the substitutions is the main reason for the narrowed HOMO-LUMO gaps. From the X-ray photoelectron spectroscopy along with cyclic voltammetry studies for the adsorbed porphyrins, we proposed that one carboxylic acid employs bidentate binding mode to anchor ZnQMA onto the TiO_2 surface, whereas the two binding groups in ZnQDA utilize one bidentate and one monodentate binding modes. Photovoltaic measurements of ZnQMA- and ZnQDA-sensitized TiO_2 cells with P25 revealed power conversion efficiencies of 5.2 % and 4.0 %, respectively. Since the light absorption capabilities of the two porphyrins are more or less similar, the number and the position of binding groups in the porphyrins have a large impact on the photovoltaic and photoelectrochemical performances.

In the third part of this dissertation, phthalocyanines with high peripheral substitutions and free from potential contamination by regioisomers have been synthesized and evaluated as photosensitizers for dye-sensitized solar cell applications. Metal free phthalocyanine-sensitized solar cell shows no photocurrent generation due to its low excited singlet state (LUMO) compared with the conduction band of the TiO2. Upon zinc metalation, the LUMO level of the phthalocyanine is pushed up, and this variation affords the exergonic free energy change for the electron injection. The zinc phthalocyanine-sensitized solar cell displays 0.57 % of power conversion efficiency (η) and 4.9 % of maximal IPCE in the near infrared region. More importantly, the cell prepared with and without the presence of chenodeoxycholic acid reveals no difference in the power conversion efficiency. This implies that the well-known aggregation tendency

of phthalocyanines that is considered to enhance the self-quenching of the phthalocyanine excited singlet state is effectively suppressed by the high degree of substitutions. Significance of the driving force for the electron injection and the distance between the dye core and the TiO_2 surface is also highlighted for devising high performance phthalocyanine photosensitizers

References

(i) Basic Research Needs for Solar Energy Utilization (U.S. Department of Energy, Washington, DC, 2005) (http://www.er.doe.gov/bes/reports/abstracts.html#SEU)

(ii) Shockley, W.; Queisser, H. J. *J. Appl. Phys.* **1961**, *32*, 510.

(iii) Service, R. F. *Science*, **2008**, *319*, 718.

(iv) Lewis, N. S. *Science*, **2007**, *315*, 798.

(v) (a) Yu, G.; Gao, J.; Hummelen, J, C.; Wudl, F.; Heeger, A. J. *Science* **1995**, *270*, 1789. (b) Gunes, S.; Neugebauer, H.; Sariciftci, N. S. *Chem. Rev.* **2007**, *107*, 1324. (c) Thompson, B. C.; Frechet, J. M. J. *Angew. Chem., Int. Ed.* **2008**, *47*, 58. (d) Nozik, A. J. *Ann. Rev. Phys. Chem.* **2001**, *52*, 193. (e) Ellingson, R. J.; Beard, M. C.; Johnson, J. C.; Yu, P.; Micic, O. I.; Nozik, A. J.; Shabaev, A.; Efros, A. L. *Nano Lett.* **2005**, *5*, 865.

(vi) (a) Hagfeldt, A.; Grätzel, M. *Acc. Chem. Res.* **2000**, *33*, 269. (b) Grätzel, M. *Pure Appl. Chem.* **2001**, *73*, 459. (c) Watson, D. F.; Meyer, G. J. *Ann. Rev. Phys. Chem.* **2005**, *56*, 119. (d) Anderson, N. A.; Lian, T. *Ann. Rev. Phys. Chem.* **2005**, *56*, 491. (e) Lewis, N. S. *Inorg. Chem*. **2005**, *44*, 6900. (f) Duncan, W. R.; Prezhdo, O. V. *Ann. Rev. Phys. Chem.* **2007**, *58*, 143. (g) Prezhdo, O. V.; Duncan, W. R.; Prezhdo, V. V. *Acc. Chem. Res.* **2008**, *41*, 339.

(vii) Gerischer, H. *Surf. Sci*. **1969**, *18*, 97.

(viii) (a) Memming, R.; Tributsch, H. *J. Phys. Chem.* **1971**, *75*, 562. (b) Memming, R. *Surf. Sci*. **1980**, *101*, 551.

(ix) O'Regan, B.; Grätzel, M. *Nature*, **1991**, *353*, 737.

(x) Cahen, D.; Hodes, G.; Grätzel, M.; Guillemoles, J. F.; Riess, I. *J. Phys. Chem. B* **2000**,

104, 2053.

(xi) (a) Galoppini, E. *Coord. Chem. Rev*. **2004**, *248*, 1283. (b) Wang, P.; Klein, C.; Moser, J.-E.; Humphry-Baker, R.; Cevey-Ha, N.-L.; Charvet, R.; Comte, P.; Zakeeruddin, S. M.; Grätzel, M. *J. Phys. Chem. B* **2004**, *108*, 17553. (c) Ramakrishna, G.; Verma, S.; Jose, D. A.; Kumar, D. K.; Das, A.; Palit, D. K.; Ghosh, H. N. *J. Phys. Chem. B* **2006**, *110*, 9012. (d) Altobello, S.; Bignozzi, C. A.; Caramori, S.; Larramona, G.; Quici, S.; Marzanni, G; Lakhmiri, R. *J. Photochem. Photobio. A* **2004**, *166*, 91. (e) Heimer, T. A.; D'Arcangelis, S. T.; Farzad, F.; Stipkala, J. M.; Meyer, G. J. *Inorg. Chem.* **1996**, *35*, 5319.

(xii) Anderson, S.; Constable, E. C.; Dare-Edwards, M. P.; Goodenough, J. B.; Hamnett, A.; Seddon, K. R.; Wright, R. D. *Nature* **1979**, *280*, 571.

(xiii) (a) Fillinger, A.; Parkinson, B. A. *J. Electrochem. Soc.* **1999**, *146*, 4559. (b) Lu, Y.; Choi, D.; Nelson, J.; Yang, O.; Parkinson, B. A. *J. Electrochem. Soc*. **2006**, *153*, E131. (c) Vittadini, A.; Selloni, A.; Rotzinger, F. P.; Grätzel, M. *J. Phys. Chem. B* **2000**, *104*, 1300. (d) Nazeeruddin, Md. K.; Humphry-Baker, R.; Liska, P.; Grätzel, M. *J. Phys. Chem. B* **2003**, *107*, 8981.

(xiv) (a) Park, H.; Bae, E.; Lee, J.-J.; Park, J.; Choi, W. *J. Phys. Chem. B* **2006**, *110*, 8740. (b) Lundqvist, M. J.; Nilsing, M.; Lunell, S.; Åkermark, B.; Persson, P. *J. Phys. Chem. B* **2006**, *110*, 20513. (c) Kilså, K.; Mayo, E. I.; Brunschwig, B. S.; Gray, H. B.; Lewis, N. S.; Winkler, J. R. *J. Phys. Chem. B* **2004**, *108*, 15640. (d) Yan, S. G.; Prieskorn, J. S.; Kim, Y.; Hupp, J. T. *J. Phys. Chem. B* **2000**, *104*, 10871. (e) Hoertz, P. G.; Carlisle, R. A.; Meyer, G. J.; Wang, D.; Piotrowiak, P.; Galoppini, E. *Nano Lett.* **2003**, *3*, 325. (f) Nilsing, M.; Persson, P.; Ojamäe, L. *Chem. Phys. Lett*. **2005**, *415*, 375. (g) Persson, P.; Lundqvist, M. J.; Ernstorfer, R.; Goddard, W. A., III,; Willig, F. *J. Chem. Theory Comput*. **2006**, *2*, 441. (h) Kilså, K.; Mayo, E. I.; Kuciauskas, D.; Villahermosa, R.; Lewis, N. S.; Winkler, J. R.; Gray, H. B. *J. Phys. Chem. A* **2003**, *107*, 3379.

(xv) Anderson, N. A.; Ai, X.; Chen, D.; Mohler, D. L.; Lian, T. *J. Phys. Chem. B* **2003**, *107*, 14231.

(xvi) Taratula, O.; Rochford, J.; Piotrowiak, P.; Galoppini, E.; Carlisle, R. A.; Meyer, G. J. *J. Phys. Chem. B* **2006**, *110*, 15734.

(xvii) Clark, C. C.; Meyer, G. J.; Wei, Q.; Galoppini, E. *J. Phys. Chem. B* **2006**, *110*, 11044.

CHAPTER 1

Effects of 5-Membered Heteroaromatic Spacers on Structures of Porphyrin Films and Photovoltaic Properties of Porphyrin-Sensitized TiO_2 Cells

Introduction

Porphyrins have been evaluated as photosensitizers for DSSC due to their strong Soret (400-450 nm) and moderate Q bands (550-600 nm) absorption properties as well as their primary role in natural photosynthetic system.[i] They have demonstrated charge-transfer kinetics indistinguishable from those of ruthenium polypyridyl complexes,[ii] which are the most efficient dyes ever reported. Moreover, optical, photophysical, and electrochemical properties can be systematically tailored by the peripheral substitutions and/or inner metal complexations. Nevertheless, compared with the high performance dyes for DSSC,[iii] porphyrins have been operated inefficiently.[iv] Moreover, even the same porphyrin displayed fairly different cell performance.[v] Such inefficiency and inconsistency has been attributed to the effects of electronic coupling between the porphyrin and the TiO_2 surface and of porphyrin aggregation.[5b,vi] For instance, argument that the identity of anchoring groups has little influence on the incident photon-to-current efficiency (IPCE) of porphyrin-sensitized TiO_2 cells was suggested,[vii] whereas strong dependence of the performances of the TiO_2 cells on the nature of spacer between the porphyrin and the TiO_2 surface was also demonstrated.[6] Thus, the various arguments arise from lack of detailed knowledge on the role of spacer including anchoring group during photoinduced interfacial electron-transfer event in porphyrin-sensitized TiO_2 cell.

In this chapter, the first syntheses, structures of porphyrin films on the TiO_2, and photovoltaic properties of porphyrins with different 5-membered heteroaromatic spacers

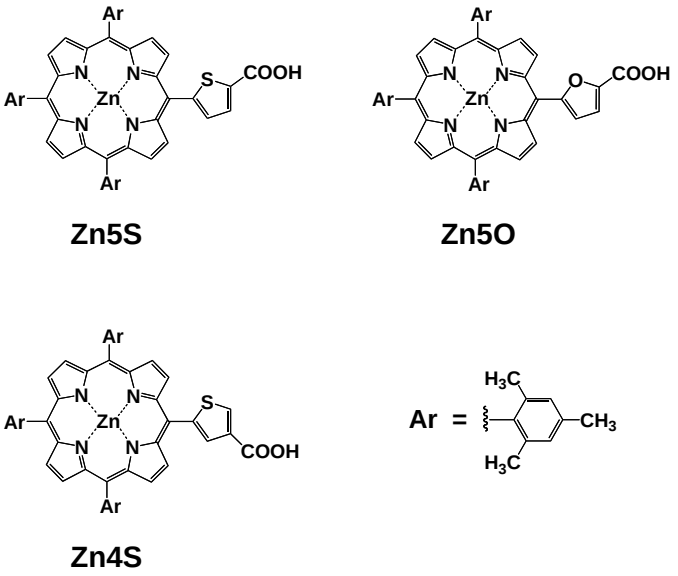

Figure 1. Structure of porphyrins used in this study

(Zn5S, Zn5O, and Zn4S), as illustrated in Figure 1, are reported. *meso*-Tetrasubstituted porphyrins are chosen as a sensitizer in this study. One carboxylic group as an anchoring group is attached on the *meso*-5-membered heteroaromatic moiety to guarantee the single anchorage of the porphyrin molecule on the TiO_2. Three methyl groups are introduced into 2,4,6-positions of three *meso*-phenyl groups of the porphyrin. The resulting large steric hindrance around the porphyrin is expected to reduce the aggregation of the porphyrin molecules on the TiO_2, leading to the suppression of undesirable quenching of the porphyrin excited singlet state and eventually efficient photocurrent generation.[viii] More importantly, a 5-membered heteroaromatic ring is employed as a bridge for connecting the porphyrin core and the anchoring group, and thereby systematically tailoring the electronic coupling between the porphyrin and the TiO_2 surface. Both relative positions of the anchoring group (i.e., 4- vs 5-position) and the different heteroatoms (i.e., sulfur vs oxygen) on the bridge molecule would have a large impact on structures of the porphyrin films on the TiO_2 and photovoltaic properties of the porphyrin-sensitized TiO_2 cells. Although porphyrins with *meso*-heteroaromatic groups have displayed unique physicochemical properties,[ix] a systematic comparison of film structures on the TiO_2 and photovoltaic properties of porphyrins with different heteroaromatic spacers has never been reported. Thus, the elucidation of a close

relationship between the molecular structure, the structure of the porphyrin film on the TiO_2, and the cell performance are anticipated in this study.

Results and Discussion

Synthesis. The syntheses of the porphyrins with *meso*-5-membered heteroaromatic carboxylic acid were all accomplished by the Lindsey methods.[x] In these methods, selection of appropriate aldehydes is the starting point for synthesizing target porphyrins. Synthetic routes of Zn5S, Zn5O, and Zn4S are displayed in SCHEMES 1 and 2.

SCHEME 1

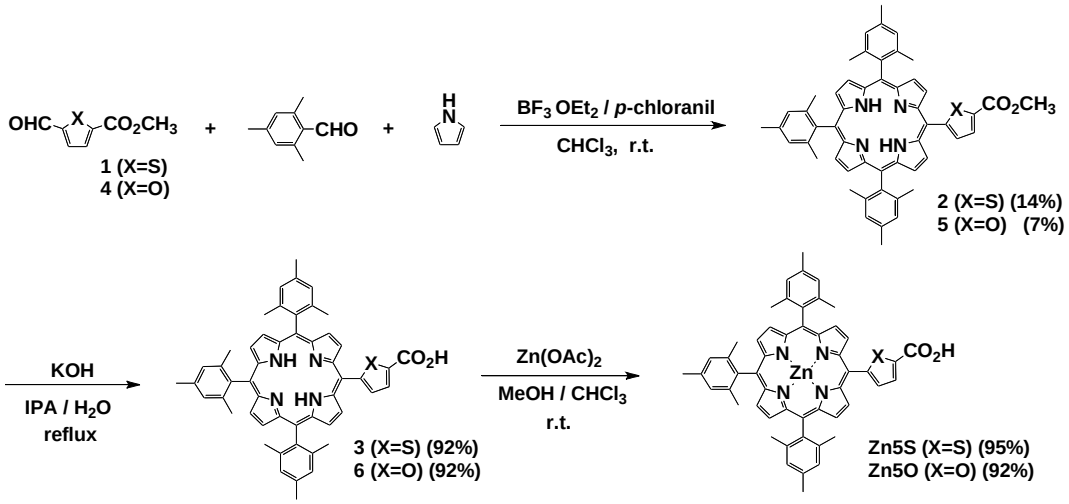

SCHEME 2

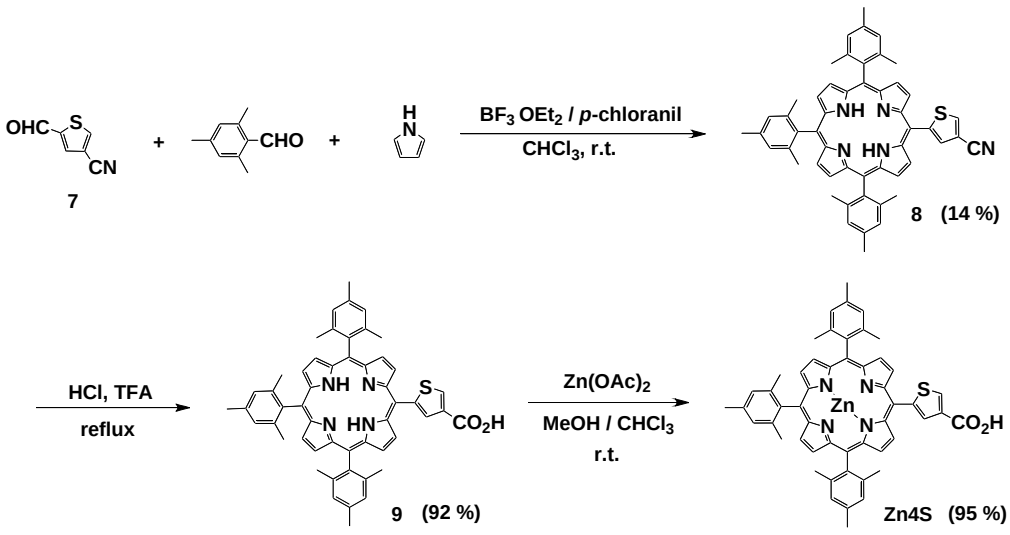

For Zn5S and Zn5O, condensation of **1** or **4** with 2,4,6-trimethylbenzaldehyde and pyrrole afforded mixtures of several porphyrins (SCHEME 1). Methoxycarbonylporphyrins **2** and **5** were separated by column chromatography and then hydrolyzed to give porphyrin carboxylic acid **3** and **6**, respectively. Zincporphyrins Zn5S and Zn5O were obtained by treatment of **3** and **6** with zinc acetate. For Zn4S, condensation of **7** with 2,4,6-trimethylbenzaldehyde and pyrrole yielded a mixture of several porphyrins (SCHEME 2). Cyanoporphyrin **8** was purified by column chromatography and then hydrolyzed to give porphyrin carboxylic acid **9**. Zincporphyrin Zn4S was prepared from **9**. Structures of the new compounds were verified by spectroscopic analyses including ^{1}H NMR and mass spectra.

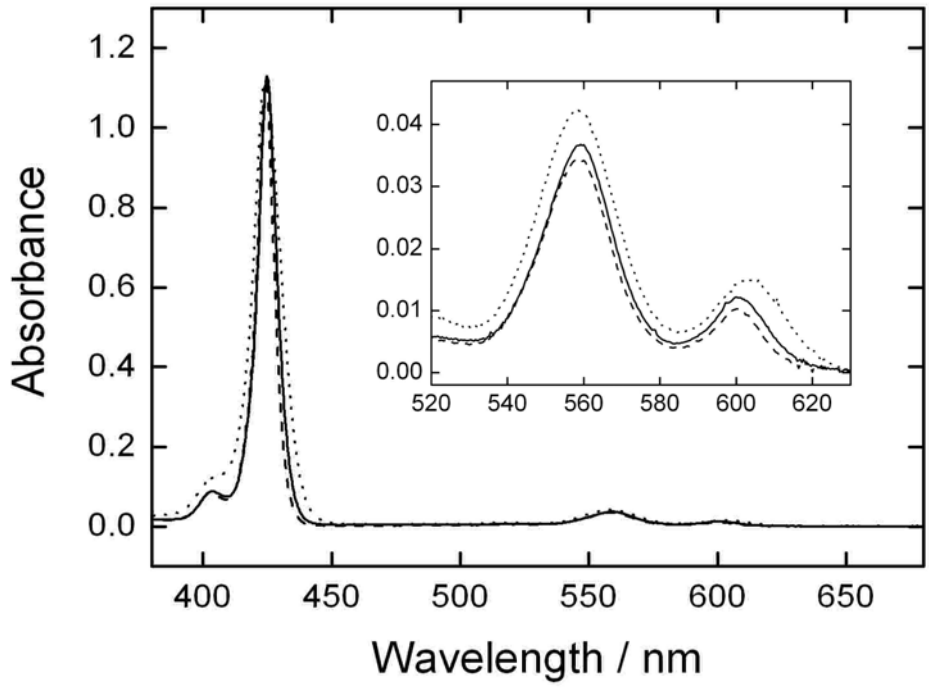

Figure 2. UV-visible absorption spectra of Zn5S (solid), Zn5O (dotted), and Zn4S (dashed) in ethanol with 2.1×10^{-6} M concentration. The spectra are normalized at the Soret band for comparison (Zn5S, ×1; Zn5O, ×2.2; Zn4S, ×0.80).

TABLE 1: Optical and Electrochemical Data for Porphyrins and Driving Forces for Electron Transfer Processes on TiO_2.

	λ^{a}_{abs} / nm	λ^{b}_{em} / nm	$E_{ox}{}^{c}$ / V	$E_{red}{}^{c}$ / V	$E_{ox}{}^{*\,d}$ / V	$\Delta G_{inj}{}^{e}$ / eV	$\Delta G_{reg}{}^{f}$ / eV
Zn5S	425 559 600	608 660	1.06	-1.34	- 0.99	- 0.49	- 0.56
Zn5O	424 558 604	614 662	1.05	-1.29	- 0.99	- 0.49	- 0.55
Zn4S	424 558 601	606 661	1.00	-1.41	- 1.06	- 0.56	- 0.50

[a] Wavelengths for Soret and Q bands absorption maxima in ethanol. [b] Wavelengths for emission maxima in ethanol by exciting at Soret wavelength. [c] Redox potentials (vs NHE). [d] Excited-state oxidation potentials approximated from E_{ox} and E_{00} (vs NHE). [e] Driving forces for electron injection from the porphyrin excited singlet state (E_{ox}*) to the conduction band of TiO_2 (-0.5 V vs NHE). [f] Driving forces for the regeneration of the porphyrin radical (E_{ox}) by I^-/I_3^- redox couple (+0.5 V vs NHE).

Optical and Electrochemical Properties in Solution. All the porphyrins displayed the characteristic spectral pattern of metalloporphyrin. The UV-visible absorption spectra of Zn5S, Zn5O, and Zn4S in ethanol are shown in Figure 2. The peak positions of the Soret and Q bands in ethanol are summarized in Table 1.

The peak positions of the Soret bands (424-425 nm) are similar, but the Soret bands become broad in the order of Zn4S, Zn5S, and Zn5O. The Q(0,0) band for

Zn5O is slightly red-shifted (604 nm) compared with those for Zn5S (600 nm) and Zn4S (601 nm), while the peak positions of the Q(1,0) band (558-559 nm) are virtually the same. The broadened Soret and slightly red-shifted Q-band for Zn5O result from smaller size of the furan bridge than the thiophene. It makes the dihedral angle between the porphyrin core and the furan bridge smaller than those between the porphyrin core and the thiophenes, leading to the large degree of conjugation in Zn5O (*vide infra*).[xi] The slightly widened Soret band of Zn5S relative to that of Zn4S may originate from a larger conjugation between the porphyrin core and the thiophene in Zn5S than in Zn4S. The steady-state fluorescence spectra of the porphyrins were measured in ethanol and the wavelengths for emission maxima are listed in Table 1. The emission maxima for Zn5O are slightly red-shifted compared to those for Zn5S and Zn4S, which is consistent with the results on the UV-visible absorption spectra. From the intercept of the normalized absorption and emission spectra, the zeroth-zeroth energies (E_{00}) are determined to be 2.05 eV for Zn5S, 2.04 eV for Zn5O, and 2.06 eV for Zn4S.[3d]

The first oxidation potentials (E_{ox}) and first reduction potentials (E_{red}) of the porphyrins were measured by using cyclic voltammetry. All porphyrins showed well-resolved and reversible one-electron redox waves and the results are listed in Table 1. The highest occupied molecular orbital-lowest unoccupied molecular orbital (HOMO-LUMO) gap for Zn5O (2.34 eV) is smaller than those for Zn5S (2.40 eV) and Zn4S (2.41 eV), which is in good agreement with the results on the UV-visible absorption and emission spectra.

From spectroscopic and electrochemical measurements, driving forces for electron injection from porphyrin excited singlet state to the conduction band (CB) of TiO_2 (-0.5 V vs NHE)[xii] (ΔG_{inj}) and for the regeneration of the porphyrin radical cation by I^-/I_3^- couple (0.5 V vs NHE)[12] (ΔG_{reg}) for the porphyrin-sensitized TiO_2 cells were determined (Table 1). Both of the processes are thermodynamically feasible and the

difference in the driving forces for the three systems are virtually negligible.[xiii]

Density Functional Theory (DFT) Calculations. DFT calculations were employed to gain the insight into the equilibrium geometry and electronic structure of the porphyrins (Figure 3). The core of each porphyrin displays analogous electronic structure. However, switching the heteroatom in the bridge (Zn5S vs Zn5O) or changing the position of carboxylic acid (Zn5S vs Zn4S) causes considerable variations in the electron densities on the spacers. They progressively increase in the order of Zn4S < Zn5S < Zn5O with a decrease in the dihedral angles between the porphyrin plane and the *meso*-heteroaromatic ring: 80° (Zn4S) > 73° (Zn5S) > 41° (Zn5O). The DFT results agree well with the abovementioned optical and electrochemical feature of the porphyrins.

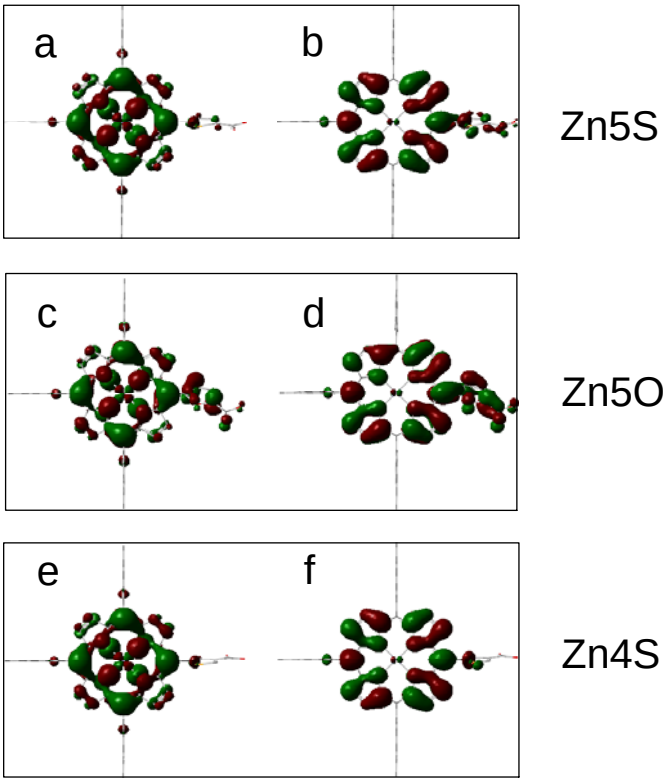

Figure 3. (a) HOMO and (b) LUMO of Zn5S, (c) HOMO and (d) LUMO of Zn5O, and (e) HOMO and (f) LUMO of Zn4S calculated by DFT methods with B3LYP/3-21G (d).

Porphyrin Adsorption on the TiO_2. Mesoporous TiO_2 films (10 μm thickness) were prepared from colloidal suspension of TiO_2 nanoparticles (P25) (See, Experimental Section). The TiO_2 electrodes were immersed into ethanol containing 0.2 mM porphyrin at room temperature to give porphyrin-modified TiO_2 electrodes (denoted as TiO_2/Zn5S,

TiO_2/Zn5O, and TiO_2/Zn4S). Total amounts of the porphyrins adsorbed on the TiO_2 films were determined by measuring absorbance of the porphyrins that were dissolved from the porphyrin-adsorbed TiO_2 films into DMF containing 0.1 M NaOH. Taking into account the surface area of P25 (54 m^2 g^{-1}),[xiv] the porphyrin densities (Γ) on the actual surface area are determined from the total amounts of the porphyrins adsorbed on the TiO_2 films.

To establish the adsorption behavior of the porphyrins on the TiO_2 surface, the time dependence of the Γ value for the porphyrin adsorption in ethanol was examined firstly (Figure 4). The initial adsorption rates of Zn5S and Zn5O are fast and similar, but the Γ values reach to different, constant maxima of 4.7×10^{-11} mol cm^{-2} and 6.9×10^{-11} mol cm^{-2}, respectively (Table 2). In contrast, the Γ value of Zn4S increases slowly by increasing the immersing time to become saturated for 12 h (Γ=2.0×10^{-11} mol cm^{-2}). The large adsorption rates of Zn5S and Zn5O relative to that of Zn4S are consistent with the large electron densities of the spacer in Zn5S and Zn5O in comparison with that of Zn4S calculated by DFT methods (Figure 3). Ruthenium dyes and porphyrins are known to make monolayers on TiO_2 surfaces.[1-7] Assuming each porphyrin monolayer with densely packed, vertical and horizontal orientations to the TiO_2 surface, Γ values are

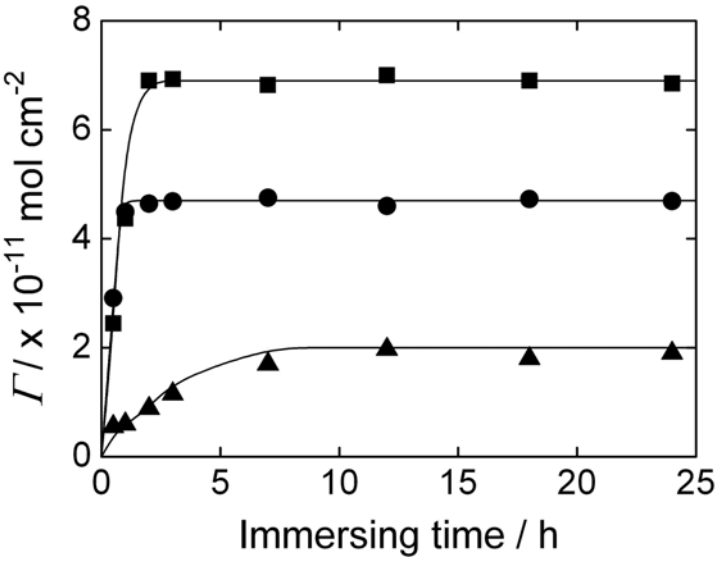

Figure 4. Time profiles of the surface coverage (Γ) of Zn5S (circle), Zn5O (square), and Zn4S (triangle) on the TiO_2 electrode for different immersing time in ethanol.

calculated to be 1.2×10^{-10} mol cm^{-2} and 6.0×10^{-11} mol cm^{-2}, respectively. Taking into account the calculated Γ values together with the adsorption behavior of Zn5S and Zn5O, both Zn5S and Zn5O molecules are tilted toward the TiO_2 surface to yield densely packed porphyrin monolayers. The small saturated Γ value of Zn4S relative to that for the horizontal orientation results from the formation of a loosely packed monolayer of Zn4S on the TiO_2 surface, owing to the weak binding ability of the carboxylic acid due to little electron density on the spacer of Zn4S.

TABLE 2: Photovoltaic Properties of Porphyrin-Sensitized Solar Cells under the Optimized Conditions.

Cell	Γ^a / 10^{-11} mol cm^{-2}	η_{max} / %	J_{sc} / mA cm^{-2}	V_{oc} / V	*ff*	$IPCE_{max}$ / %
TiO_2/Zn5S	4.7±0.1	3.1±0.2 (1 h)[b]	7.2±0.2	0.67±0.02	0.67±0.04	65±3[c]
TiO_2/Zn5O	6.9±0.1	2.3±0.2 (2 h)[b]	5.8±0.2	0.62±0.02	0.65±0.04	55±3[d]
TiO_2/Zn4S	2.0±0.1	1.8±0.3 (12 h)[b]	4.3±0.3	0.62±0.03	0.67±0.04	34±4[c]

[a] Saturated, maximum Γ value. [b] Numbers in parentheses represent the immersing time for the porphyrin adsorption in ethanol. [c] At 420 nm. [d] At 430 nm.

Spectroscopic Characterization of Porphyrin Films on TiO_2. To gain further insight into the structures of the porphyrin monolayers on the TiO_2 surface, absorption spectra were measured at the initial (solid line in Figure 5) and final (dashed line in Figure 5) stages of the equilibrated coverage for TiO_2/Zn5S (1 and 12 h), TiO_2/Zn5O (2 and 12 h), and TiO_2/Zn4S (12 and 24 h). Thickness of the TiO_2 substrate was adjusted

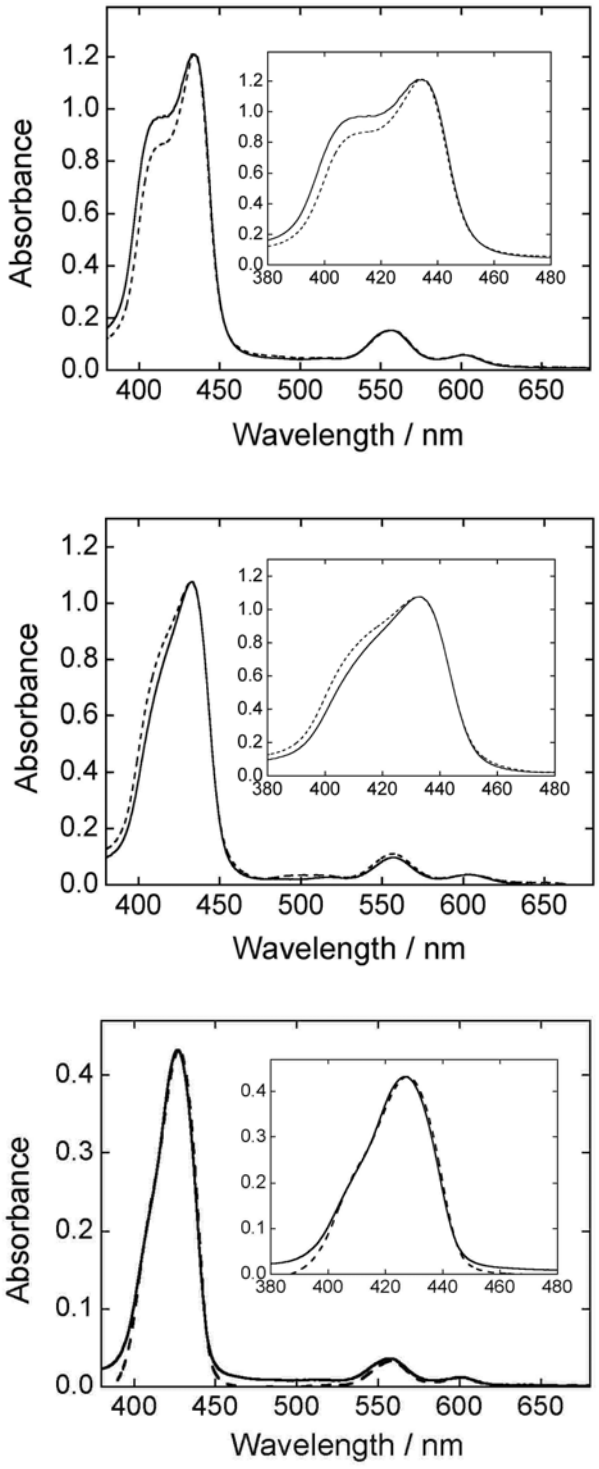

Figure 5. UV-visible absorption spectra of (a) TiO_2/Zn5S for the immersing time of 1 h (solid line) and 12 h (dashed line), (b) TiO_2/Zn5O for the immersing time of 2 h (solid line) and 12 h (dashed line), and (c) TiO_2/Zn4S for the immersing time of 12 h (solid line) and 24 h (dashed line) in ethanol. Thickness of the TiO_2 films was adjusted to be 0.7 – 1.0 μm to obtain the shape and peak position of the spectra accurately.

to be 0.7 – 1.0 μm to obtain the shape and peak position of the whole spectra accurately. The peak positions of TiO_2/Zn5S, TiO_2/Zn5O, and TiO_2/Zn4S are virtually similar for the different immersing times, whereas the difference in the shape of the Soret bands at the initial and final stages of the equilibrated coverage become large in the order of TiO_2/Zn4S, TiO_2/Zn5O, and TiO_2/Zn5S. It should be noted here that the splittings of the Soret bands arising from the exciton coupling of the porphyrins[xv] are observed for TiO_2/Zn5S (λ_{max}=411, 434 nm) and TiO_2/Zn5O (λ_{max}=411, 433 nm), while TiO_2/Zn4S exhibits a single Soret band (λ_{max}=427 nm), of which the peak position is slightly red-shifted from that in ethanol (λ_{max}=424 nm). These results agree well with the formation of densely packed porphyrin monolayers for TiO_2/Zn5S and TiO_2/Zn5O and of loosely packed monolayer for TiO_2/Zn4S.

ATR-FTIR spectroscopy is known to be a useful tool for gaining the information on the binding mode of the molecules adsorbed on the TiO_2 surface.[xvi] In this study, the interpretations for the ATR-FTIR spectra of the porphyrin monolayers are aided by comparison with the FTIR spectra of the corresponding porphyrin powder in a KBr pellet. Figure 6 shows the FTIR spectra of Zn5S and Zn5O and the ATR-FTIR spectra of TiO_2/Zn5S and TiO_2/Zn5O. The reliable ATR-FTIR spectrum of TiO_2/Zn4S could not be obtained probably because of the low coverage of Zn4S on the TiO_2 due to the weak binding ability of the anchoring group to the TiO_2. Both FTIR spectra of Zn5S and Zn5O reveal the characteristic band of ν (C=O) of the carboxylic acid group at around 1700 cm^{-1} (Figure 6a, c).[xvii] This diagnostic for the ν (C=O) disappears for the ATR-FTIR spectra of TiO_2/Zn5S and TiO_2/Zn5O. The ATR-FTIR spectra of TiO_2/Zn5S and TiO_2/Zn5O exhibit a marked increase in symmetric carboxylate band, ν (COO_s^-), at around 1400 cm^{-1} (Figure 6b, d). A band can be assigned for asymmetric carboxylate, ν (COO_{as}^-), at around 1600 cm^{-1} for TiO_2/Zn5S and TiO_2/Zn5O also gains intensity, but is not so significant as that for ν (COO_s^-). The disappearance of ν (C=O) and the increased intensities of ν (COO_s^-) and ν (COO_{as}^-) demonstrate that a proton is

detached from the carboxylic acid group during the adsorption of the porphyrin on the TiO_2 surface through the bidentate binding carboxylate group.[4a,4b,16b,17]

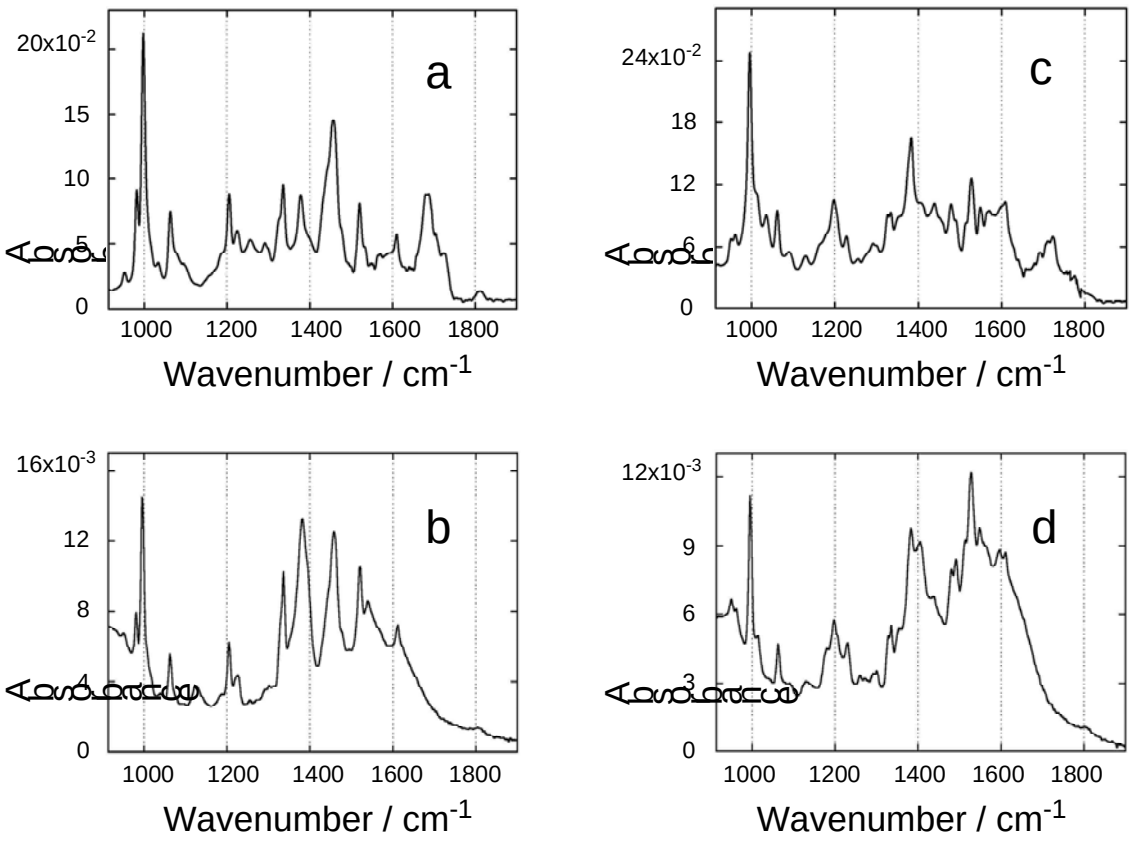

Figure 6. FTIR spectra of (a) Zn5S and (c) Zn5O in a KBr pellet and ATR-FTIR spectra of (b) TiO_2/Zn5S (Γ=(4.7±0.1)×10^{-11} mol cm^{-2}) and (d) TiO_2/Zn5O (Γ=(6.9±0.1) × 10^{-11} mol cm^{-2}) with 10 μm-thickness TiO_2 films. The TiO_2/Zn5S and TiO_2/Zn5O electrodes were prepared by immersing the TiO_2 films into the porphyrin ethanol solutions for 1 and 2 h, respectively. ATR-FTIR spectra of porphyrin monolayers on the TiO_2 were referenced to the spectra of blank TiO_2 film. Before measurements, the blank TiO_2 film was heated to 100 ^oC for 10 min to remove adsorbed water.

To further shed light on the adsorption states of porphyrins on the TiO_2 surface, XPS measurements were performed for TiO_2/Zn5S, TiO_2/Zn5O, and TiO_2/Zn4S together with the samples of the corresponding porphyrin multilayers prepared by casting the porphyrin solutions onto the TiO_2 (denoted as TiO_2/Zn5S$_M$, TiO_2/Zn5O$_M$, and TiO_2/Zn4S$_M$). All porphyrin molecules in the monolayer directly contact with the TiO_2 surface, whereas most of the molecules in the multilayer are anticipated to have no interaction with the surface.

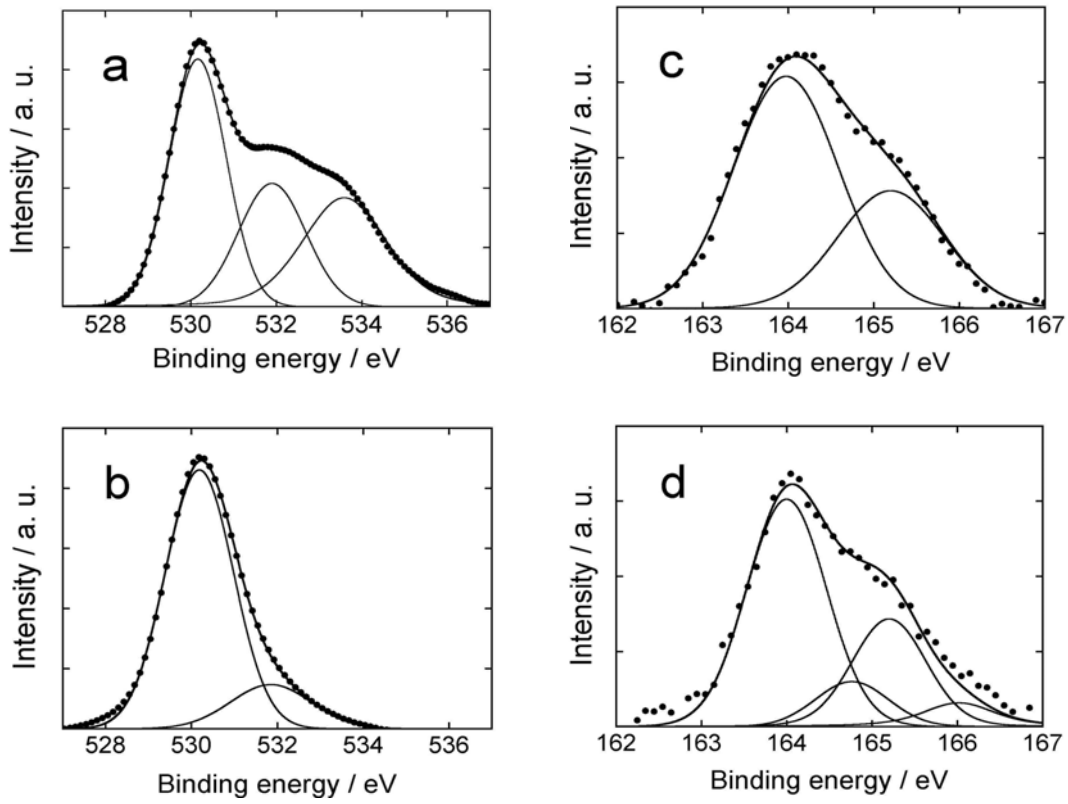

Figure 7. X-ray photoelectron O1s spectra of (a) TiO_2/Zn5S$_M$ and (b) TiO_2/Zn5S and X-ray photoelectron S2p spectra of (c) TiO_2/Zn5S$_M$ and (d) TiO_2/Zn5S. The TiO_2/Zn5S electrode was prepared by immersing the TiO_2 film into the porphyrin ethanol solution for 1 h. The TiO_2/Zn5$_M$ electrode was prepared by casting the porphyrin ethanol solution onto the TiO_2. The spectra are normalized for comparison.

Figure 7 shows the X-ray photoelectron O1s and S2p spectra of TiO_2/Zn5S and TiO_2/Zn5S_M. The O1s spectrum of TiO_2/Zn5S_M exhibits three chemically different peaks (Figure 7a). The most intense peak appearing at 530.2 eV can be assigned to the oxygen atom of the TiO_2 surface.[xviii] The peaks arising at 531.9 and 533.6 eV originate from the oxygen atoms of the carbonyl group and of the hydroxy group in the carboxylic acid, respectively.[xix] The O1s spectrum of TiO_2/Zn5S (Figure 7b), in contrast to that of TiO_2/Zn5S_M, reveals the same two O1s peaks as those for the XPS spectrum of TiO_2/Zn5S_M, with the disappearance of the peak at 533.6 eV. The comparison also supports that the hydroxy group loses a proton during the adsorption on the TiO_2, and consequently the two oxygens in the carboxylate bind to the TiO_2 surface with the same binding energy,[xx] which is in good agreement with the results on the ATR-FTIR spectra (*vide supra*). S2p of thiophene typically shows one pair of peaks at 164.0 and 165.2 eV by spin-orbit split, and the ratio of intensity is 2:1.[xxi] This fingerprint for S2p from the XPS spectrum of TiO_2/Zn5S_M is also found (Figure 7c). The S2p spectrum of TiO_2/Zn5S (Figure 7d), which is unlikely to TiO_2/Zn5S_M, displays one additional pair of peaks at 164.8 and 166.0 eV with the intensity ratio of 2:1 as well as the pair of peaks at 164.0 and 165.2 eV. This implies that the sulfur atom in TiO_2/Zn5S is not necessarily equivalent with that in TiO_2/Zn5S_M.[xxii] The Ti^{4+} cation in the TiO_2 surface has a Lewis-acidic character,[xxiii] and the sulfur atom in the bridge of Zn5S holds the lone pair of electrons. This leads to coordination of the sulfur atom via the lone pair to Ti^{4+} cation.[xxiv] The Zn5S is, therefore, envisaged to possess 2-fold adhesive interactions with the TiO_2: one by the sulfur atom in the bridge and the other by the carboxylic acid. Under these circumstances, the Zn5S molecule tilts heavily toward the plane of the TiO_2 surface, resulting in the low saturated Γ value compared to that for the Zn5O (*vide supra*).

Figure 8 displays the XPS spectra for O1s of TiO_2/Zn5O and TiO_2/Zn5O$_M$. For TiO_2/Zn5O$_M$ (Figure 8a), each XPS peak for the O1s appears at 530.2, 531.5, 532.4, and 533.4 eV. The peaks at 530.2, 531.5, and 533.4 eV can be attributed to the oxygen atoms from the TiO_2 surface, the carbonyl group, and the hydroxy group, respectively,[18,19] as in the case for TiO_2/Zn5S$_M$. The peak at 532.4 eV can be assigned to the oxygen atom of furan in the bridge. For TiO_2/Zn5O (Figure 8b), the three O1s peaks at 530.2, 531.5, and 532.4 eV are appeared with the disappearance of the O1s peak at 533.4 eV, as seen for the comparison of XPS spectra of TiO_2/Zn5S$_M$ and TiO_2/Zn5S.[20] It is noteworthy that the XPS peak arising from the interaction between the oxygen atom of the furan bridge and the TiO_2 surface could not be detected. This suggests that the Zn5O molecule does not tilt heavily toward the TiO_2 surface relative to the Zn5S, which also agrees well with the large saturated Γ value of Zn5O compared to that of Zn5S (*vide supra*). On the other hand,

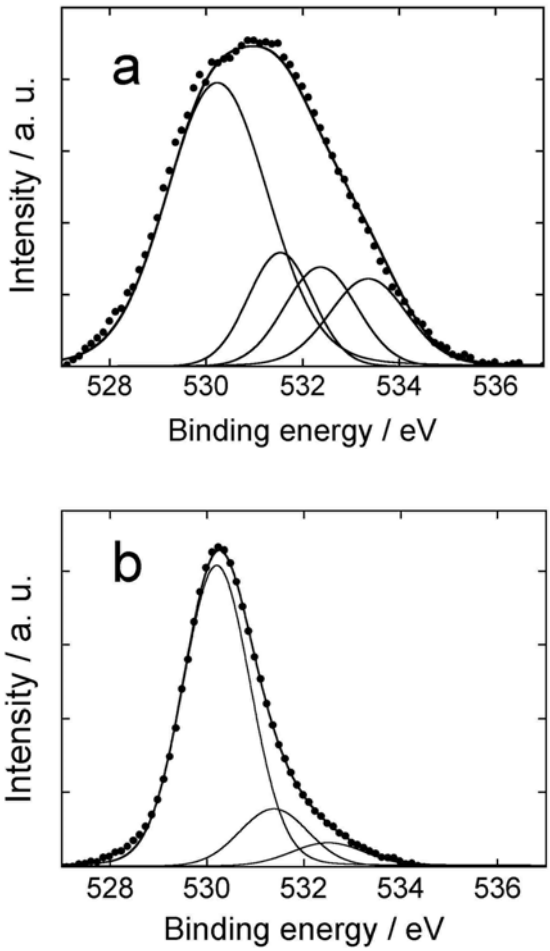

Figure 8. X-ray photoelectron O1S spectra of (a) TiO_2/Zn5O$_M$ and (b) TiO_2/Zn5O. The TiO_2/Zn5O electrode was prepared by immersing the TiO_2 films into the porphyrin ethanol solutions for 2 h. The TiO_2/Zn5O$_M$ electrode was prepared by casting the porphyrin ethanol solution onto the TiO_2. The spectra are normalized for comparison.

comparison of the XPS spectra of TiO_2/Zn4S$_M$ and TiO_2/Zn4S could not be performed, because the sample of TiO_2/Zn4S did not give a satisfactory XPS spectrum due to the low coverage of the Zn4S on the TiO_2.

Photovoltaic and Photoelectrochemical Properties of Porphyrin-Sensitized TiO_2 Cell. Since the photovoltaic performance of dye-sensitized solar cell strongly depends on the TiO_2 preparation and electrolytes, the cell performance with N719 dye as a reference system under the present conditions employing P25 TiO_2 film was firstly examined. A 10-μm-thick TiO_2 electrode was modified with N719 (0.2 mM) in *t*-butanol and acetonitrile (1:1) for 12 h. Current-voltage characteristics were measured using the N719 modified electrode and a Pt counter electrode under AM 1.5 conditions. The η value is derived from the equation: $\eta = J_{SC} \times V_{OC} \times ff$ in where η is the power conversion efficiency, J_{SC} is the short circuit current, V_{OC} is the open circuit potential, and *ff* is the fill factor. N719-sensitized cell yields 6.5 % of η value with 14.0 mA cm^{-2} of J_{SC}, 0.74 V of V_{OC}, and 0.63 of *ff* (Figure 9). Except for V_{OC}, the cell shows rather inferior performance compared with the reported results.[3h]

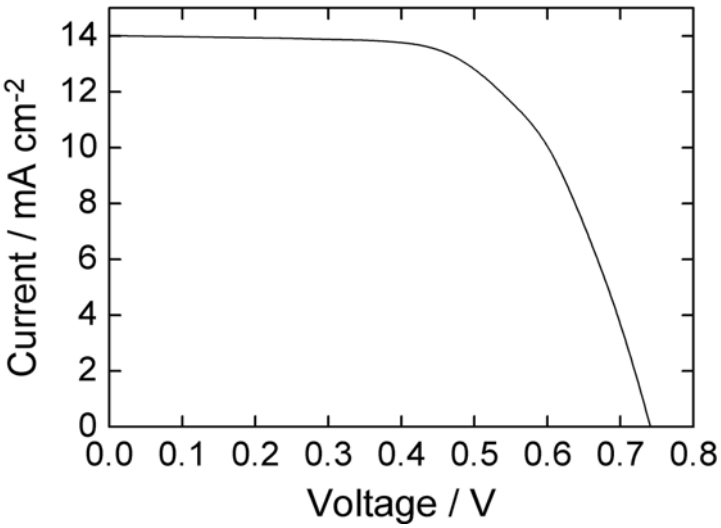

Figure 9. Photocurrent-voltage characteristics of N719-sensitized TiO_2 cell (η = 6.5 %, J_{sc} = 14.0 mA cm^{-2}, V_{oc} = 0.74 V, *ff* = 0.63). Conditions: electrolyte 0.1 M LiI, 0.05 M I_2, 0.6 M 2,3-dimethyl-1-propyl imidazolium iodide, and 0.5 M 4-*t*-butylpyridine in CH_3CN. Input power: AM 1.5 under simulated solar light (100 mW cm^{-2}). $\eta = J_{sc} \times V_{oc} \times ff$.

To further establish the cell performance of the porphyrin-sensitized solar cells under the present conditions using P25, the time dependence of η value for the adsorption of each porphyrin (0.2 mM) in ethanol was examined (Figure 10). The η values of Zn5S- and Zn5O-sensitized cells increase rapidly by increasing the immersing time to reach maximum η values (η_{max}) of 3.1% for 1 h and of 2.3% for 2 h. Further increase of the adsorption time leads to gradual decreases of the η values, reaching to constant η values of 1.9% and 1.2% for 12-18 h, respectively. The initial time profiles of the η values correlate well with those of the Γ values (Figure 4), but the decreases of the η values do not match the saturated behavior of the Γ values as porphyrin monolayers. The behaviors are believed to be associated with the increment in the degree of aggregation of porphyrins on the TiO_2 surface along with the prolonged adsorption. In contrast, the η value of the Zn4S-sensitized cell increases slowly by increasing the immersing time to reach a constant, maximum η value of 1.8% for 12 h. The trend of the η value parallels that of the Γ value for the Zn4S (Figure 4). Table 2 summarizes the photovoltaic performance of the porphyrin-sensitized TiO_2 cells under the optimized conditions exhibiting the η_{max} value. The current-voltage characteristics are also shown in Figure 11. The η_{max} value increases in the order of Zn4S - (1.8%) < Zn5O- (2.3%) < Zn5S- (3.1%) sensitized cells.

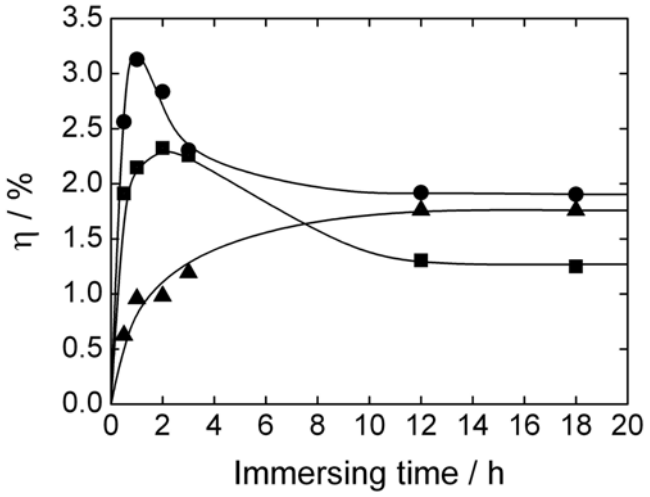

Figure 10. Time profiles of the η values of Zn5S- (circle), Zn5O- (square), and Zn4S- (triangle) sensitized cells with the TiO_2 electrodes prepared under different immersing time for the porphyrin adsorption in ethanol.

The η_{max} values are much smaller than that of N719-sensitized cells under the same experimental conditions. The smaller η_{max} values of the porphyrin-sensitized cells originate mainly from the small J_{SC} values, which reflect the difference in the IPCE values of the porphyrin- and N719-sensitized cells. The porphyrin-sensitized cells show slightly small V_{OC} value compared with that of N719-sensitized cell, however, to a large extent, the three cells display rather similar V_{OC} and *ff* values. The trend of η_{max} value matches the order of J_{SC}. Thus, the small η_{max} value of the Zn4S-sensitized TiO_2 cell relative to those of the Zn5S- and Zn5O-sensitized cells largely results from the small, saturated Γ value of TiO_2/Zn4S compared to those of TiO_2/Zn5S and TiO_2/Zn5O (Figure 4). It is noteworthy that the Zn5S-sensitized TiO_2

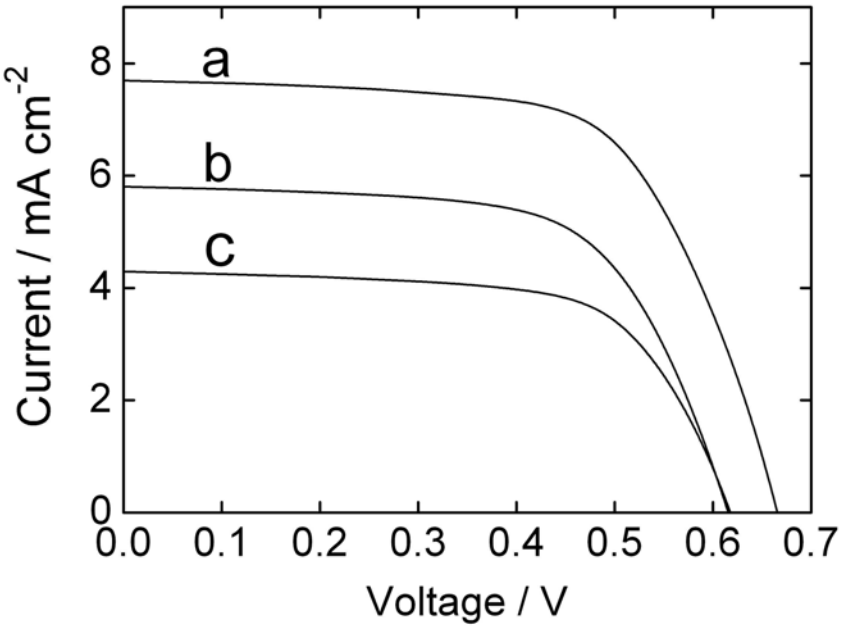

Figure 11. Photocurrent-voltage characteristics under the optimized conditions exhibiting maximum η values for respective TiO_2 cells. (a) Zn5S-sensitized TiO_2 cell (η_{max} = 3.1 %, J_{sc} = 7.2 mA cm^{-2}, V_{oc} = 0.67 V, *ff* = 0.67), (b) Zn5O-sensitized TiO_2 cell (η_{max} = 2.3 %, J_{sc} = 5.8 mA cm^{-2}, V_{oc} = 0.62 V, *ff* = 0.65), and (c) Zn4S-sensitized TiO_2 cell (η_{max} = 1.8 %, J_{sc} = 4.3 mA cm^{-2}, V_{oc} = 0.62 V, *ff* = 0.67). Conditions: electrolyte 0.1 M LiI, 0.05 M I_2, 0.6 M 2,3-dimethyl-1-propyl imidazolium iodide, and 0.5 M 4-*t*-butylpyridine in CH_3CN. Input power: AM 1.5 under simulated solar light (100 mW cm^{-2}). $\eta = J_{sc} \times V_{oc} \times ff$.

cell exhibits larger η value than the Zn5O-sensitized cell, irrespective of the rather small, saturated Γ value of TiO_2/Zn5S relative to that of TiO_2/Zn5O.

A series of photocurrent action spectra are recorded and compared against the absorption spectra on the TiO_2 (Figure 12). The overall photoelectrochemical responses parallel the absorption feature of the porphyrin on the TiO_2 (Figure 5), implying the involvement of the porphyrin moiety in the photocurrent generation. These results are in good agreement with the photoelectrochemical and photovoltaic behavior of porphyrin-sensitized TiO_2 cells.[4] The maximum IPCE ($IPCE_{max}$) value also increases in the order of Zn4S- (34%) < Zn5O- (55%) < Zn5S- (65%) sensitized cells, which correlates well with the trend of the η_{max} value. At longer wavelength

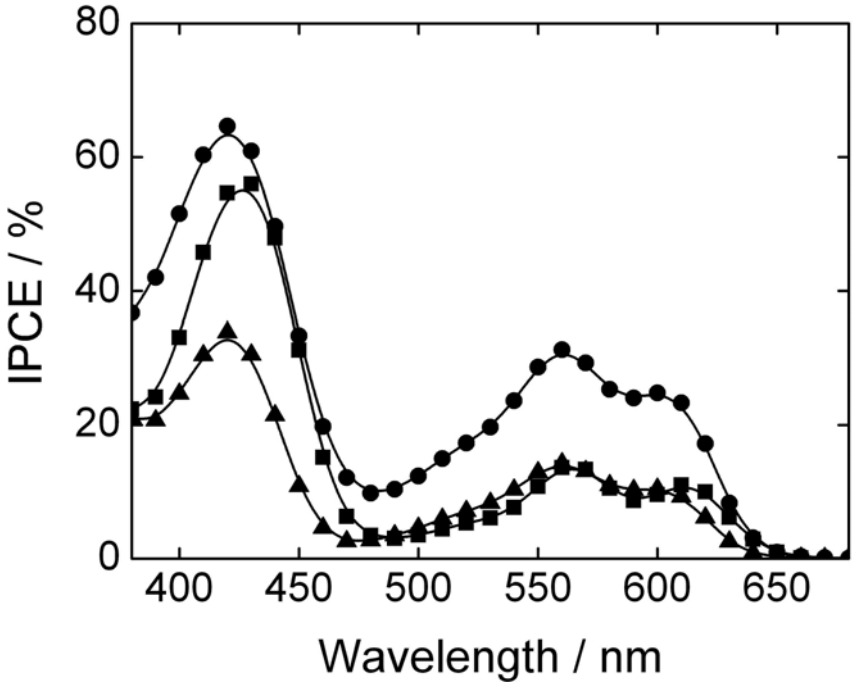

Figure 12. Action spectra of Zn5S-sensitized TiO_2 cell (circle), Zn5O-sensitized TiO_2 cell (square), and Zn4S-sensitized TiO_2 cell (triangle). Each of the porphyrin-modified TiO_2 electrodes was prepared under the same conditions exhibiting the maximum η values for the corresponding TiO_2 cells. Conditions: electrolyte 0.1 M LiI, 0.05 M I_2, 0.6 M 2,3-dimethyl-1-propyl imidazolium iodide, and 0.5 M 4-*t*-butylpyridine in CH_3CN. Input power: AM 1.5 under simulated solar light (100 mW cm^{-2}).

region (> 500 nm), the Zn5S-sensitized TiO_2 cell displays a higher IPCE value than those of the Zn5O- and Zn4S-sensitized cells. The photocurrent at the short and long wavelength regions stems from the porphyrin S_2 and S_1 states, respectively. At present the rationale is not clear, but it may be associated with the difference in the interaction between the porphyrin excited singlet states[2] and/or between the porphyrin excited singlet states and the TiO_2 surface.[xxv]

To explain the difference in the η_{max} and $IPCE_{max}$ values of the Zn5S-, Zn5O-, and Zn4S-sensitized cells, the IPCE value is divided into three parts. Namely, IPCE is defined as the following equation (1).

$$IPCE = LHE \times APCE = LHE \times \phi_{inj} \times \eta_{col} \quad (1)$$

where LHE (light harvesting efficiency) is the number of absorbed photons per the number of incident photons, APCE (absorbed photon-to-current efficiency) is the number of electrons collected in the external circuit per the number of absorbed photons, ϕ_{inj} is the quantum yield for electron injection from the porphyrin excited-state to the CB of the TiO_2 electrode, and η_{col} is the efficiency of the charge collection. The APCE values at the Soret and Q bands regions for each of the porphyrin-sensitized TiO_2 cells are determined by literature procedures[xxvi] (Table 3). The Zn5S-sensitized TiO_2 cell exhibits a larger IPCE value than the Zn5O-sensitized one, irrespective of a rather small, saturated Γ value of TiO_2/Zn5S relative to that of TiO_2/Zn5O. This indicates that the difference in the APCE values is responsible for the large IPCE value of the Zn5S-sensitized TiO_2 cell relative to that of the Zn5O-sensitized cell. APCEs of the two Zn4S-sensitized TiO_2 cells with different Γ values are similar (Table 3), when taking into account light losses by multiple reflection at the interfaces of the TiO_2 electrode, scattering by the porous TiO_2 network, and absorption by electrolyte.[xxvii] Therefore, small Γ value of TiO_2/Zn4S compared with those of TiO_2/Zn5S and

TiO_2/Zn5O can be invoked to rationalize the small IPCE value of the Zn4S-sensitized TiO_2 cell relative to those of the Zn5S- and Zn5O-sensitized TiO_2 cells. The photocurrent generation mechanism in the present cells is considered as follows. First, ultrafast electron injection takes place from the porphyrin excited singlet state to the CB of the TiO_2 electrode with the time constants ranging from <100 fs to ~10 ps.[7,xxviii] I^- in the electrolyte solution diffuses to the resulting porphyrin radical cation to give electrons with the time constant of ~10^{-8} s,[1-7] yielding to the neutral porphyrin and I_3^-. The intermolecular quenching process is much faster than the charge recombination from the CB of the TiO_2 electrode to the porphyrin radical cation with the time constant ranging from 10^{-4}~10^{-1} s.[7] I_3^- diffuses to the counter electrode to receive electrons to regenerate the initial state. Thus, the IPCE values are limited by the initial electron injection and/or charge recombination between the electrons on the CB of TiO_2 and I_3^-. Since the porphyrins are not involved in the latter process, the former process contributes the difference in the IPCE values. Namely, the nonparallel rates of electron injection between the Zn5S- and Zn5O-sensitized cells may be attributed to the difference in the IPCE values. Given the similar driving forces for the electron

TABLE 3: APCE of Porphyrin-Sensitized Solar Cells.

cell	Γ / 10^{-11} mol cm^{-2}	APCE(IPCE) / %
TiO_2/Zn5S	4.7	65(65),[a] 48(31),[b] 82(25)[c]
TiO_2/Zn5O	6.9	55(55),[a] 23(14),[b] 34(10)[c]
TiO_2/Zn4S	2.0	36(34),[a] 38(14),[b] 78(10)[c]
TiO_2/Zn4S	0.6	26(23),[a] 46(7),[b] 98(5)[c]

[a] At 420 nm. [b] At 560 nm. [c] At 600 nm.

injection (Table 1), the difference in the electronic coupling between the two systems is likely to have an impact on the large IPCE value of the Zn5S-sensitized cell in comparison with the Zn5O-sensitized cell.[xxix] However, the electron density of LUMO in the spacer of Zn5O is rather larger than that of Zn5S (Figure 4). Thus, the dual electron-transfer pathways given by the sulfur atom residing in the bridge as well as by the carboxylic acid for the Zn5S-sensitized TiO_2 cell against single pathway for the Zn5O-sensitized cell, accelerate the electron injection from the Zn5S excited singlet state to the CB of the TiO_2 electrode, leading to the larger IPCE value are proposed (Figure 13). The results obtained from optical spectroscopy, DFT calculations, dye coverage, ATR-FTIR spectroscopy, and XPS measurements are consistent with the additional electron injection pathway through the interaction between the sulfur atom in the spacer and the TiO_2 surface.

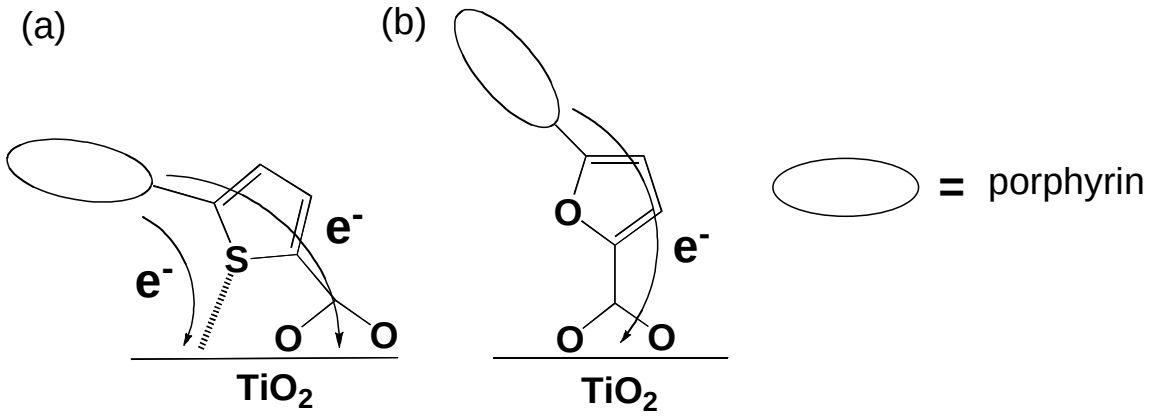

Figure 13. Schematic view of proposed adsorption geometry and electron transfer pathways of (a) Zn5S and (b) Zn5O on the TiO_2 surface.

Conclusions

Novel porphyrins with *meso* 5-membered heteroaromatic spacers are designed and synthesized to evaluate the effects of the spacers on the structures of the porphyrin films on TiO_2 and photovoltaic properties of porphyrin-sensitized TiO_2 cells. Modifications

in spacers including switching one element (i.e., sulfur vs oxygen) in the bridge or changing the position of the anchoring group (i.e., 4- vs 5-position) are found to have significant effects on the dye coverage and the structures of the porphyrin monolayers on the TiO_2 surface, and photovoltaic properties of the porphyrin-sensitized TiO_2 cells. The high photovoltaic properties of the Zn5S-sensitized cell can be rationalized by the additional electron-transfer pathway through specific interaction between the sulfur atom inherent in the bridge and the TiO_2 surface. Theses findings will provide a useful tactic for devising novel dyes for dye-sensitized solar cells.

Experimental Section

Synthesis

General. All solvents and chemicals were of reagent grade quality, purchased and used without further purification unless otherwise noted. All of the reactions were carried out under nitrogen or argon atmosphere in the dark. Column chromatography and thin-layer chromatography (TLC) were performed with UltraPure Silica Gel (230-400 mesh, SiliCycle) and Silica gel 60 F_{254} (Merck), respectively. ^{1}H-NMR spectra were measured on a JEOL EX-400 (400 MHz) or a JEOL AL300 (300 MHz) spectrometer. Matrix assisted laser desorption/ionization time-of-flight (MALDI-TOF) mass spectra were made on a Shimadzu KOMPACT MALDI II using CHCA as a matrix. UV-vis absorption spectra were measured using a Perkin-Elmer Lambda 900 UV/VIS/NIR Spectrometer with a spectroscopy grade ethanol. FT-IR spectra were acquired using by a JASCO FT/IR-470 plus spectrometer with a KBr pellet. Melting points were recorded on a Yanagimoto micro-melting point apparatus and were not corrected.

Methyl 5-formylthiophene-2-carboxylate (1). This procedure was based upon the literature protocol for similar compound.[xxx] 5-Formylthiophene-2-carboxylic acid (1.07 g, 6.9 mmol), sodium hydrogen carbonate (0.88 g, 10 mmol), and dimethyl sulfate

(1.3 mL, 14 mmol) were dissolved in hexamethylphosphoamide (5.5 mL) and heated at 100 ^{o}C for 1h. Subsequently, the reaction mixture was cooled to room temperature, extracted with diethyl ether, and then the solvent was removed in vacuo. The crude product was purified by silica column chromatography (ethyl acetate/n-hexane = 1:4) to give **1** as a pale yellow solid (0.84 g, 4.9 mmol, 73 % yield). Mp 87 ^{o}C; ^{1}H NMR (400 MHz, $CDCl_3$) δ 9.98 (s, 1H), 7.84 (d, *J*=4.0 Hz, 1H), 7.73 (d, *J*=4.0 Hz, 1H), 3.94 (s, 3H); IR (KBr) ν_{max} 1670 cm^{-1} (CO aldehyde), 1730 cm^{-1} (CO ester); MS (MALDI-TOF) *m/z* 170.4 $(M+H)^+$.

5-(5-Methoxycarbonyl-2-thienyl)-10,15,20-tris(2,4,6-trimethylphenyl)porphyrin (2). This procedure was based upon the literature protocol for similar compound.[xxxi] Methyl 5-formylthiophene-2-carboxylate (**1**) (0.39 g, 2.3 mmol), pyrrole (0.7 mL, 9.3 mmol), and 2,4,6-trimethyl benzaldehyde (1.0 mL, 7.0 mmol) were dissolved in chloroform at room temperature. Dry nitrogen was bubbled through the solution for 30 min before adding boron trifluoride diethyl etherate (0.6 mL, 4.6 mmol). The solution was stirred for 1h, then *p*-chloranil (2.33 g, 9.4 mmol) was added and stirring was continued for 1h. After triethylamine (0.7 mL, 4.6 mmol) was added, the solvent was removed in vacuo. Purification of the crude product by flash column chromatography on alumina ($CHCl_3$) and subsequent column chromatography on silica gel (CH_2Cl_2/n-hexane = 1:1) and reprecipitation from CH_2Cl_2/hexane afforded **2** as a purple red solid (0.25 g, 0.32 mmol, 14 % yield). Mp > 300 ^{o}C; ^{1}H NMR (400 MHz, $CDCl_3$) δ 8.95 (d, *J*=4.8 Hz, 2H), 8.70 (d, *J*=4.8 Hz, 2H), 8.63 (s, 4H), 8.18 (d, *J*=3.6 Hz, 1H), 7.89 (d, *J*=3.6 Hz, 1H), 7.28 (s, 6H), 4.03 (s, 3H), 2.63 (s, 6H), 2.62 (s, 3H), 1.85 (s, 6H), 1.84 (s, 12H), -2.52 (s, 2H); MS (MALDI-TOF) *m/z* 805.3 $(M+H^+)$.

5-(5-Carboxy-2-thienyl)-10,15,20-tris(2,4,6-trimethylphenyl)porphyrin (3). To a solution of **2** (0.26 g, 0.32 mmol) in 2-propanol (118 mL) was added a solution of potassium hydroxide (1.97 g, 35 mmol) in water (29.5 mL). The solution was refluxed for 2h. After the reaction mixture was cooled to room temperature, aqueous 3M

hydrochloric acid was added until the color of reaction mixture turned to green from red. The solution was washed with saturated aqueous sodium bicarbonate and water, dried over anhydrous sodium sulfate, and then the solvent was removed in vacuo. Reprecipitation from CH_2Cl_2/hexane gave **3** as a purple red solid (0.24 g, 0.30 mmol, 92 %). Mp > 300 ^oC; ^1H NMR (400 MHz, $CDCl_3$) δ 8.97 (d, *J*=4.4 Hz, 2H), 8.72 (d, *J*=4.4 Hz, 2H), 8.63 (s, 4H), 8.26 (d, *J*=3.2 Hz, 1H), 7.94 (d, *J*=3.2 Hz, 1H), 7.28 (s, 6H), 2.63 (s, 6H), 2.62 (s, 3H), 1.85 (s, 18H), -2.52 (s, 2H); MS (MALDI-TOF) *m/z* 791.0 ($M+H^+$).

5-(5-Carboxy-2-thienyl)-10,15,20-tris(2,4,6-trimethylphenyl)porphyrinatozinc(II) (Zn5S). To a solution of **3** (36 mg, 0.046 mmol) in chloroform (60 mL) was added saturated methanolic solution of zinc acetate dihydrate (12 mL). The solution was stirred at room temperature for 2h. The reaction mixture was washed with water, dried over anhydrous sodium sulfate, and then the solvent was removed in vacuo. Reprecipitation from CH_2Cl_2/hexane gave **Zn5S** as a red solid (37 mg, 0.043 mmol, 95 % yield). Mp > 300 ^oC; ^1H NMR (400 MHz, $CDCl_3$) δ 9.14 (d, *J*=4.4 Hz, 2H), 8.78 (d, *J*=4.4 Hz, 2H), 8.67 (s, 2H), 8.66 (s, 2H), 8.47 (d, *J*=3.6 Hz, 1H), 7.95 (d, J=3.6 Hz, 1H), 7.27 (s, 6H), 2.60 (s, 9H), 1.81 (s, 6H), 1.78 (s, 12H); MS (MALDI-TOF) *m/z* 854.0 ($M+H^+$).

Methyl 5-formylfuran-2-carboxylate (4). 5-Formylfuran-2-carboxylic acid (1.01 g, 7.2 mmol) was dissolved in methanol (9.65 mL) with concentrated sulfuric acid (0.96 mL) and heated at reflux for 6h. After the reaction mixture was cooled to room temperature, methanol was removed by vacuum evaporator. The resulting solid was extracted with diethyl ether and dried in vacuo. Column chromatography on silica gel (ethyl acetate/acetone/hexane = 1:1:8) gave **4** as a yellow solid (0.99 g, 6.4 mmol, 89 % yield). Mp 87-88 ^oC; ^1H NMR (400 MHz, $CDCl_3$) δ 9.81 (s, 1H), 7.27 (s, 2H), 3.96 (s, 3H); IR (KBr) ν_{max} 1672 cm^{-1} (CO aldehyde), 1727 cm^{-1} (CO ester); MS (MALDI-TOF) m/z 152.5 ($M+H^+$).

5-(5-Methoxycarbonyl-2-furyl)-10,15,20-tris(2,4,6-trimethylphenyl)porphyrin (5). This procedure was based upon the literature protocol for similar compound.[31] Methyl 5-formylfuran-2-carboxylate (**4**) (0.36 g, 2.3 mmol), pyrrole (0.7 mL, 9.3 mmol), and 2,4,6-trimethyl benzaldehyde (1.0 mL, 7.0 mmol) were dissolved in chloroform at room temperature. Dry nitrogen was bubbled through the solution for 30 min before adding boron trifluoride diethyl etherate (0.6 mL, 4.6 mmol). The solution was stirred for 2h, then *p*-chloranil (2.33 g, 9.4 mmol) and stirring was continued for 2h. After triethylamine (0.7 mL, 4.6 mmol) was added, the solvent was removed in vacuo. Purification of the crude product by flash column chromatography on alumina ($CHCl_3$) and subsequent column chromatography on silica gel (CH_2Cl_2/hexane = 1:1) and reprecipitation from CH_2Cl_2/hexane afforded **5** as a purple red solid (0.13 g, 0.17 mmol, 7 % yield). Mp > 300 ^oC; ^1H NMR (400 MHz, $CDCl_3$) δ 9.05 (d, *J*=4.8 Hz, 2H), 8.74 (d, *J*=4.8 Hz, 2H), 8.64 (d, *J*=4.8 Hz, 2H), 8.61 (d, *J*=4.8 Hz, 2H), 7.76 (d, *J*=3.6 Hz, 1H), 7.32 (d, *J*=3.6 Hz, 1H), 7.28 (s, 6H), 4.05 (s, 3H), 2.63 (s, 6H), 2.62 (s, 3H), 1.86 (s, 6H), 1.84 (s, 12H), -2.50 (s, 2H); MS (MALDI-TOF) *m/z* 790.9 ($M+H^+$).

5-(5-Carboxy-2-furyl)-10,15,20-tris(2,4,6-trimethylphenyl)porphyrin (6). To a solution of **5** (134 mg, 0.17 mmol) in 2-propanol (63 mL) was added a solution of potassium hydroxide (1.05 g, 18.7 mmol) in water (15.8 mL). The solution was refluxed for 2h. After the reaction mixture was cooled to room temperature, aqueous 3M hydrochloric acid was added until the color of the reaction mixture turned to green from red. The solution was washed with saturated aqueous sodium bicarbonate and water, dried over anhydrous sodium sulfate, and then the solvent was removed in vacuo. Reprecipitation from CH_2Cl_2/hexane gave **6** as a purple red solid (121 mg, 0.16 mmol, 92 %). Mp > 300 ^oC; ^1H NMR (400 MHz, $CDCl_3$) δ 9.08 (d, *J*=4.8 Hz, 2H), 8.76 (d, *J*=4.8 Hz, 2H), 8.64 (d, *J*=4.8 Hz, 2H), 8.61 (d, *J*=4.8 Hz, 2H), 7.89 (d, *J*=3.4 Hz, 1H), 7.38 (d, *J*=3.4 Hz, 1H), 7.28 (s, 6H), 2.63 (s, 9H), 1.86 (s, 6H), 1.84 (s, 12H), -2.50 (s, 2H); MS (MALDI-TOF) *m/z* 773.9 ($M+H^+$).

5-(5-Carboxy-2-furyl)-10,15,20-tris(2,4,6-trimethylphenyl)porphyrinatozinc(II) (Zn5O). To a solution of **6** (80 mg, 0.10 mmol) in chloroform (100 mL) was added saturated methanolic solution of zinc acetate dihydrate (25 mL). The solution was stirred at room temperature for 2h. The reaction mixture was washed with water, dried over anhydrous sodium sulfate, and then the solvent was removed in vacuo. Reprecipitation from CH_2Cl_2/hexane gave **Zn5O** as a purple red solid (80 mg, 0.095 mmol, 92 % yield). Mp > 300 ^oC; ^1H NMR (400 MHz, $CDCl_3$) δ 9.12 (s, 2H), 8.77 (s, 2H), 8.67 (s, 4H), 7.87 (s, 1H), 7.27 (s, 6H), 7.05 (s, 1H), 2.61 (s, 9H), 1.83 (s, 6H), 1.78 (s, 12H); MS (MALDI-TOF) *m/z* 834.6 ($M+H^+$).

4-Cyanothiophene-2-aldehyde (7). This procedure was based upon the literature protocol for similar compound.[xxxii] 4-bromothiophene-2-aldehyde (2.40 g, 13 mmol) and copper cyanide (2.24 g, 25 mmol) was dissolved in N,N'-dimethylformamide (50 mL) and heated at 145 ^oC for 20h. After the reaction mixture was cooled to room temperature, $FeCl_3 \bullet 6H_2O$ (16.50 g, 61 mmol) in water (12.2 mL) with hydrochloric acid (12M, 3.1 mL) was added. The reaction mixture was heated at 75 ^oC for 30 min and then extracted with dichloromethane. The combined extracts were washed with saturated aqueous sodium chloride and water, dried over anhydrous sodium sulfate, and then the solvent was removed in vacuo. Purification of the crude product by silica column chromatography (ethyl acetate/hexane = 1:4) gave **7** as a white solid (1.32 g, 9.7 mmol, 77 % yield). Mp 83–84 ^oC; ^1H NMR (400 MHz, $CDCl_3$) 9.95 (s, 1H), 8.27 (s, 1H), 7.94 (s, 1H); IR (KBr) ν_{max} 1673 cm^{-1} (CO), 2232 cm^{-1} (CN); MS (MALDI-TOF) *m/z* 136.8 ($M+H^+$).

5-(4-Cyano-2-thienyl)-10,15,20-tris(2,4,6-trimethylphenyl)porphyrin (8). This procedure was based upon the literature protocol for similar compound.[31] 4-Cyanothiophene-2-aldehyde **7** (0.59 g, 4.3 mmol), pyrrole (1.2 mL, 17 mmol), and 2,4,6-trimethyl benzaldehyde (1.9 mL, 13 mmol) were dissolved in chloroform (350 mL) at room temperature. Dry nitrogen was bubbled through the solution for 30 min

before adding boron trifluoride diethyl etherate (1.1 mL, 8.4 mmol). The solution was stirred for 1h, then *p*-chloranil (4.22 g, 17 mmol) was added and stirring was continued for 1h. After triethylamine (1.2 mL, 8.5 mmol) was added, the solvent was removed in vacuo. Purification of the crude product by column chromatography on silica gel (CH_2Cl_2/ hexane = 2:3) and reprecipitation from CH_2Cl_2/hexane afforded **8** as a purple red solid (0.46 g, 0.59 mmol, 14 % yield). Mp > 300 ^oC; ^1H NMR (400 MHz, $CDCl_3$) δ 8.96 (d, *J*=4.8 Hz, 2H), 8.71 (d, *J*=4.8 Hz, 2H), 8.63 (d, *J*=4.8 Hz, 2H), 8.61 (d, *J*=4.8 Hz, 2H), 8.32 (s, 1H), 8.03 (s, 1H), 7.28 (s, 6H), 2.63 (s, 6H), 2.62 (s, 3H), 1.85 (s, 6H), 1.84 (s, 12H), -2.53 (s, 2H); IR (KBr) ν_{max} 2229 cm^{-1} (CN); MS (MALDI-TOF) *m/z* 771.7 ($M+H^+$).

5-(4-Carboxy-2-thienyl)-10,15,20-tris(2,4,6-trimethylphenyl)porphyrin (9). This procedure was based upon the literature protocol for similar compound.[xxxiii] Cyanoporphyrin **8** (163 mg, 0.21 mmo1) was dissolved in a mixture of hydrochloric acid (12M, 5.75 mL) and trifluoroacetic acid (9.59 mL). The solution was refluxed for 6h, and quenched with lump sodium bicarbonate. Filtering, washing with water, and drying of resulting precipitate gave **9** as a red solid (158 mg, 0.20 mmol, 92 % yield). Mp > 300 ^oC; ^1H NMR (400 MHz, $CDCl_3$) δ 8.95 (d, *J*=4.8 Hz, 2H), 8.71 (d, *J*=4.8 Hz, 2H), 8.64 (d, *J*=4.8 Hz, 2H), 8.62 (d, *J*=4.8 Hz, 2H), 8.41 (s, 1H), 8.12 (s, 1H), 7.28 (s, 4H), 7.27 (s, 2H), 2.63 (s, 6H), 2.62 (s, 3H), 1.85 (s, 6H), 1.84 (s, 12H), -2.54 (s, 2H); MS (MALDI-TOF) *m/z* 789.9 ($M+H^+$).

5-(4-Carboxy-2-thienyl)-10,15,20-tris(2,4,6-trimethylphenyl)porphyrinatozinc(II) (Zn4S). To a solution of **9** (0.26 g, 0.32 mmol) in chloroform (425 mL) was added saturated methanolic solution of zinc acetate dihydrate (85 mL). The solution was stirred at room temperature for 2h. The reaction mixture was washed with water, dried over anhydrous sodium sulfate, and then the solvent was removed in vacuo. Reprecipitation from CH_2Cl_2/hexane gave **Zn4S** as a red solid (0.26 g, 0.31 mmol, 95 % yield). Mp > 300 ^oC; ^1H NMR (400 MHz, $CDCl_3$) d 8.90 (d, *J*=6.0 Hz, 2H), 8.74 (d,

J=6.0 Hz, 2H), 8.70 (d, *J*=6.0 Hz, 2H), 8.67 (d, *J*=6.0 Hz, 2H), 8.07 (s, 1H), 7.66 (s, 1H), 7.25 (s, 6H), 2.62 (s, 9H), 1.85 (s, 6H), 1.83 (s, 12H); MS (MALDI-TOF) *m/z* 852.2 ($M+H^+$).

Optical Spectroscopy. UV-visible absorption spectra of the porphyrins in ethanol and the porphyrin monolayers on the TiO_2 electrodes were recorded using a Perkin-Elmer Lambda 900 UV/VIS/NIR Spectrometer. Steady-state fluorescence spectra were acquired by a SPEX Fluoromax-3 Spectrofluorometer. Spectroscopy grade ethanol was used for the measurements of UV-visible absorption and fluorescence spectra.

Electrochemistry. Electrochemical measurements were made using an ALS 630a electrochemical analyzer. Redox potentials were determined in dichloromethane containing 0.1M tetrabutylammonium hexafluorophosphate ($TBAPF_6$) at a scan rate of 0.1 V s^{-1}. A glassy carbon working electrode, $Ag/AgNO_3$ reference electrode, and Pt wire counter electrode were employed. Ferrocene/ferrocenium (0.64 V vs NHE) was used as an internal standard for all measurements. Dichloromethane was purified[xxxiv] just before use, and $TBAPF_6$ was recrystallized from methanol.

Density Functional Theory (DFT) Calculations. Geometry optimization and electronic structure calculations of the porphyrins were performed using B3LYP functional and 3-21G (d) basis set implemented in the Gaussian 03 program package.[xxxv] Molecular orbitals were visualized by GaussView 3.0 software.

Preparation of Porphyrin-Modified TiO_2 Electrode. Mesoporous TiO_2 films were prepared from a colloidal suspension of TiO_2 nanoparticles (P25, Nippon Aerogel) dispersed in deionized water and Triton X-100. The suspension was deposited on a transparent conducting glass (Asahi Glass, SnO_2/F, 9.4 ohm/sq) by using doctor blade technique. The films were annealed at 673 K for 10 min, followed by similar deposition and annealing (723 K, 2 h) for the 10-μm-thick TiO_2 films. The thickness of the films was determined using the surface roughness/profile measuring instrument (SURFCOM 130A, ACCRETECH). The TiO_2 electrodes were immersed into each of

the 0.2 mM ethanol solution of the porphyrins at room temperature. After dye adsorption, the dye-coated electrodes were copiously rinsed with ethanol. The amounts of the porphyrins adsorbed on the TiO_2 films were determined by measuring absorbance at the Soret band of the dye molecules that were dissolved from the dye-adsorbed TiO_2 films into DMF containing 0.1 M NaOH. Porphyrin multilayer was prepared by successive dropping of the respective 0.2 mM ethanol solution of the porphyrins onto the TiO_2 for the measurements of X-ray photoelectron spectra.

Photovoltaic Measurements. The photovoltaic measurements were performed in a sandwich cell consisting of the porphyrin-sensitized TiO_2 electrode as the working electrode and a platinum-coated conducting glass as the counter electrode. The two electrodes were placed on top of each other using a thin transparent film of Surlyn polymer (Dupont) as a spacer to form the electrolyte space. A thin layer of electrolyte (0.1 M LiI, 0.05 M I_2, 0.6 M 2,3-dimethyl-1-propylimidazolium iodide, and 0.5 M 4-*t*-butylpyridine in acetonitrile) was introduced into the interelectrode space. The IPCE values and photocurrent-voltage characteristics were determined by using a potentiostat (Bunko–Keiki Co., Ltd., model HCSSP-25) irradiated with simulated AM 1.5 solar light (100 mW cm^{-2}, Bunko–Keiki Co., Ltd., model CEP-2000). All the experimental values were given as an average from six independent measurements.

Fourier transform infrared (FTIR) and Attenuated total reflectance-Fourier transform infrared (ATR-FTIR) Measurements. FTIR spectra for the porphyrins were acquired using by a JASCO FT/IR-470 plus spectrometer at a resolution of 1 cm^{-1} by co-addition of 32 scans with a KBr pellet. ATR-FTIR spectra for the adsorbed porphyrins on the TiO_2 were collected by a Thermo Electron Corporation Nicolet 380 FTIR with the Golden Gate diamond anvil ATR accessory at a resolution of 4 cm^{-1} by co-addition of 64 scans with the porphyrin monolayers. ATR-FTIR spectra for the porphyrin monolayers were referenced to the spectra of blank TiO_2 films. All the samples for ATR-FTIR measurements were made by the same method for preparing the

porphyrin monolayers on the TiO_2 electrodes (*vide supra*).

X-ray Photoelectron Spectroscopy (XPS) Measurements. The XPS data were acquired using an ULVAC-PHI 5500MT system equipped with Mg Kα X-ray source (1253.6 eV) and a hemispherical energy analyzer. Samples were mounted on indium foil and then transferred to an analyzer chamber. The electron takeoff angle was set at 45 deg. The pressure of the main XPS chamber was maintained at less than 1×10^{-8} Torr during analysis. All the XPS peak positions were referenced to the O1s peak of TiO_2 substrate at 530.2 eV. Peaks of interests were deconvoluted by Gaussian/Lorentzian mixed functions with PeakFit 4.12 program. All the samples for XPS measurements were made by the same method for preparing the porphyrin monolayers and multilayers on the TiO_2 electrodes.

References and Notes

(i) (a) Kay, A.; Grätzel, M. *J. Phys. Chem.* **1993**, *97*, 6272. (b) Nazeeruddin, Md. K.; Humphry-Baker, R.; Officer, D. L.; Campbell, W. M.; Burrell, A. K.; Grätzel, M. *Langmuir* **2004**, *20*, 65. (c) Schmidt-Mende, L.; Campbell, W. M.; Wang, Q.; Jolley, K. W.; Officer, D. L.; Nazeeruddin, Md K.; Grätzel, M. *ChemPhysChem* **2005**, *6*, 1253.

(ii) Tachibana, Y.; Haque, S. A.; Mercer, I. P.; Durrant, J. R.; Klug, D. R. *J. Phys. Chem. B* **2000**, *104*, 1198.

(iii) (a) Hara, K.; Sato, T.; Katoh, R.; Furube, A.; Ohga, Y.; Shinpo, A.; Suga, S.; Sayama, K.; Sugihara, H.; Arakawa, H. *J. Phys. Chem. B* **2003**, *107*, 597. (b) Horiuchi, T.; Miura, H.; Sumioka, K.; Uchida, S. *J. Am. Chem. Soc*. **2004,** *126*, 12218. (c) Haque, S. A.; Handa, S.; Peter, K; Palomares, E.; Thelakkat, M.; Durrant, J. R. *Angew. Chem., Int. Ed*. **2005**, *44*, 5740. (d) Hagberg, D. P.; Edvinsson, T.; Marinado, T.; Boschloo, G.; Hagfeldt, A.; Sun, L. *Chem. Commun*. **2006**, 2245. (e) Chen, C.-Y.; Wu, S.-J.; Wu, C.-G.; Chen, J.-G.; Ho, K.-C. *Angew. Chem., Int. Ed*. **2006**, *45*, 5822. (f) Kitamura, T.; Ikeda, M.; Shigaki, K.; Inoue, T.; Anderson, N. A.; Ai, X.; Lian, T.; Yanagida, S. *Chem. Mater.* **2004**, *16*, 1806.

(g) Wang, P.; Klein, C.; Humphry-Baker, R.; Zakeeruddin, S. M.; Grätzel, M. *J. Am. Chem. Soc*. **2005**, *127*, 808. (h) Nazeeruddin, Md. K.; Humphry-Baker, R.; Liska, P.; Grätzel, M. *J. Phys. Chem. B* **2003**, *107*, 8981.

(iv) (a) Ma, T.; Inoue, K.; Noma, H.; Yao, K.; Abe, E. *J. Photochem. Photobiol., A* **2002**, *152*, 207. (b) Wang, Q.; Campbell, W. M.; Bonfantani, E. E.; Jolley, K. W.; Officer, D. L.; Walsh, P. J.; Gordon, K.; Humphry-Baker, R.; Nazeeruddin, Md. K.; Grätzel, M. *J. Phys. Chem. B* **2005**, *109*, 15397. (c) He, J.; Benkö, G.; Korodi, F.; Polívka, T.; Lomoth, R.; Åkermark, B.; Sun, L.; Hagfeldt, A.; Sundström, V. *J. Am. Chem. Soc.* **2002**, *124*, 4922. (d) Watson, D. F.; Marton, Stux, A. M.; Meyer, G. J. *J. Phys. Chem. B* **2004**, *108*, 11680.

(v) (a) Cherian, S.; Wamser, C. C. *J. Phys. Chem. B* **2000**, *104*, 3624. (b) Jasieniak, J.; Johnston, M.; Waclawik, E. R. *J. Phys. Chem. B* **2004**, *108*, 12962. (c) Ma, T. L.; Inoue, K.; Yao, K.; Noma, H.; Shuji, T.; Abe, E.; Yu, J.; Wang, X.; Zhang, B. *J. Electroanal. Chem.* **2002**, *537*, 31.

(vi) Campbell, W. M.; Burrell, A. K.; Officer, D. L.; Jolley, K. W. *Coord. Chem. Rev.* **2004**, *248*, 1363.

(vii) Odobel, F.; Blart, E.; Lagree, M.; Villieras, M.; Boujtita, H.; El Murr, N.; Caramori, S.; Bignozzi, C. A. *J. Mater. Chem.* **2003**, *13*, 502.

(viii) Huijser, A.; Savenije, T. J.; Kroeze, J. E.; Siebbeles, L. D. A. *J. Phys. Chem. B* **2005**, *109*, 20166.

(ix) (a) Vollmer, M. S.; Würthner, F.; Effenberger, F.; Emele, P.; Meyer, D. U.; Stümpfig, T.; Port, H.; Wolf, H. C. *Chem. Eur. J.* **1998**, *4*, 260. (b) Bhyrappa, P.; Bhavana, P. *Chem. Phys. Lett.* **2001**, *349*, 399. (c) Friedlein, R.; von Kieseritzky, F.; Braun, S.; Linde, C.; Osikowicz, W.; Hellberg, J.; Salaneck, W. R. *Chem. Commun.* **2005**, 1974. (d) Gupta, I.; Ravikanth, M. *Tetrahedron Lett.* **2002**, *43*, 9453.

(x) (a) Lindsey, J, S.; Prathapan, S.; Johnson, T. E.; Wagner, R. W. *Tetrahedron* **1994**, *50*, 8941. (b) Lindsey, J. S. In *The Porphyrin Handbook*; Kadish, K. M., Smith, K. M., Guilard, R., Eds.; Academic Press: New York, 2000; Vol. 1, pp 46-118.

(xi) Gupta, I.; Ravikanth, M. *Tetrahedron* **2003**, *59*, 6131.

(xii) Kamat, P. V.; Haria, M.; Hotchandani, S. *J. Phys. Chem. B* **2004**, *108*, 5166.

(xiii) Kuang, D.; Ito, S.; Wenger, B.; Klein, C.; Moser, J.-E.; Humphry-Baker, R.;

Zakeeruddin, S. M.; Grätzel, M. *J. Am. Chem. Soc*. **2006**, *128*, 4146.

(xiv) Nakade, S.; Matsuda, M.; Kambe, S.; Saito, Y.; Kitamura, T.; Sakata, T.; Wada, Y.; Mori, H.; Yanagida, S. *J. Phys. Chem. B* **2002**, *106*, 10004.

(xv) Osuka, A.; Maruyama, K. *J. Am. Chem. Soc.* **1988**, *110*, 4454.

(xvi) (a) Weisz, A, D.; Regazzoni, A. E.; Blesa, M. A. *Solid State Ionics*, **2001**, *143*, 125. (b) Nazeeruddin, Md. K.; Humphry-Baker, R.; Officer, D. L.; Campbell, W. M.; Burrell, A. K.; Grätzel, M. *Langmuir* **2004**, *20*, 6514.

(xvii) Finnie, K. S.; Bartlett, J. R.; Woolfrey, J. L. *Langmui*r **1998**, *14*, 2744.

(xviii) Johansson, E. M. J.; Hedlund, M.; Siegbahn, H.; Rensmo, H. *J. Phys. Chem. B* **2005**, *109*, 22256.

(xix) (a) Schnadt, J.; O'Shea, J. N.; Patthey, L.; Schiessling, J.; Krempasky, J.; Shi, M.; Mårtensson, N.; Br□ ühwiler, P. A. *Surf. Sci*. **2003**, *544*, 74. (b) Mahrov, B.; Boschloo, G.; Hagfeldt, A.; Siegbahn, H.; Rensmo, H. *J. Phys. Chem. B* **2004**, *108*, 11604.

(xx) Patthey, L.; Rensmo, H.; Persson, P.; Westermark, K.; Vayssieres, L.; Stashans, A.; Petersson, Å.; Brühwiler, P. A.; Siegbahn, H.; Lunell, S.; Mårtensson, N. *J. Chem. Phys*. **1999**, *110*, 5913.

(xxi) (a) Clark, D. T.; Lilley, D. M. J. *Chem. Phys. Lett.* **1971**, *9*, 234. (b) Hitchcock, A. P.; Horsely, J. A.; Stöhr, J. *J. Chem. Phys*. **1986**, *85*, 4835. (c) Elfeninat, F.; Fredriksson, C.; Sacher, E.; Selmani, A. *J. Chem. Phys*. **1995**, *102*, 6153.

(xxii) XPS measurements of monolayers of ruthenium dyes (i.e., N719 and N3) adsorbed on the TiO2 surface also revealed similar interaction between the surface and sulfur atoms of NCS groups.[18]

(xxiii) (a) Rehm, J. M.; McLendon, G. L.; Nagasawa, Y.; Yoshihara, K.; Moser, J.; Grätzel, M. *J. Phys. Chem*. **1996**, *100*, 9577. (b) Casarin, M.; Ferrigato, F.; Maccato, C.; Vittadini, A. *J. Phys. Chem. B* **2005**, *109*, 12596. (c) Farfan-Arribas, E.; Madix, R. J. *J. Phys. Chem. B* **2003**, *107*, 3225.

(xxiv) Liu, G.; Rodriguez, J. A.; Hrbek, J.; Long, B. T.; Chen, D. A. *J. Mol. Catal. A* **2003**, *202*, 215.

(xxv) A charge-transfer complex between the excited N3 dye and surface states of ZnO was suggested as an intermediate state between the locally excited N3 dye and the

resulting N3 radical cation after injection of electron into the conduction band of ZnO. Furube, A.; Katoh, R.; Hara, K.; Murata, S.; Arakawa, H.; Tachiya, M. *J. Phys. Chem. B* **2003**, *107*, 4162.

(xxvi) Grätzel, M. *Inorg. Chem.* **2005**, *44*, 6841.

(xxvii) (a) Usami, A.; Ozaki, H. *J. Phys. Chem. B* **2005**, *109*, 2591. (b) Tachibana, Y.; Akiyama, H. Y.; Kuwabata, S. *Sol. Energy Mater. Sol. Cells.* **2007**, *91*, 201.

(xxviii) Luo, L.; Lo, C.-F.; Lin, C.-Y.; Chang, I.-J.; Diau, E. W.-G. *J. Phys. Chem. B* **2006**, *110*, 410.

(xxix) The separation distance between the center of the porphyrin and the TiO2 surface in the Zn5S is smaller than that in the Zn5O owing to the heavily tilted orientation of the porphyrin ring on the TiO2 surface in the Zn5S compared to the Zn5O. Therefore, we cannot rule out the possibility that small reorganization energy of the electron injection in the Zn5S-sensitized cell relative to that in the Zn5O-sensitized cell accelerates the electron injection, resulting in the large IPCE value in the Zn5S-sensitized cell.

(xxx) Colburn, V. M.; Iddon, B.; Suschitzky, H. *J. Chem. Soc. Perkin I* **1977**, 2436.

(xxxi) Lindsey, J, S.; Prathapan, S.; Johnson, T. E.; Wagner, R. W. *Tetrahedron* **1994**, *50*, 8941.

(xxxii) (a) Moorthy, J. N.; Mal, P.; Singhal, N.; Venkatakrishnan, P.; Malik, R.; Venugopalan, P. *J. Org. Chem.* **2004**, *69*, 8459. (b) Friedman, L.; Shechter, H. *J. Org. Chem.* **1961**, *26*, 2522.

(xxxiii) Shin, E. J.; Jung, H. *J. Photosci*. **2004**, *11*, 83.

(xxxiv) Perrin, D. D.; Armarego, W. L. F. In *Purification of Laboratory Chemicals,* 3rd ed.; Pergamon: Elmsford, NY, 1988; p 145.

(xxxv) Frisch, M. J. *et al*. *Gaussian 03*, revision C.02; Gaussian, Inc.: Wallingford, CT, 2004.

CHAPTER 2

Quinoxaline-Fused Porphyrins for Dye-Sensitized Solar Cells

Introduction

Although porphyrins have strong Soret and moderate Q bands absorption properties, typically the absorption windows are narrow and thereby poorly matched to the solar light distribution. This limits the light harvesting efficiency, the short circuit current (J_{sc}), and consequently the power conversion efficiency (η) of the porphyrin-sensitized solar cells. A strategy to tackle this problem is to make an unnecessarily strong and narrow Soret band broad and weak Q bands strong and to fill out the light absorption gap which typically lies in between 450 nm and 550 nm. For instance, elongating the π-system and lowering the symmetry by *meso*- and β-naphthalene-fused porphyrin carboxylic acid materialized the improved η by 50 % relative to the non-fused counterpart.[i] Extension of the porphyrin π-system by modifying a β position with olefinic linkage has been reported to be an effective method to broaden the absorption window,[ii] and this concept has been successfully applied to design the best performing porphyrin photosensitizers (η=7.1%).[iii]

Another promising way for achieving it is to construct β, β'-edge fused porphyrin with quinoxaline moiety. This strategy has been employed to construct a variety of model systems, especially for molecular wires.[iv] Tailoring the electrochemical properties, accordingly the electronic properties of the system, by systematic switching of the substituents that are located outside of the porphyrin macrocycle, has been reported.[v] It typically affords rigid structure and well-defined molecular length as well as relatively broad absorption spectra. Nevertheless, β, β'-edge fused porphyrins with quinoxaline moiety have never been employed for dye-sensitized solar cells.

In this chapter, synthesis and the optical, electrochemical, and photovoltaic properties of mono- and di-carboxyquinoxalino[2,3-β]porphyrins (ZnQMA and ZnQDA) for dye-sensitized solar cells are reported (Figure 1). Both of the compounds are expected to have a broader absorption, compared with that of reference porphyrin without the carboxyquinoxalino moiety (ZnP), leading to the high value of J_{sc} and η. Four *meso*-2,4,6-trimethylphenyl groups are introduced to provide the oxidative stability of the porphyrins[vi] and to reduce the aggregation between the neighboring porphyrins adsorbed onto the TiO_2 surface by the steric hindrance around the porphyrin core. Only difference between the two molecules is the number of the peripheral carboxylic acid groups. This alteration may make the electronic coupling of the structurally related porphyrins to the TiO_2 surface different and affect the photoinduced electron transfer, thereby the photoelectrochemical and/or photovoltaic performances. It is an effective approach to control the photoinduced electron-transfer properties by the subtle modifications in molecular structures. As such, this study would afford a hands-on framework to devise novel photosensitizers for dye-sensitized solar cell applications.

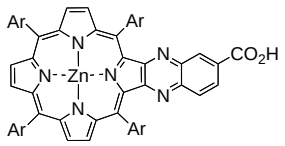

ZnQMA

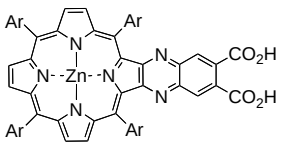

ZnQDA

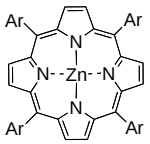

ZnP

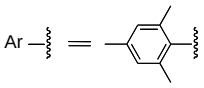

Figure 1. Porphyrins used in this study

Results and Discussion

Synthesis. The syntheses of the monocarboxyquinoxalino[2,3-β]porphyrin (ZnQMA) and dicarboxyquinoxalino[2,3-β]porphyrin (ZnQDA) were accomplished by the protocol explored by Crossley and co-workers.[vii] A key step in this protocol is the dual Schiff base forming reaction between porphyrin 2,3-dione and diamine. Synthetic routes to ZnQMA

and ZnQDA are displayed in SCHEME 1. Starting compounds, 5,10,15,20-tetrakis(2,4,6-trimethylphenyl)porphyrin **1**, copper porphyrin **2**, zinc porphyrin reference (ZnP), methyl 3,4-diaminobenzoate, and dimethyl 4,5-diaminophthalate are known compounds and were prepared by the literature procedures.[viii] One of the β positions of copper porphyrin **2** was nitrated by mild electrophilic substitution reaction.[ix] Because the selectivity for the nitration to porphyrin periphery heavily depends on the identity of inner metal, free base porphyrin **1** was coordinated by copper (II) before the reaction.[x] After obtaining the β-nitro copper porphyrin **3**, copper (II) inside the porphyrin was drawn out to yield **4**.

SCHEME 1

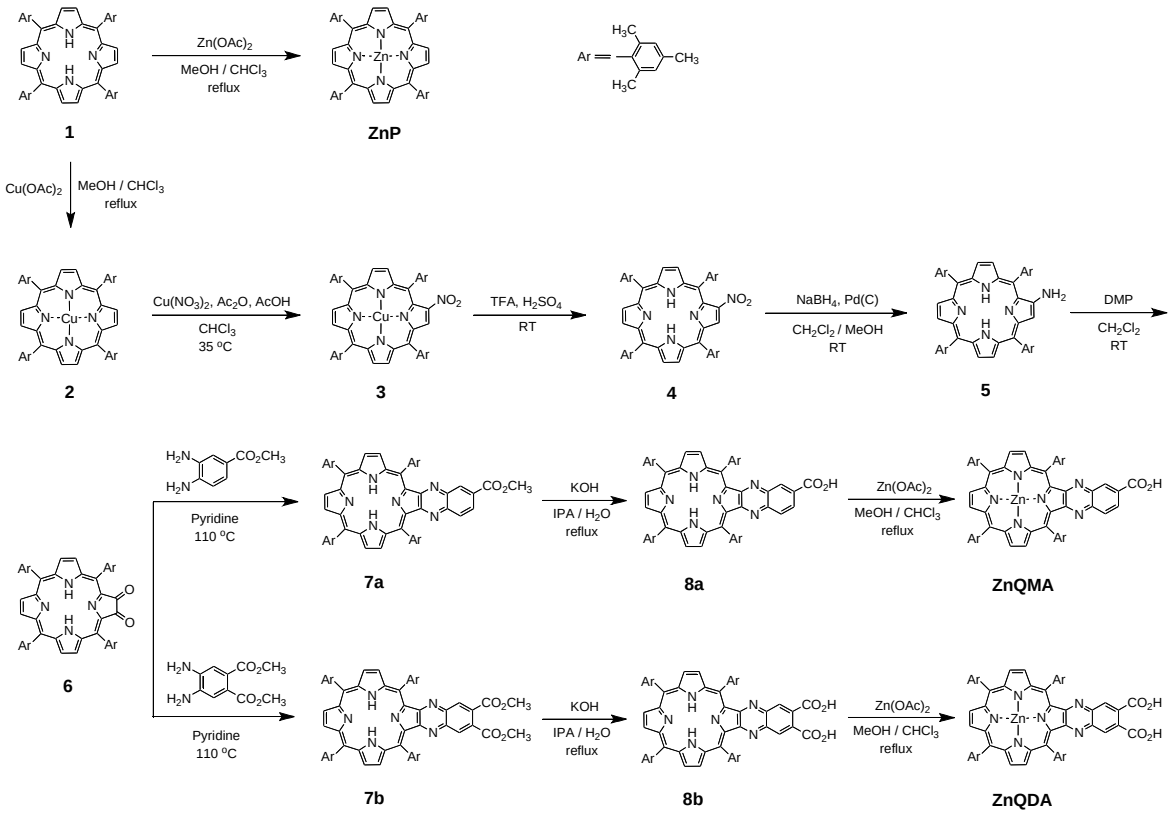

2,3-Dioxo-5,10,15,20-tetrakis(2,4,6-trimethylphenyl)chlorin **6** was prepared by the oxidation of the amino porphyrin **5** with Dess-Martin periodinane (DMP), which had

been generated through the hydrogenation of the β-nitro porphyrin **4** with sodium borohydride. Since **5** and **6** are unstable compounds, both of them were directly employed for the respective next reactions.[xi] The condensation of **6** with methyl diaminobenzoate and dimethyl diaminophthalate in pyridine[xii] solution afforded the desired methoxycarbonylquinoxalino[2,3-β]porphyrin **7a** and bis(methoxycarbonyl)quinoxalino[2,3-β]porphyrin **7b**, respectively. Both **7a** and **7b** were hydrolyzed under basic conditions to obtain the corresponding porphyrin carboxylic acids **8a** and **8b**, followed by the treatment of zinc acetate to yield ZnQMA and ZnQDA, respectively. Zinc (II) insertion into porphyrins usually takes 30 min or more, but it needed about 18 h to complete the insertion of Zn atom into **8a** and **8b**. In addition, the solution color changed from red to green by zinc metalation, which is in sharp contrast with the typical change in color (i.e., from red to pink) of the solution for tetraphenylporphyrins. Drastic changes in the molecular structure and/or electronic structure of the porphyrins by the metalation are insinuated (*vide infra*). Structures of all the new compounds were verified by spectroscopic analyses including ^{1}H NMR, FT-IR and mass spectra.

Figure 2 depicts ^{1}H NMR spectra of ZnQMA, ZnQDA, **8a**, and **8b** in a mixture of acetone d_6 and CD_3OD. Notably, the splitting patterns are different in the 7,8,17,18-protons of ZnQMA (Figure 2a) and **8a** (Figure 2c): Two skewed doublets for **8a** are changed to a multiplet for ZnQMA; thus, the molecular symmetry along with the long axis is supposed to be broken due to the zinc insertion reaction. However, **8a** already has no formal symmetry along with the long axis due to the presence of single carboxylic acid group. Therefore, it is understood that the nonplanarity that is resulted from the collective effects of unsymmetric molecular structure and zinc metalation is the origin of the phenonema. However, similar occurrences could not be found in case for ZnQDA (Figure 2b) and **8b** (Figure 2d). The estimation of equilibrium geometry for ZnQMA and ZnQDA by DFT calculations also supports the results of ^{1}H NMR spectroscopy (*vide*

infra). To the best of the author's knowledge, it is the first report of the distortion of the porphyrin macrocycle induced by rather long-distance substitutions along with zinc (II) metalation. Complete structural analysis based on X-ray diffraction could not be performed due to the failure to obtain a high quality of single crystal.

DFT Calculations. DFT calculations were employed to gain insight into the equilibrium geometry and electronic structures for the frontier orbitals of the porphyrins. The

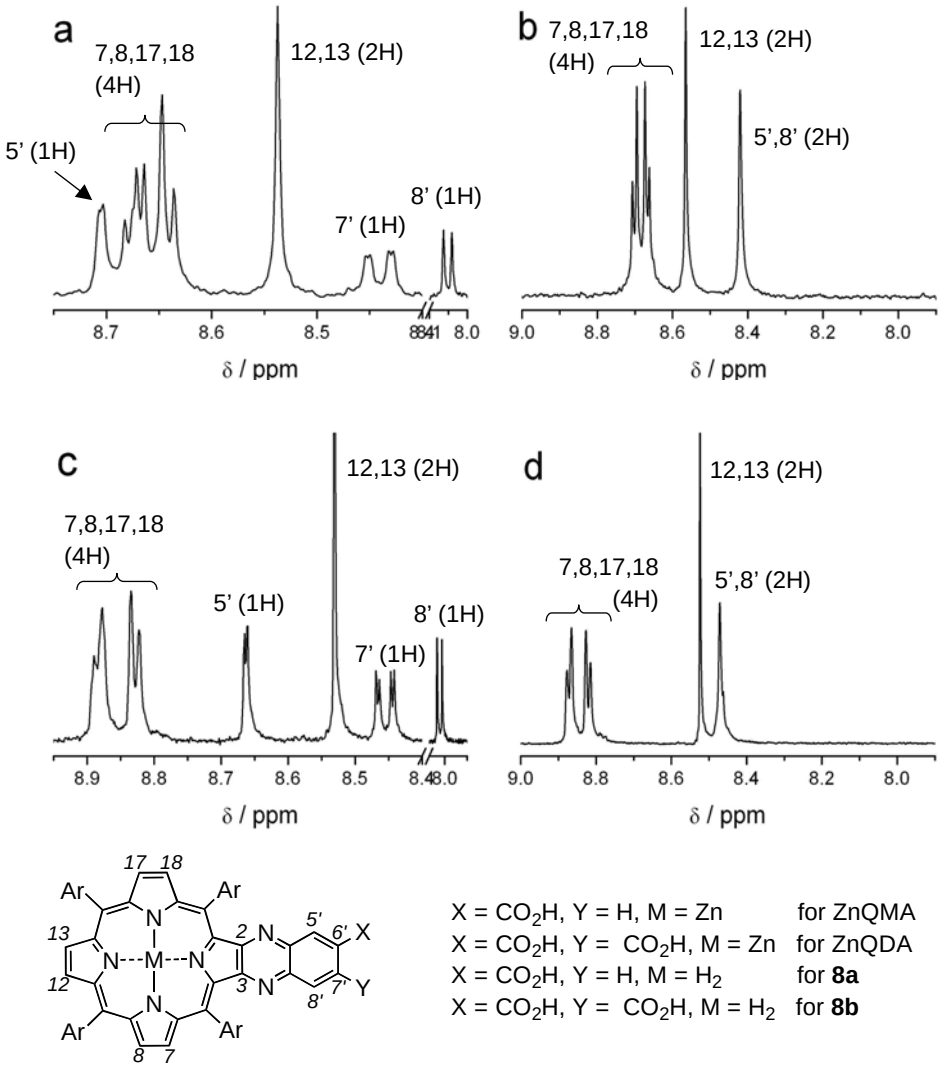

Figure 2. Part of the 400 MHz ^{1}H NMR spectra of (a) ZnQMA, (b) ZnQDA, (c) **8a**, and (d) **8b** in acetone d_6 + CD_3OD solution at 293 K. The peaks in the aliphatic regions are omitted for clarity.

calculated structures do not show negative frequencies, implying that the optimized geometries are in the global energy minima.[xiii] As expected from the results of ^{1}H NMR spectroscopy, ZnQMA and ZnQDA are found to adopt saddle and planar structures in their respective optimized geometries (Figure 3).

Porphyrins with D_{4h} symmetry generally show energetically degenerate two lowest unoccupied molecular orbitals (LUMO+1, LUMO) and nearly degenerate two highest occupied molecular orbitals (HOMO, HOMO-1). Degenerate energy levels of the LUMO and LUMO+1 of ZnP are split both in ZnQMA and ZnQDA, whereas the near

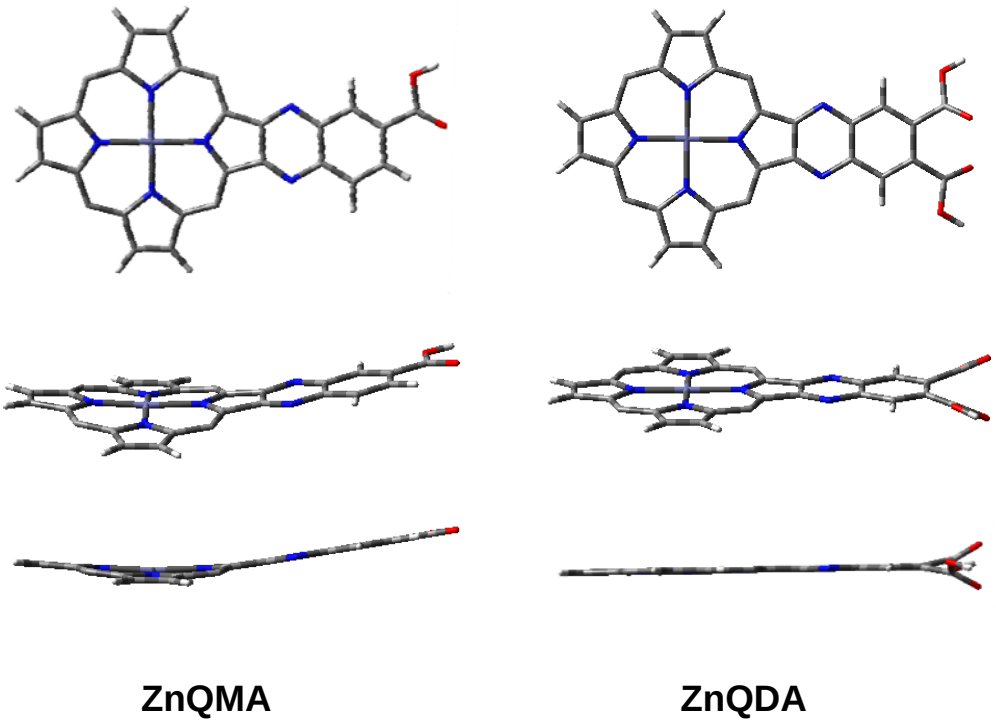

Figure 3. Optimized geometries for ZnQMA and ZnQDA estimated by DFT calculations with B3LYP/3-21G(d) with various viewing angles. *Meso* substituents are omitted for clarity.

degeneracy of the HOMO and HOMO-1 remains intact by the quinoxalino substitutions (Figure 4). In addition, variations in energies by the structural modifications for the

LUMO (-0.55 eV for ZnQMA and -0.63 eV for ZnQDA vs ZnP) are larger than those for the HOMO (-0.19 eV for ZnQMA and -0.27 eV for ZnQDA vs ZnP). These results reveal that the substitutions onto the β, β'-edge of the porphyrins mainly affect the energy levels for the unoccupied orbitals of the porphyrins.

Figure 5 displays the electron density distributions of ZnQMA and ZnQDA in their respective LUMOs. Sufficient electron densities around the carboxylic acid binding group on the LUMO of dye are requested for the strong electronic coupling between the

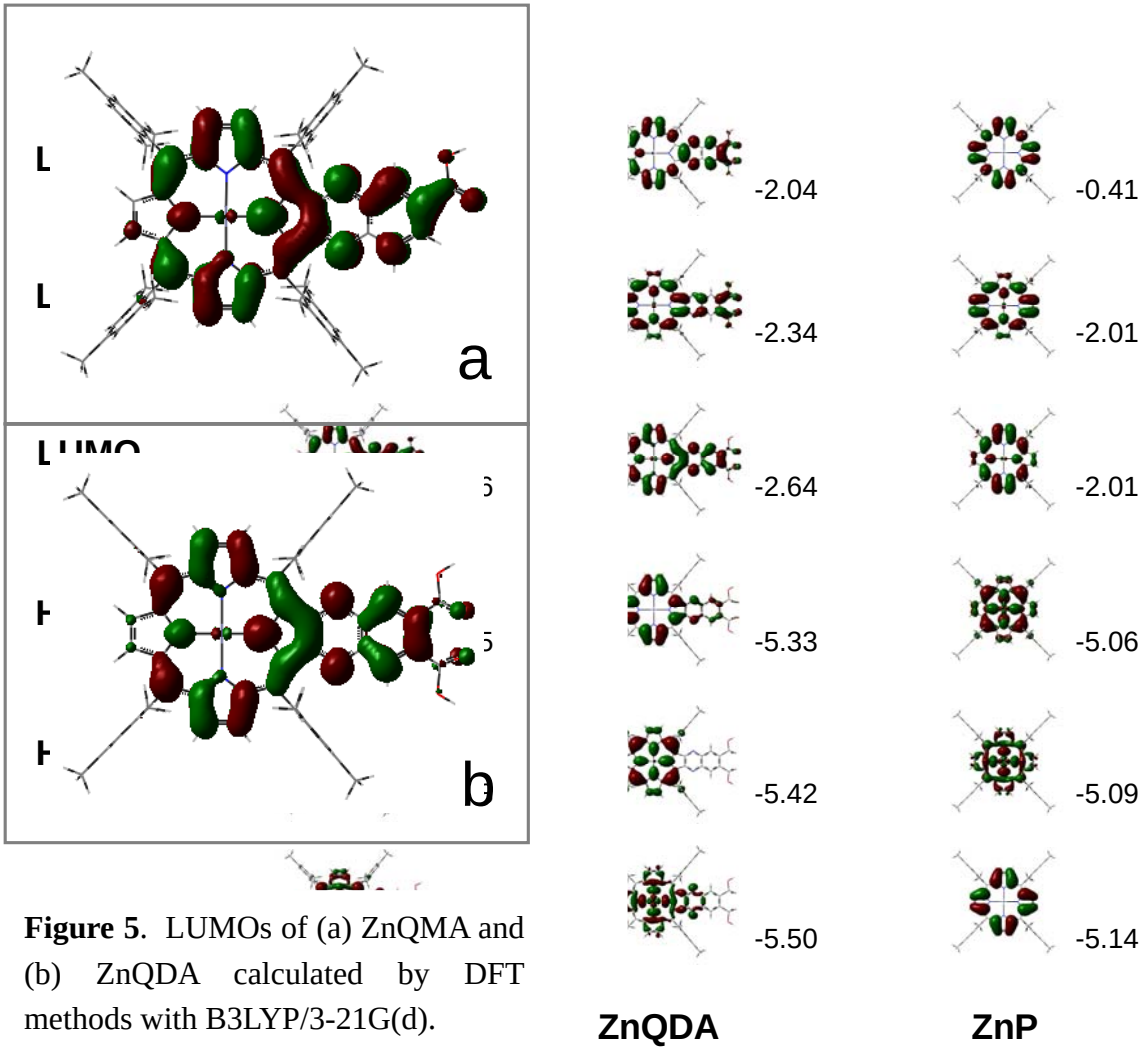

Figure 5. LUMOs of (a) ZnQMA and (b) ZnQDA calculated by DFT methods with B3LYP/3-21G(d).

Figure 4. Some sets of molecular orbital diagrams and corresponding energies for ZnQMA, ZnQDA, and ZnP estimated by DFT calculations with B3LYP/3-21G(d). The energies in eV are quoted with respect to the vacuum (1 Hartree = 27.2116 eV).

excited state of dye and the 3d orbital of TiO_2.[xiv] Bridging carbon atom between the porphyrin and the carboxylic acid as well as the carboxylic acid on the LUMO of ZnQMA (Figure 5a) has larger electron density than those of ZnQDA (Figure 5b). Accordingly, fast electron injection from the excited singlet state of ZnQMA to the CB of TiO_2 compared with that for ZnQDA, leading to high cell performance of ZnQMA relative to that of ZnQDA are expected (*vide infra*).[xv]

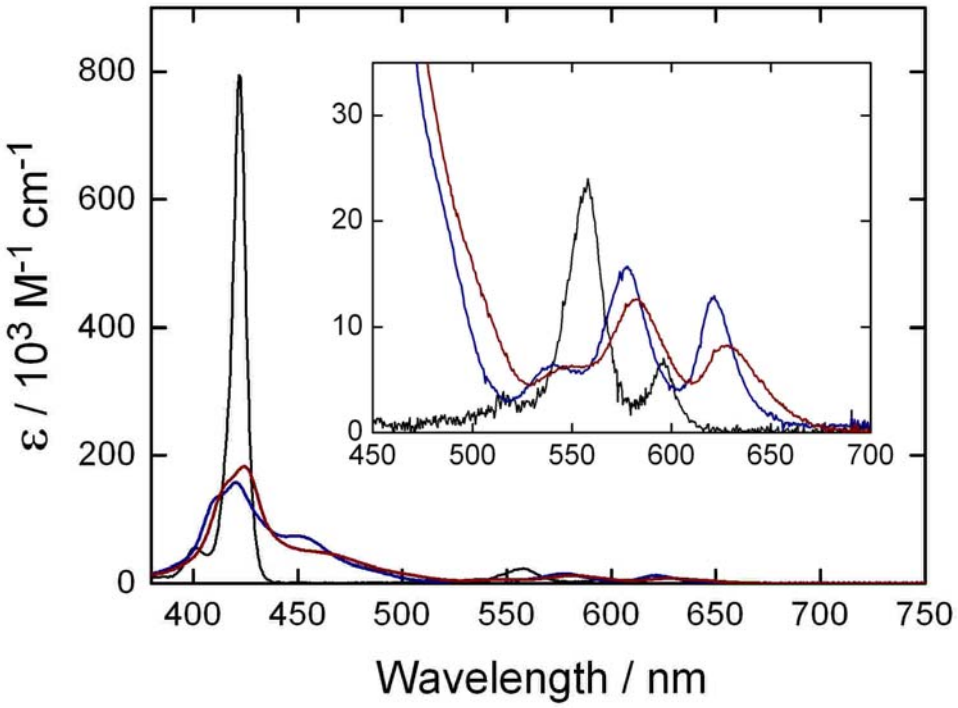

Figure 6. UV-visible absorption spectra of ZnQMA (blue), ZnQDA (red), and ZnP (black) measured in 1μM of methanol solution.

Optical and Electrochemical Properties. Figure 6 displays the UV-visible absorption spectra of ZnQMA, ZnQDA, and ZnP in MeOH. As expected from the molecular structure and DFT calculations, narrow-width Soret band of ZnP is dramatically broadened by introducing the substituents with aromatic and electron-withdrawing characters; the red-shifted and widened Q-bands for both ZnQMA and ZnQDA are clearly demonstrated. The significant improvements of light harvesting capabilities by extensions of the π-systems are verified by comparing the relative ratio of integrated absorption cross section from 380 to 750 nm (ZnP : ZnQMA : ZnQDA = 1.000 : 1.070 : 1.072). Remarkable is the intense absorption arising between 435 and 500 nm for ZnQMA and ZnQDA, while there is no substantial absorption at the same region for ZnP. The neighborhood of 500 nm is the most abundant region of solar light spectrum, thus the utilization of the light in this area is particularly important. Because the solvent

employed for the absorption measurements is methanol and it would occupy the fifth coordination site of the zinc, the observed absorption features of ZnQMA and ZnQDA are thought to be originated from the π-extension. However, the probability to treat it as the indication of the self-assembly through the interactions between the zinc and the carboxylic acid group still cannot be ruled out. To discern the cause of the widened and red-shifted optical features unambiguously, the UV-visible absorption spectra in toluene, a non-coordinating solvent, with different concentrations (1 ~ 10 μM) were measured. The absorption features display more or less similar trend with those measured in methanol (Figure 7). Moreover, the characteristic spectral patterns of ZnQMA and

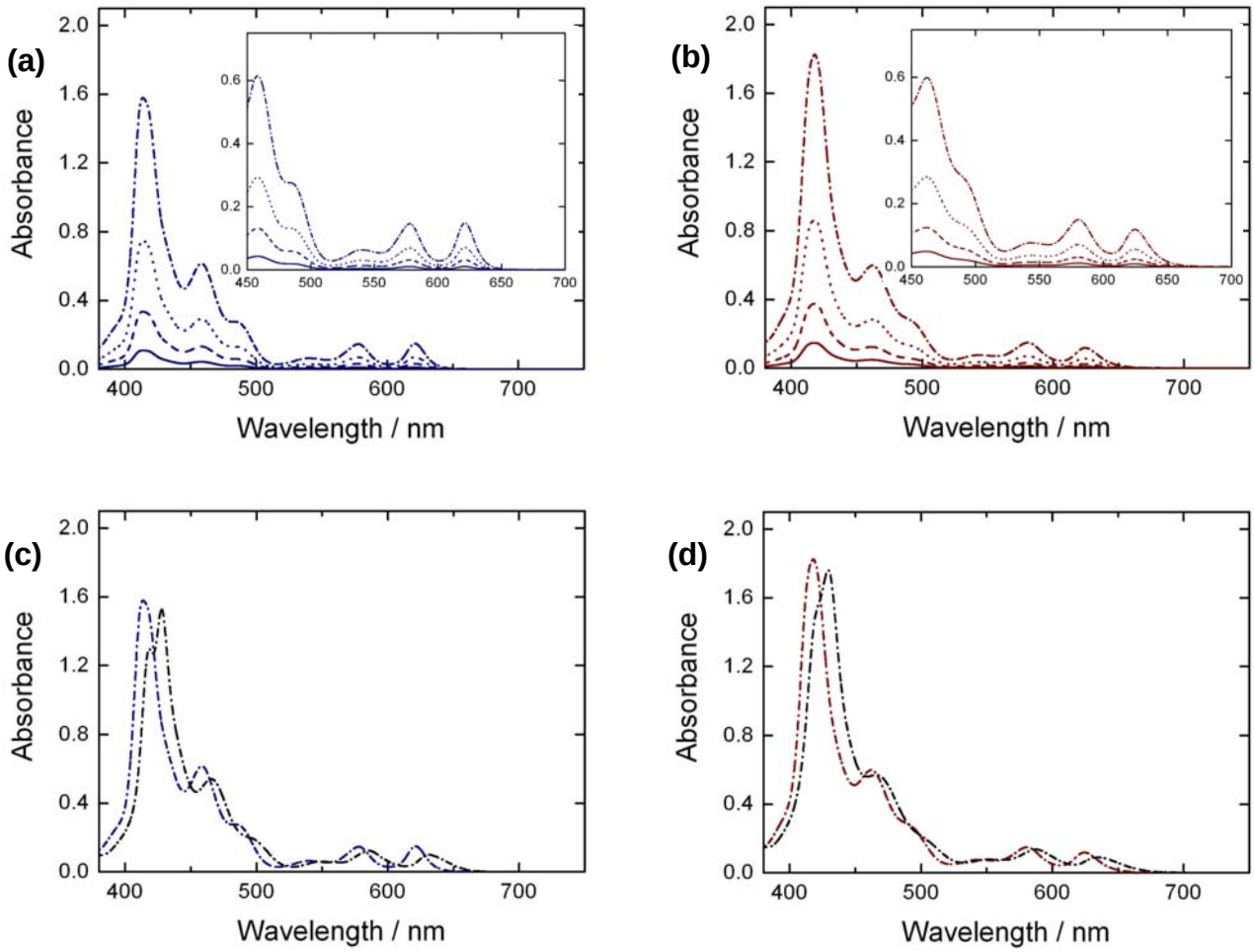

Figure 7. UV-visible absorption spectra of (a) ZnQMA and (b) ZnQDA measured in toluene solution with different concentrations of 1.0 μM (solid), 2.5 μM (dashed), 5.0 μM (dotted), and 10.0 μM (dashed dot). UV-visible absorption spectra of (c) ZnQMA and (d) ZnQDA measured in 10.0 μM with the addition of 2.5 mM of pyridine (black). Optical length = 1 cm.

ZnQDA can still be found even after the addition of an excess amount of pyridine (2.5 mM), a highly coordinating ligand to the zinc. The observed optical features of ZnQMA and ZnQDA, therefore, should be invoked by the carboxyquinoxalino substitutions. On the basis of the Gouterman's four orbital model, absorption features of the porphyrins are interpreted by the configuration interaction of the electronic transitions between the two

occupied orbitals (HOMO-1, HOMO) and the two unoccupied orbitals (LUMO, LUMO+1).[xvi] Detailed optical features between ZnQMA and ZnQDA are not exactly the same, and it can be understood by nonequivalent configuration interaction caused by the difference in symmetry and/or planarity of the two macrocycles.

TABLE 1: Optical and Electrochemical Data for Porphyrins and Driving Forces for Electron-Transfer Processes on TiO_2.

	λ_{abs} [a] / nm (ε / 10^3 M^{-1} cm^{-1})	λ_{em} [b] / nm	E_{ox} [c] / V	E_{red} [c] / V	E_{00} / eV	E_{ox}^* [d] / V	ΔG_{inj} [e] / eV	ΔG_{reg} [f] / eV
ZnQMA	420.5 (157.6) 578.0 (15.7) 621.5 (13.0)	637 690	0.98 (1.10)[g]	-1.13	1.98	-0.99 (-0.88)[g]	-0.49 (-0.38)[g]	-0.48 (-0.60)[g]
ZnQDA	424.5 (182.8) 583.5 (12.7) 627.5 (8.3)	635 689	0.98 (1.10)[g]	-1.05	1.96	-0.98 (-0.86)[g]	-0.48 (-0.37)[g]	-0.48 (-0.60)[g]
ZnP	422.0 (794.6) 558.0 (24.0) 596.5 (6.8)	599 655	0.95	-1.29	2.08	-1.12	-	-

[a] Wavelengths for Soret and Q bands maxima in methanol. [b] Wavelengths for emission maxima in methanol by exciting at Soret wavelength. [c] Ground state redox potentials (vs NHE). [d] Excited-state oxidation potentials approximated from E_{ox} and E_{00} (vs NHE). [e] Driving forces for electron injection from the porphyrin singlet excited state (E_{ox}*) to the CB of TiO_2 (-0.5 V vs NHE). [f] Driving forces for the regeneration of porphyrin radical cation (E_{ox}) by I^-/I_3^- redox couple (+0.5 V vs NHE). [g] Energies estimated with reference to the oxidation potentials of the adsorbed porphyrins.

The steady-state fluorescence spectra of the porphyrins were measured in methanol and the wavelengths for emission maxima are listed in Table 1. From the intersection of the normalized absorption and emission spectra, the zeroth-zeroth excitation energies (E_{00})[xvii] are determined to be 1.98 eV for ZnQMA, 1.96 eV for ZnQDA, and 2.08 eV for ZnP. The fluorescence lifetimes (τ) of ZnQMA, ZnQDA, and ZnP were measured in methanol by the time-correlated single photon counting technique at an emission wavelength of 650 nm with excitation at 400 nm. The decay curves of fluorescence intensity were fitted as a single exponential to give τ=0.99 ns for ZnQMA and τ=2.36 ns for ZnP, whereas the fluorescence lifetime for ZnQDA could be analyzed by two components with τ =0.73 ns (62 %) and τ =1.52 ns (38 %). As electron injection processes from excited-state dyes to the TiO_2 surface have been reported to take place in a time scale of 10^{12} - 10^{13} s^{-1},[xviii] the reduced fluorescence lifetime due to the quinoxalino substitutions would have little influence on the electron injection efficiency.

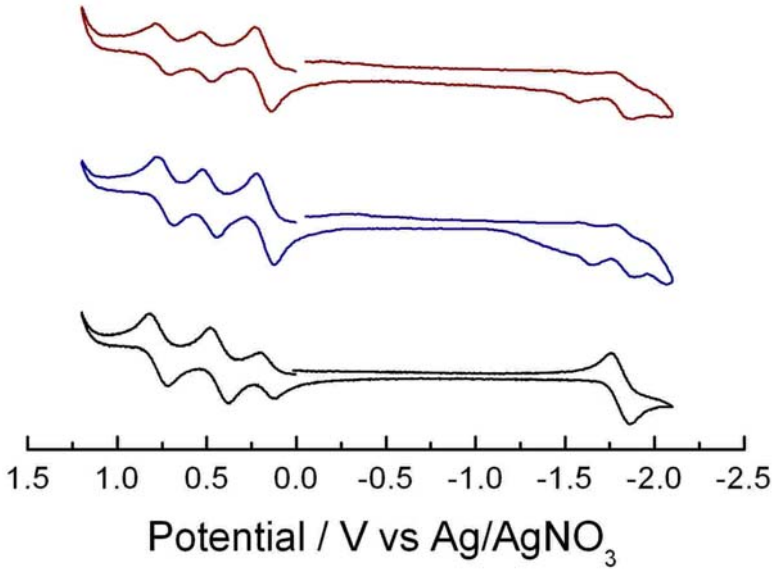

Figure 8. Cyclic voltammograms for ZnP (black), ZnQMA (blue), and ZnQDA (red) in CH_2Cl_2 containing 0.1M TBAP as a supporting electrolyte. A glassy carbon working electrode (3 mm diameter), $Ag/AgNO_3$ reference electrode, and Pt wire counter electrode were employed. Ferrocene/ferrocenium (+0.642 V vs NHE) was used as an internal standard for all measurements.

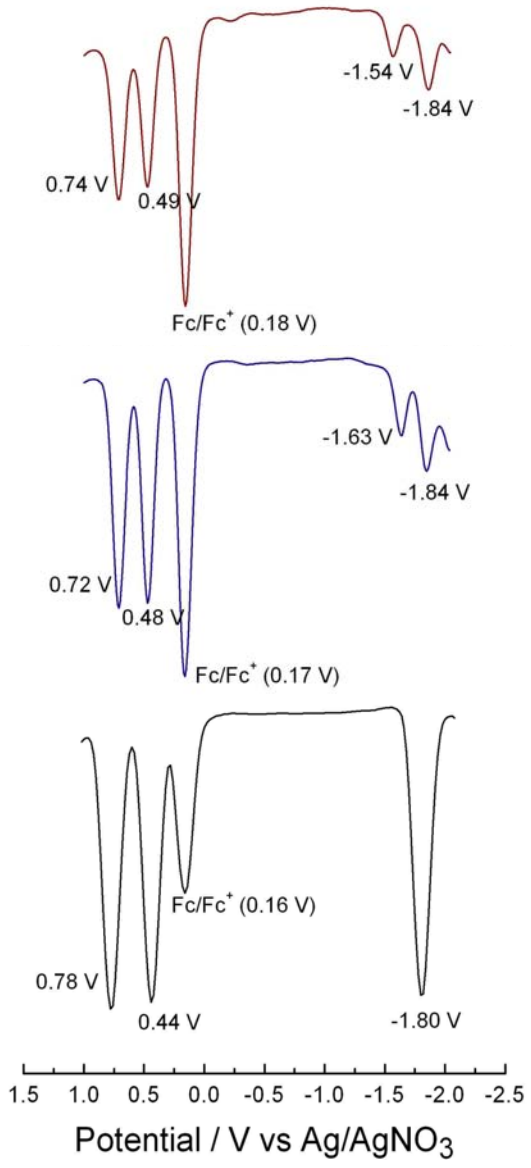

Figure 9. Differential pulse voltammograms for ZnP (black), ZnQMA (blue), and ZnQDA (red) in CH_2Cl_2 containing 0.1M TBAP as a supporting electrolyte. Scan rate of 50 mV s^{-1} and pulse amplitude of 50 mV were used for measurements. Other conditions for measurements were the same for CV measurements.

To determine the first oxidation potential (E_{ox}) and first reduction potential (E_{red}) of the porphyrins in solutions, cyclic voltammetry measurements were performed in dichloromethane containing 0.1 M tetrabutylammonium perchlorate (TBAP) as a supporting electrolyte. Both ZnQMA and ZnQDA show well-resolved reversible one- and two-electron oxidation waves, but the waves for the reduction are irreversible and vague (Figure 8). ZnP displays two oxidation waves and one reduction wave under the same sweep conditions (+1.2 V to -2.1 V vs $Ag/AgNO_3$). Differential pulse voltammerty (DPV) was applied to determine the redox potentials accurately (Figure 9), and the results are displayed in Table 1. Both ZnQMA and ZnQDA show two oxidation peaks corresponding to the porphyrin radical cation and radical dication and two reduction peaks corresponding to the porphyrin radical anion and radical dianion, respectively. ZnP gives two oxidation peaks and one

reduction peak, as observed in the CV measurements. The first oxidation peaks for both ZnQMA (0.98 V vs NHE) and ZnQDA (0.98 V vs NHE) are shifted to a more positive direction

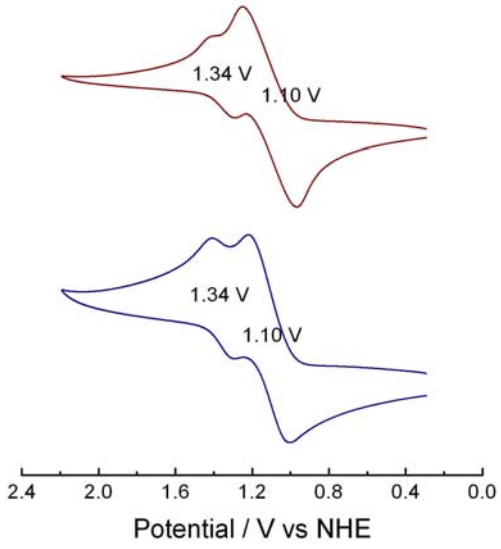

Figure 10. Cyclic voltammograms for TiO_2/ZnQMA (blue) and TiO_2/ZnQDA (red) in acetonitrile containing 0.1M TBAP at a scan rate of 100 mV s^{-1}. The porphyrin-modified TiO_2 was employed as a working electrode along with the Ag/AgCl reference electrode (+0.197 V vs NHE) and Pt wire counter electrode.

ca. 0.03 V from that of ZnP, whereas the first reduction peaks are shifted to a more positive direction by ca. 0.16 V for ZnQMA (-1.13 V vs NHE) and 0.24 V for ZnQDA (-1.05 V vs NHE) with respect to that of ZnP. This corroborates that the carboxyquinoxalino substituents affect mainly the LUMO of the porphyrins, as suggested from the results of DFT calculations (*vide supra*). ZnQMA and ZnQDA are easier to be reduced than ZnP. Recent study by Kadish et al. has also reported that the substitutions of the periphery of quinoxalino[2,3-β]porphyrins with electron-withdrawing groups result in the stabilization of LUMO and narrowed electrochemical HOMO-LUMO gaps.[5] The electrochemical HOMO-LUMO gaps are determined to be 2.11 eV for ZnQMA, 2.03 eV for ZnQDA, and 2.24 eV for ZnP, which is consistent with the aforementioned trend for the optical HOMO-LUMO gaps.

Cyclic voltammetry with the adsorbed porphyrins on the TiO_2 surfaces was also made (Figure 10). Half-wave potentials for the adsorbed porphyrins are estimated by averaging the anodic and cathodic peak potentials. TiO_2/ZnQMA electrode shows two oxidation waves, and the half-wave potentials are determined to be +1.10 vs NHE for

porphyrin radical cation and +1.34 vs NHE for radical dication. About 0.12 V of positive shift on the first oxidation potential is noted for ZnQMA after being adsorbed on the TiO_2. This is the fingerprint for the electron-withdrawing character from the TiO_2 to the porphyrin for forming the chemical bond. Because ZnQDA holds two carboxylic acid groups, it is expected to make a far stronger chemical bond to the TiO_2 surface compared with ZnQMA. However, shifts in the first and second oxidation potentials for TiO_2/ZnQDA are evidenced as the same magnitude as for TiO_2/ZnQMA, indicating that one of the two carboxylic acid binding groups in ZnQDA has a very weak interaction to the TiO_2 surface and/or the binding groups in the two porphyrins utilize different adsorption modes onto the TiO_2. This aspect is studied in more detail by X-ray photoelectron spectroscopy measurement (*vide infra*).

Cyclic voltammograms for TiO_2/ZnQMA under different scan rate conditions are shown in Figure 11. Regardless of the scan rate employed, the half-wave potential for one-electron oxidation is determined to be +1.10 V vs NHE. The growth of anodic and cathodic peak currents follows more or less the increment of square root of the scan rate. For chemically adsorbed electroactive species, the voltammogram typically displays the symmetric anodic and cathodic current waves at the same peak potential irrespective of the scan rate; only the current is proportionally augmented with the increment of the scan rate.[xix]

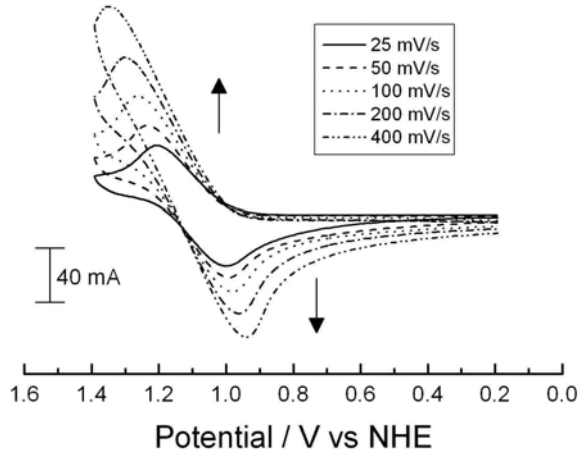

Figure 11. Cyclic voltammograms for TiO_2/ZnQMA with different scan rates of 25 mV s^{-1} (solid), 50 mV s^{-1} (dashed), 100 mV s^{-1} (dotted), 200 mV s^{-1} (dashed dotted), and 400 mV s^{-1} (dashed dotted dotted). The TiO_2/ZnQMA electrode was prepared by immersing the TiO_2 film into the porphyrin methanol solution for 1 h.

Although ZnQMA is adsorbed on the electrode, electron transport between the porphyrin and the back contact should occur through the highly porous TiO_2 network. The electron transport under this situation is believed to be controlled by diffusion,[xx] and therefore the anodic and cathodic peak potentials are not necessarily the same. Progressive widening in the anodic and cathodic waves along with the increments of the scan rates is not yet fully understood, but changes in the diffusion coefficients of electrons depending on the scan rates would be the main reason; difference in the scan rates, thereby the different degrees of surface trap filling affects the motion of the electrons.[xxi]

From spectroscopic and electrochemical measurements, driving forces for electron injection from porphyrin excited singlet state to the CB of TiO_2 (-0.5 V vs NHE)[xxii] (ΔG_{inj}) and the regeneration of porphyrin radical cation by I^-/I_3^- redox couple (+0.5V vs NHE)[22] (ΔG_{reg}) for the porphyrin-sensitized solar cells are evaluated (Table 1). Both of the processes are thermodynamically feasible and the differences in the driving forces for the two systems are negligible.

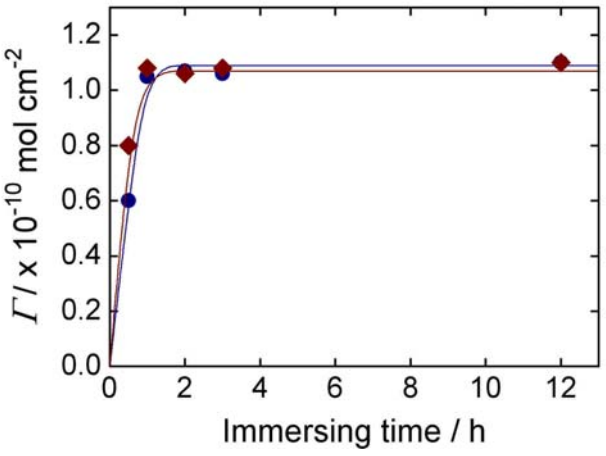

Figure 12. Time profiles of the surface coverage (Γ) of ZnQMA (blue) and ZnQDA (red) on the TiO_2 electrode for different immersing time in methanol solution.

Porphyrin Adsorption on TiO_2. Mesoporous TiO_2 films (10-μm-thick) were prepared from a colloidal suspension of TiO_2 nanoparticles (P25) (see Experimental Section).[xxiii] The TiO_2 electrodes were immersed into methanol containing 0.2 mM porphyrin at room temperature to give porphyrin-modified TiO_2 electrodes. Total amounts of the porphyrins adsorbed on the

TiO_2 films were determined by measuring the changes in the absorbance of the porphyrin solutions before and after immersing the TiO_2 films. After the immersion, both the ZnQMA and ZnQDA dissolved in methanol make the TiO_2 films green and reach saturated surface coverage (Γ) on the films for 0.5 - 1 h (Figure 12); the trend is very similar to the results in the chapter 1 on the surface coverage of similar porphyrins on the TiO_2.[1,23] Porphyrin concentrations on the TiO_2 films (0.25 cm^2 of area with thickness of 10 μm) are determined to be about 1.1×10^{-10} mol cm^{-2}. Assuming the porphyrin monolayer has a densely packed and vertical orientation to the TiO_2 surface, the Γ value is calculated to be 1.2×10^{-10} mol cm^{-2}. Taking into account the good agreement between the calculated and experimental Γ values together with the adsorption behavior of ZnQMA and ZnQDA, both of them are almost perpendicular to the TiO_2 surface, leading to the densely packed monolayers of ZnQMA and ZnQDA on the TiO_2.

Carboxylic acid groups are known to be spontaneously adsorbed onto TiO_2 surfaces. They form bidentate chelating, bidentate bridging, and/or ester-like binding

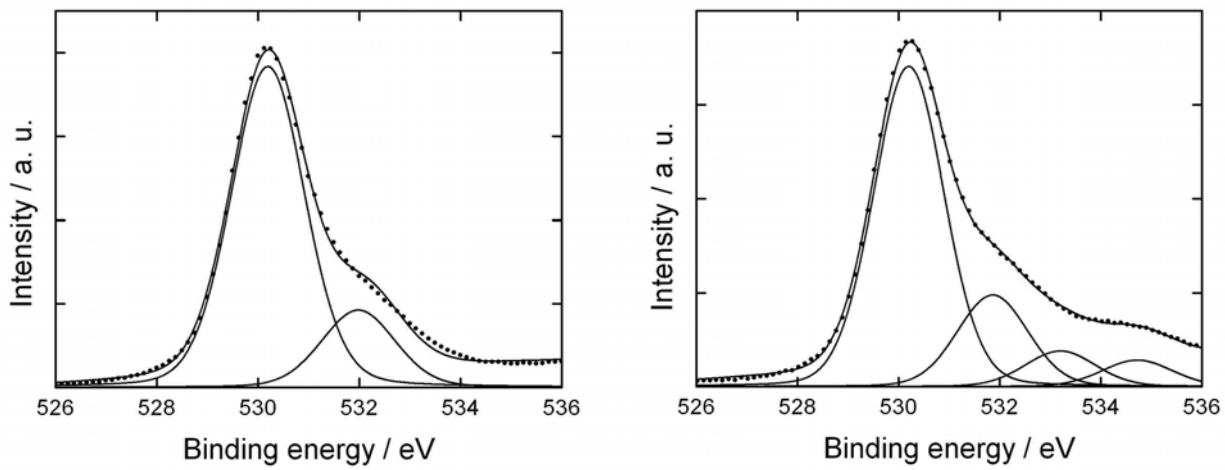

Figure 13. O1s XPS spectra for (a) ZnMQA and (b) ZnQDA on the TiO_2 surface. The modified TiO_2 surface was prepared by immersing the TiO_2 film into the porphyrin methanol solution for 1 h.

with the TiO_2 surfaces depending on the experimental conditions.[xxiv] To gain detailed

information on the adsorption modes of the porphyrins on the TiO_2 surface, X-ray photoelectron spectroscopy (XPS) measurements for TiO_2/ZnQMA and TiO_2/ZnQDA were made (Figure 13). The O1s photoelectron spectrum of TiO_2/ZnQMA (Figure 13a) exhibits two distinct oxygen peaks. The most intense peak (530.2 eV) originates from the oxygen from the TiO_2 surface.[xxv] The remaining peak (532.1 eV) can be assigned to the two oxygen atoms from the carboxylate that are anchored to the TiO_2 surface with the same binding energy through bidentate coordination.[xxvi] The O1s spectrum of TiO_2/ZnQDA (Figure 13b) shows four chemically nonequivalent oxygen signatures. One peak that appears at 530.2 eV is assigned to the oxygen atom from the TiO_2; the other peak at 531.9 eV originates from carboxylate with bidentate coordination. Considering the intensity ratio of 2 : 1 : 1 among the three small peaks except for the large one from the TiO_2, the remaining two peaks arising at 533.2 and 534.7 eV can be assigned to the two oxygen atoms of carboxylate which coordinates weakly or adsorbs physically on the TiO_2 in an ester-like monodentate manner. The larger binding energy of the electron for monodentate O1s than that for bidentate O1s supports this interpretation. This is consistent with the results of the above-mentioned cyclic voltammetry measurements for TiO_2/ZnQMA and TiO_2/ZnQDA (*vide supra*).

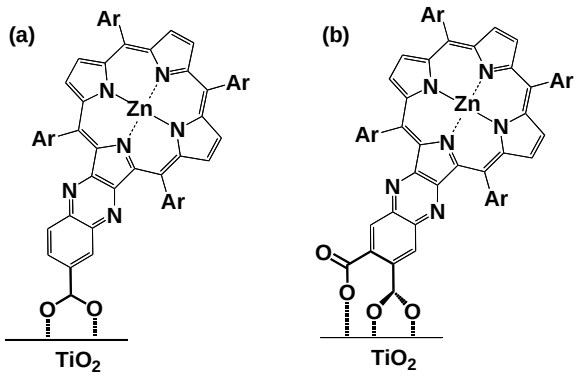

Figure 14. Proposed adsorption geometries of (a) ZnQMA and (b) ZnQDA on the TiO_2 surface.

From the collective results of the XPS and electrochemistry measurements, the adsorption geometries of ZnQMA and ZnQDA on the TiO_2 surface are proposed as illustrated in Figure 14.[xxvii] Namely, carboxylic group in ZnQMA binds to the TiO_2 surface with bidentate coordination. In contrast, one

carboxylic group in ZnQDA binds to the TiO_2 surface with bidentate coordination, while the other carboxylic group in ZnQDA binds to the TiO_2 surface with monodentate coordination.

Photovoltaic and Photoelectrochemical Properties of Porphyrin-Sensitized TiO_2 Cells. To judge the potential of ZnQMA and ZnQDA as photosensitizers for DSSC, their cell performances using P25 TiO_2 film were evaluated. 10-μm-thick TiO_2 electrode was modified with ZnQMA or ZnQDA (0.2 mM) dissolved in methanol for the immersing time of 0.5-12 h. The power conversion efficiency (η) is derived from the equation: $\eta = J_{SC} \times V_{OC} \times ff$, where J_{SC} is the short circuit current, V_{OC} is the open circuit potential, and ff is the fill factor. The η values of ZnQMA- and ZnQDA-sensitized TiO_2 cells show the dependency on the immersing time, as observed in the time profile of η values of the TiO_2 cells modified with similar porphyrin carboxylic acids[1,23] (Figure 15). Figure 16 depicts the photocurrent-voltage characteristics of ZnQMA- and ZnQDA-sensitized TiO_2 cells under the respective maximal η conditions with immersing time of 1 h.

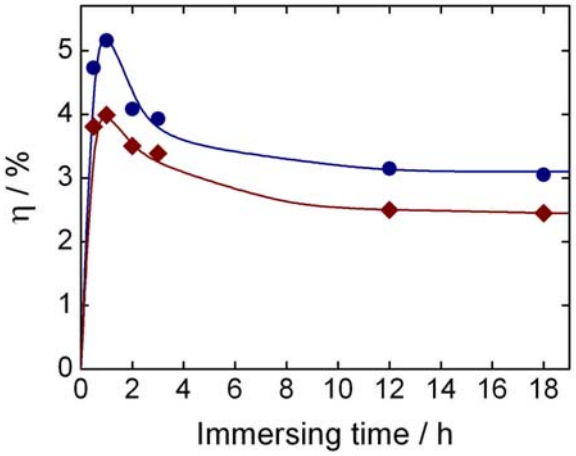

Figure 15. Time profiles of the η values of ZnQMA- (blue) and ZnQDA- (red) sensitized solar cells with the TiO_2 electrodes prepared under different immersing time for porphyrin adsorption in methanol.

ZnQMA-sensitized cell exhibits η=5.2% with J_{SC}=11.2 mA cm^{-2}, V_{OC}=0.72 V, and ff =0.68, while ZnQDA-sensitized one yields η=4.0% with J_{SC}=9.3 mA cm^{-2}, V_{OC}=0.67 V, and ff =0.64. Both η values are smaller than that of N719-sensitized cell under our optimized conditions (η = 6.5 %, J_{SC} = 14.0 mA cm^{-2}, V_{OC} = 0.74 V, ff = 0.63);[23] this result did not reach the level that had been reported by Grätzel et al. (η =

10-11 %).[xxviii] Different photovoltaic performances even for the same dye sensitizer among the different groups is not unusual, and such differences are mainly explained by the experimental conditions such as electrolytes and morphological and structural aspects of TiO_2.[xxix] The smaller value of the porphyrin-sensitized cell arises mainly from the inferior J_{SC}, which reflects the difference in the spectral coverage between the porphyrins and N719.

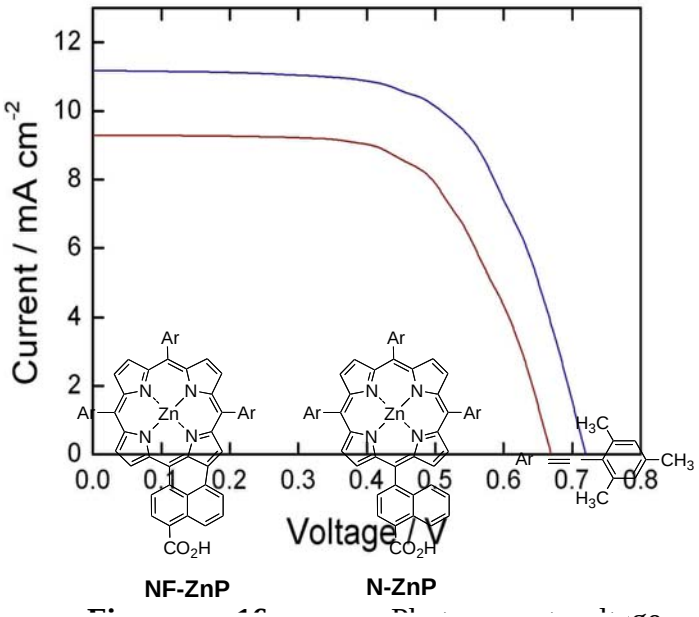

Figure 17. Molecular structures of naphthalene-fused porphyrin, NF-ZnP and the reference porphyrin, N-ZnP.

To a large extent, η=5.2 % for ZnQMA-sensitized TiO_2 cell is the promising result compared to that of N719-sensitized one under our optimized conditions. We have proposed that constructing π-expansion to achieve widened and red-shifted light absorption would be effective to improve the performance of porphyrins for dye-sensitized solar cell applications. In the report,[1] we have prepared the *meso*- and β-naphthalene-fused zinc porphyrin carboxylic acid, NF-ZnP as well as its non-fused counterpart, N-ZnP (Figure 17), and evaluated their respective photovoltaic performances. The power conversion efficiency (η) of the NF-ZnP cell (η=4.1% with J_{SC}=10.6 mA cm^{-2}, V_{OC}=0.62 V, and *ff* =0.62) was larger by ca. 50 % due to the π-expansion than that of the N-ZnP cell (η=2.8% with J_{SC}=6.7 mA cm^{-2}, V_{OC}=0.61 V, and *ff* =0.68). The enhanced performance should be

invoked by the improved J_{SC}, and it was clearly demonstrated in the photocurrent action spectra. To consider the similar molecular structures of ZnP and N-ZnP, π-extension by constructing β, β'-edge fused porphyrin would be a useful strategy to devise an efficient porphyrin photosensitizer for DSSC applications.

Difference in the η values between the two porphyrin-sensitized solar cells primarily results from the nonparallel value of *J*sc. This trend can also be found in the photocurrent action spectra of ZnQMA- and ZnQDA-sensitized TiO_2 cells (Figure 18a). The ZnQMA-sensitized TiO_2 cell discloses superior incident photon-to-photocurrent efficiency (IPCE) to the ZnQDA-sensitized one in all wavelength regions. Each of the photoelectrochemical responses follows the absorption feature of the corresponding porphyrin adsorbed on the electrodes (Figure 18b), indicating that the porphyrin is the main source for the photocurrent generation. The maximal IPCE ($IPCE_{max}$) at the respective Soret and Q bands are 72 % (at Soret), 56 % (at Q(1,0)), and 52 % (at Q(0,0)) for ZnQMA-sensitized cell, and 64 % (at Soret), 41 % (at Q(1,0)), and 35 % (at Q(0,0)) for ZnQDA-sensitized one, respectively (Table 2).

To rationalize the difference in η as well as IPCE between the two porphyrin-sensitized TiO_2 cells, the IPCE is divided into three components as the following equation (1).

$$IPCE = LHE \times APCE = LHE \times \phi_{inj} \times \eta_{col} \qquad (1)$$

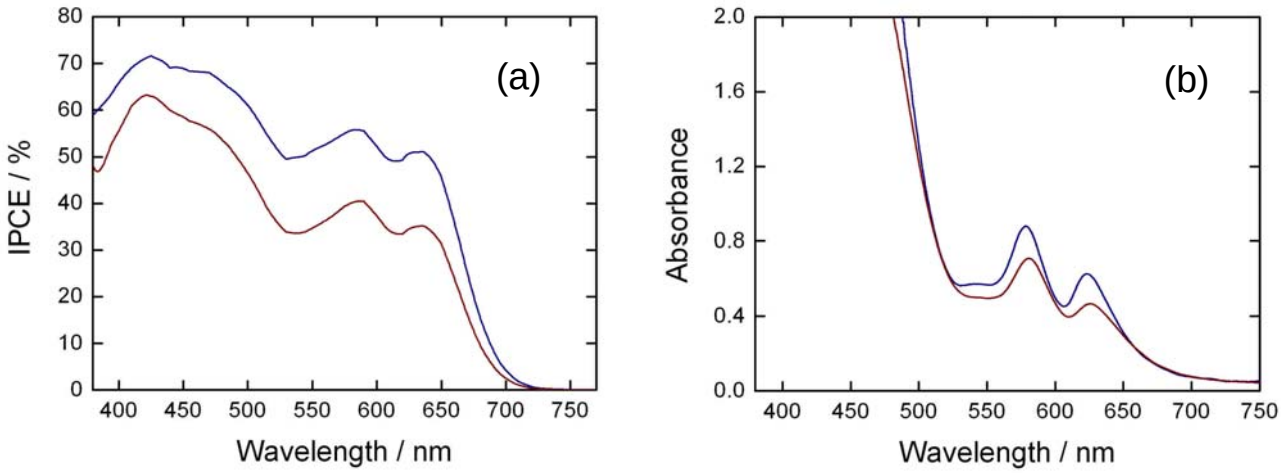

Figure 18. (a) Photocurrent action spectra of ZnQMA-sensitized TiO_2 cell (blue) and ZnQDA-sensitized TiO_2 cell (red) and (b) UV-visible absorption spectra of TiO_2/ZnQMA (blue) and TiO_2/ZnQDA (red). Each of the porphyrin-modified TiO_2 electrodes was prepared under the same conditions for the power conversion efficiency (η) measurements. Conditions: electrolyte 0.1 M LiI, 0.05 M I_2, 0.6 M 2,3-dimethyl-1-propyl imidazolium iodide, and 0.5 M 4-*t*-butylpyridine in CH_3CN; input power: AM 1.5 under simulated solar light (100 mW cm^{-2}).

where LHE (light harvesting efficiency) is the number of absorbed photons per the number of incident photons, APCE (absorbed photon-to-current efficiency) is the number of electrons collected in the external circuit per the number of absorbed photons, ϕ_{inj} is the quantum yield for electron injection from the porphyrin excited state to the CB of the TiO_2 electrode, and η_{col} is the efficiency of charge collection. Namely, high value of IPCE is anticipated provided that the conditions of broad and strong light absorption as well as favorable charge transfer/transport kinetics are accomplished. Given the comparable surface coverages and molar absorptivities between the two porphyrins, difference in APCE should be attributed to the main reason for the nonequivalent IPCE between the two cells. Maximal APCE ($APCE_{max}$) values at the Soret and Q bands regions for each of the porphyrin-sensitized TiO_2 cells are determined[xxx] and summarized in Table 2. As expected, the ZnQMA-sensitized cell reveals a higher value of APCE than that of the ZnQDA-sensitized one. The ϕ_{inj} for the

TABLE 2: $APCE_{max}$ and $IPCE_{max}$ Values of ZnQMA- and ZnQDA-Sensitized TiO_2 Cells at the Soret and Q Bands.

Cell	$APCE_{max}$ ($IPCE_{max}$) / %
TiO_2/ZnQMA	80 (72),[a] 65 (56),[b] 61 (52) [c]
TiO_2/ZnQDA	71 (64),[a] 48 (41),[b] 41 (35) [c]

[a] At Soret. [b] At Q(1,0). [c] At Q(0,0).

ZnQMA cell should be anticipated to be larger than that for the ZnQDA cell, considering the strong electronic coupling between the LUMO of ZnQMA and the CB of the TiO_2 compared with that between the LUMO of ZnQDA and the CB of TiO_2 (*vide supra*). The η_{col} primarily depends on the relative rates of charge transport against charge recombination. The recombination between the injected electrons on the CB of the TiO_2 and the I^-/I_3^- is known to be the main pathway for charge recombination in dye-sensitized solar cell systems.[xxxi] To clarify the effect of the charge recombination, we measured the current-voltage characteristics under dark conditions (Figure 19).

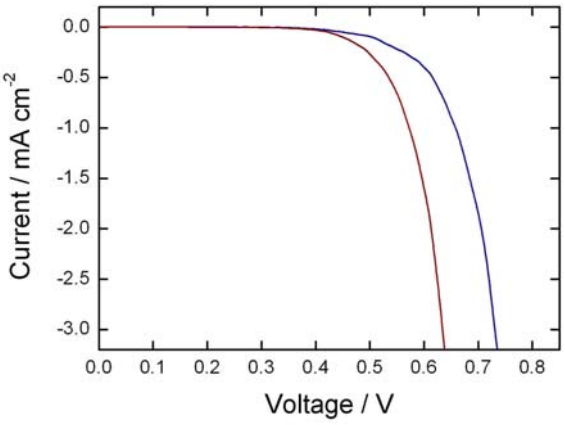

Figure 19. Current-voltage characteristics of ZnQMA- (blue) and ZnQDA-sensitized TiO_2 cells (red) under dark conditions.

Obviously, the onset of the dark current for the ZnQMA cell appears at a more positive value than that for the ZnQDA cell, indicating that the degree of the charge

recombination for the ZnQDA cell is higher than that for the ZnQMA one.[xxxii] Some of the protons of carboxylic acid groups are known to be transferred to the TiO_2 surface during the adsorption, and it would induce the positive shift of the Fermi level of the TiO_2.[xxxiii] The decreased Fermi level indicates that there is a narrowed gap between the CB of the TiO_2 and the redox level of the I^-/I_3^-. Namely, the proton-induced Fermi level shift would increase the overlap of the CB of the TiO_2 with oxidized electrolyte.[xxxiv] It hinders the efficient charge collection, and consequently makes the η_{col} lower. The ZnQDA holds one more carboxylic acid group compared with the ZnQMA. The degree of the proton transfer, and thereby the degree of charge recombination for the ZnQDA-sensitized TiO_2 cell is anticipated to be higher than that for the ZnQMA-sensitized one. Because any source of charge recombination is known to have an effect to decrease V_{OC},[xxxv] we can also rationalize the smaller V_{OC} for ZnQDA cell than that for ZnQMA cell. The open circuit potential (V_{OC}) is the maximum Gibbs free energy that can be attained from the given system and is defined as the energy difference between the Fermi level of the TiO_2 and the redox potential of the I^-/I_3^- electrolyte for DSSC. The lower value of V_{OC} for ZnQDA cell can be understood based on the positive shift of the Fermi level. Grätzel et al. have reported that the influence of the number of transferable protons (4 protons for N3 dye, 2 protons for N719 dye, and 0 proton for N712 dye) on the J_{SC} and V_{OC} of DSSC; J_{SC} = 19±0.5 mA cm^{-2} and V_{OC} = 0.60±0.03 V for N3, J_{SC} = 17±0.5 mA cm^{-2} and V_{OC} = 0.73±0.03 V for N719, and J_{SC} = 13±0.5 mA cm^{-2} and V_{OC} = 0.90±0.03 V for N712.[xxxvi] The highest V_{OC} value for N712 cell was explained by the negative shift of the Fermi level of the TiO_2. The highest J_{SC} value for N3 cell was, in turn, rationalized by the positive shift of the Fermi level, which is considered to increase the photocurrent injection; a tradeoff between J_{SC} and V_{OC} in dye-sensitized TiO_2 cells due to the variations in the Fermi level was suggested. This tradeoff relation, however, cannot be found in our present ZnQMA- and ZnQDA-sensitized solar cells. Although the photocurrent injection yield in the ZnQDA cell is expected to be high compared with that

of the ZnQMA cell due to the more positively shifted Fermi level, it is compensated by the stronger electronic coupling between the LUMO of ZnQMA and the CB of the TiO_2 than that between the LUMO of ZnQDA and the CB of the TiO_2. The coplanarity of the carboxylic acid group with respect to the macrocycle plane in the ZnQMA, different from the ZnQDA, can be attributed to the main reason for this nonequivalent coupling effect (Figure 3). Finally, it can be concluded that the superior performance of ZnQMA-sensitized TiO_2 cell to ZnQDA-sensitized one is originated from both the more favorable electron injection and charge collection efficiency.

Conclusions

Two β, β'-quinoxalino porphyrins containing different numbers of carboxylic acid binding groups have been synthesized and evaluated as photosensitizers for DSSC. Both of the compounds showed broadened, red-shifted, and amplified light absorption with the aid of π-extensions. Electrochemistry along with DFT calculations revealed that the low-lying LUMO by the substitutions is the main reason for the narrowed HOMO-LUMO gaps. From the X-ray photoelectron spectroscopy, FTIR spectroscopy, and cyclic voltammetry studies for the adsorbed porphyrins, we proposed that one carboxylic acid employs bidentate binding mode to anchor ZnQMA onto the TiO_2 surface, whereas the two binding groups in ZnQDA utilize one bidentate and one monodentate binding modes. Photovoltaic measurements of the ZnQMA- and the ZnQDA-sensitized TiO_2 cells with P25 revealed power conversion efficiencies of 5.2 % and 4.0 %, respectively. Since the light absorption capabilities of the two porphyrins are more or less similar, the number and the position of binding groups in the porphyrins have a large impact on the photovoltaic and photoelectrochemical performances. The results for the ZnQMA-sensitized TiO_2 cell could be called "promising", considering the result of N719-sensitized cell (η = 6.5 %) under present optimized conditions.

Experimental Section

Synthesis

General. All solvents and chemicals were of reagent grade quality, purchased, and used without further purification unless otherwise noted. All of the reactions were carried out under a nitrogen or argon atmosphere in the dark. Column chromatography and thin-layer chromatography (TLC) were performed with UltraPure Silica Gel (230-400 mesh, SiliCycle) and Silica gel 60 F_{254} (Merck), respectively. ^{1}H-NMR spectra were measured on a JEOL EX-400 (400 MHz) or a JEOL AL300 (300 MHz) spectrometer. Matrix assisted laser desorption/ionization time-of-flight (MALDI-TOF) mass spectra were made on a Shimadzu KOMPACT MALDI II using CHCA as a matrix. UV-vis absorption spectra were measured using a Perkin-Elmer Lambda 900 UV/VIS/NIR Spectrometer with a spectroscopy grade methanol. FT-IR spectra were acquired using by a JASCO FT/IR-470 plus spectrometer with a KBr pellet. 5,10,15,20-Tetrakis(2,4,6-trimethylphenyl)porphyrin (1), 5,10,15,20-tetrakis(2,4,6-trimethylphenyl)porphyrinatocopper (II) (2), 5,10,15,20-tetrakis(2,4,6-trimethylphenyl)porphyrinatozinc (II) (ZnP), methyl 3,4-diaminobenzoate, and dimethyl 4,5-diaminophthalate were prepared according to the known procedures.[8]

2-Nitro-5,10,15,20-tetrakis(2,4,6-trimethylphenyl)porphyrinatocopper (II) (3). This procedure was based upon the literature protocol for similar compound.[9] To a solution of **2** (1.69 g, 2.0 mmol) in chloroform (1.3 L) was added a solution of copper nitrate trihydrate (1.19 g, 4.9 mmol) in a mixed solution of acetic anhydride (160 mL) and acetic acid (30 mL). The reaction mixture was stirred at 35 ~ 40 °C for 2 h until the reactant was not detected by silica TLC (hexane/CH_2Cl_2 = 3:1). After cooling to room temperature, the reaction mixture was treated with sodium carbonate and washed with water, subsequently dried over anhydrous magnesium sulfate and then concentrated in vacuo.

Purification by silica column chromatography (hexane/CH_2Cl_2 = 3:1), and subsequent reprecipitation from CH_2Cl_2/methanol afforded **3** as a deep red solid (1.3 g, 1.5 mmol, 73 % yield). UV-vis (CH_2Cl_2) λ_{max} (nm) 419.20, 544.81, 585.14 (lit.[8b] 420, 546, 584); FT-IR (KBr) ν_{max} 3422, 2916, 1610, 1527 (NO_2), 1450, 1375, 1334, 999, 803 cm^{-1}; MS (MALDI-TOF) *m/z* 888.2 ($M+H^+$).

2-Nitro-5,10,15,20-tetrakis(2,4,6-trimethylphenyl)porphyrin (4). This procedure was based upon the literature protocol for similar compound.[xxxvii] To a vigorously stirred solution of **3** (1.20 g, 1.35 mmol) in trifluoroacetic acid (91 mL) was added a concentrated sulfuric acid (98%, 20 mL). After 2.5 h of stirring, the reaction mixture was neutralized with saturated aqueous sodium bicarbonate and extracted with chloroform. The extract was washed with water, dried over anhydrous magnesium sulfate, and concentrated in vacuo. Purification by silica column chromatography (hexane/CH_2Cl_2 = 3:1 ~ 2:1), and subsequent reprecipitation from CH_2Cl_2/hexane afforded **4** as a brownish violet solid (793 mg, 0.96 mmol, 71 % yield). ^1H NMR (300 MHz, $CDCl_3$) δ 8.84-8.53 (m, 7H, β-pyrrolic H), 7.27 (s, 6H, phenyl H), 7.17 (s, 2H, phenyl H), 2.62-2.58 (m, 12H, methyl H), 1.89-1.84 (m, 24H, methyl H), -2.48 (s, 2H, inner H); FT-IR (KBr) ν_{max} 3329, 2917, 1611, 1529 (NO_2), 1473, 1376, 1341, 983, 968, 851, 802 cm^{-1}; MS (MALDI-TOF) *m/z* 829.4 ($M+H^+$).

2-Amino-5,10,15,20-tetrakis(2,4,6-trimethylphenyl)porphyrin (5). This procedure was based upon the literature protocol for similar compound.[xxxviii] All glassware used was oven dried at 100 °C for 2 h and cooled by the stream of nitrogen. Two-neck round-bottomed flask was charged with **4** (562 mg, 0.679 mmol), dry dichloromethane (120 mL), and dry methanol (30 mL). Palladium (10% on carbon, 590 mg) was added to the solution and the flask was shielded from light. The solution was purged with nitrogen and stirred at room temperature for 1 h, and placed into the ice-bath. Sodium borohydride (640 mg, 16.9 mmol) was added to the solution in small portions over a 10 min period. Progress of the reaction was monitored by silica TLC (hexane/CH_2Cl_2 = 1:1), where the

reactant (**4**) moved slightly faster than the amino product (**5**) on the plate, as described in the literature for similar compound.[8b] The reactant seemed to be completely consumed after 1.2 h of the reaction. Solvent was removed by using rotary evaporator, and the residue was passed through a plug of Celite using dichloromethane as eluent in the dark. The crude product was concentrated in vacuo, and was directly used for the next reaction without further purification due to the unstability against photo-oxidation.[7] (499 mg, 0.63 mmol, 92.0 % yield). MS (MALDI-TOF) *m/z* 799.2 ($M+H^+$).

2,3-Dioxo-5,10,15,20-tetrakis(2,4,6-trimethylphenyl)chlorin (6). This procedure was based upon the literature protocol for similar compound.[7c] To a solution of **5** (430 mg, 0.54 mmol) in a dichloromethane (140 mL) was added a Dess-martin periodinane (250 mg, 0.59 mmol). Progress of the reaction was monitored by mass spectrometry (MALDI-TOF) due to the reactant and product showed indistinguishable color and R_f values on silica TLC (hexane:CH_2Cl_2 = various ratios).[xxxix] The reaction mixture was stirred for 30 h in the dark. Hydrochloric acid (1.0 M, 90 mL) was added to the solution and stirred for 1 h to hydrolyze undesirable imine products. The reaction mixture was treated with saturated aqueous sodium bicarbonate and washed with water. Organic layer was collected, dried over anhydrous magnesium sulfate, and then the solvent was removed in vacuo. Column chromatography on silica gel (hexane/CH_2Cl_2 = 3:2 ~ 1:1) afforded **6** as a greenish brown solid. (163 mg, 0.2 mmol, 37 % yield). Unstable product was directly employed for the next reaction. MS (MALDI-TOF) *m/z* 812.6 ($M+H^+$).

5,10,15,20-Tetrakis(2,4,6-trimethylphenyl)-6'-methoxycarbonylquinoxalino[2,3-β]porphyrin (7a). This procedure was based upon the literature protocol for similar compound.[xl] Methyl 3,4-diaminobenzoate (27 mg, 0.16 mmol) and **6** (120 mg, 0.15 mmol) were charged into the Schlenk tube. Dry pyridine (3.2 mL) was added and the solution was stirred at 110 °C. Progress of the reaction was monitored by silica TLC (hexane/CH_2Cl_2 = 3:2). Although the reactant seemed to be completely consumed after 1 h, the reaction was made to proceed for 14 h. The reaction mixture was cooled to room

temperature, dissolved in dichloromethane, and separated with brine and water. Collected organic layer was dried over anhydrous sodium sulfate and the solvent was removed in vacuo. Purification by silica column chromatrography (hexane/CH_2Cl_2 = 1:1 ~ 2:3), and subsequent reprecipitation from CH_2Cl_2/MeOH gave **7a** as a deep violet solid. (102 mg, 0.11 mmol, 73 % yield). ^{1}H NMR (400 MHz, $CDCl_3$) δ 8.85 (d, *J*=4.9 Hz, 2H, β-pyrrolic H), 8.75 (d, *J*=4.9 Hz, 2H, β-pyrrolic H), 8.66 (d, ^4J=2.0 Hz, 1H, quinoxaline H), 8.54 (s, 2H, β-pyrrolic H), 8.36 (dd, *J*=8.8 and 2.0 Hz, quinoxaline H), 7.97 (d, *J*=8.8 Hz, 1H, quinoxaline H), 7.35 (s, 2H, phenyl H), 7.33 (s, 2H, phenyl H), 7.28 (s, 4H, phenyl H), 2.76 (s, 3H, methyl H), 2.75 (s, 3H, methyl H), 2.63 (s, 6H, methyl H), 1.89 (s, 12H, methyl H), 1.75 (s, 12H, methyl H), -2.36 (s, 2H, inner H); FT-IR (KBr) ν_{max} 3348, 2917, 2859, 1728 (ester), 1611, 1437, 1341, 1304, 1254, 1140, 1119, 979, 851, 819, 803, 725 cm^{-1}; MS (MALDI-TOF) *m/z* 942.6 ($M+H^+$).

5,10,15,20-Tetrakis(2,4,6-trimethylphenyl)-6'-carboxyquinoxalino[2,3-β]porphyrin (8a). To a solution of **7a** (100 mg, 0.11 mmol) in 2-propanol (40 mL) was added a solution of potassium hydroxide (0.66 g, 11.8 mmol) in water (10 mL). The solution was refluxed (80 °C) for 2 h. After cooling to room temperature, the reaction mixture was treated with aqueous HCl (1M, 12 mL) solution. The solution was washed with saturated aqueous sodium bicarbonate and water. Organic layer was collected, dried over anhydrous magnesium sulfate, and then the solvent was removed in vacuo. Reprecipitation from CH_2Cl_2/hexane gave **8a** as a deep violet solid (91 mg, 0.098 mmol, 89 %). Mp > 300 ^{o}C; ^{1}H NMR (400 MHz, acetone-d_6) δ 8.76 (d, *J*=4.9 Hz, 2H, β-pyrrolic H), 8.70 (d, *J*=4.9 Hz, 2H, β-pyrrolic H), 8.54 (d, ^4J=2.0 Hz, 1H, quinoxaline H), 8.40 (s, 2H, β-pyrrolic H), 8.33 (dd, *J*=8.8 and 2.0 Hz, quinoxaline H), 7.90 (d, *J*=8.8 Hz, 1H, quinoxaline H), 7.27 (s, 2H, phenyl H), 7.26 (s, 2H, phenyl H), 7.23 (s, 4H, phenyl H), 2.61 (s, 3H, methyl H), 2.60 (s, 3H, methyl H), 2.49 (s, 6H, methyl H), 1.76 (s, 12H, methyl H), 1.65 (s, 6H, methyl H), 1.65 (s, 6H, methyl H), -2.35 (s, 2H, inner H); FT-IR (KBr) ν_{max} 3436, 3350, 2918, 2856, 1736, 1706, 1612, 1446, 1344, 1212, 1141, 1120, 980,

803, 725 cm^{-1}; MS (MALDI-TOF) *m/z* 926.2 ($M+H^+$).

5,10,15,20-Tetrakis(2,4,6-trimethylphenyl)-6'-carboxyquinoxalino[2,3-β]porphyrin atozinc (II) (ZnQMA). To a solution of **8a** (85 mg, 0.091 mmol) in chloroform (148 mL) was added a solution of zinc acetate dihydrate (300 mg, 1.37 mmol) in methanol (25 mL). The solution was stirred at reflux for 18 h. The solvent was removed by using a rotary evaporator, and the residue dissolved in dichloromethane and passed through filter paper (ADVANTEC). The filtrate was washed with water, dried over anhydrous sodium sulfate, and then the solvent was removed in vacuo. Reprecipitation from CH_2Cl_2/acetonitrile gave **ZnQMA** as a deep purple solid (57 mg, 0.057 mmol, 63 % yield). ^{1}H NMR (400 MHz, acetone-d_6 + CD_3OD) δ 8.73 (d, ^4J=1.4 Hz, 1H, quinoxaline H), 8.70-8.66 (m, 4H, β-pyrrolic H), 8.56 (s, 2H, β-pyrrolic H), 8.46 (dd, *J*=8.8 and 1.4 Hz, quinoxaline H), 8.07 (d, *J*=8.8 Hz, 1H, quinoxaline H), 7.36 (s, 2H, phenyl H), 7.35 (s, 2H, phenyl H), 7.32 (s, 4H, phenyl H), 2.72 (s, 6H, methyl H), 2.61 (s, 6H, methyl H), 1.89 (s, 12H, methyl H), 1.78 (s, 6H, methyl H), 1.77 (s, 6H, methyl H); UV-vis (MeOH) λ_{max} (nm) 420.5, 578.0, 621.5; MS (MALDI-TOF) *m/z* found 991.3($M+H^+$).

5,10,15,20-Tetrakis(2,4,6-trimethylphenyl)-6',7'-bis(methoxycarbonyl)quinoxalino[2,3-β]porphyrin (7b). This procedure was based upon the literature protocol for similar compound.[40] Dimethyl 4,5-diaminophthalate (37 mg, 0.17 mmol) and **6** (130 mg, 0.16 mg) were charged into the Schlenk tube. Dry pyridine (3.5 mL) was added and the solution was stirred at 110 °C. Progress of the reaction was monitored by silica TLC (hexane/CH_2Cl_2 = 3:2). Although the reactant seemed to be completely consumed after 1 h, the reaction was made to proceed for 14 h. The reaction mixture was cooled to room temperature, dissolved in dichloromethane, and separated with brine and water. Collected organic layer was dried over anhydrous sodium sulfate and the solvent was removed in vacuo. Purification by silica column chromatography (hexane/CH_2Cl_2 = 3:2 ~ 1:1), and subsequent reprecipitation from CH_2Cl_2/MeOH gave **7b** as a deep violet solid. (130 mg, 0.13 mmol, 81 % yield). ^{1}H NMR (400 MHz, $CDCl_3$) δ 8.84 (d, *J*=4.9 Hz, 2H,

β-pyrrolic H), 8.75 (d, *J*=4.9 Hz, 2H, β-pyrrolic H), 8.54 (s, 2H, β-pyrrolic H), 8.32 (s, 2H, quinoxaline H), 7.33 (s, 4H, phenyl H), 7.28 (s, 4H, phenyl H), 2.74 (s, 6H, methyl H), 2.63 (s, 6H, methyl H), 1.89 (s, 12H, methyl H), 1.73 (s, 12H, methyl H), -2.37 (s, 2H, inner H); FT-IR (KBr) ν_{max} 3450, 3350, 2949, 2917, 2856, 1735 (ester), 1611, 1437, 1342, 1261, 1215, 1135, 1057, 979, 970, 851, 802, 726, 714 cm^{-1}; MS (MALDI-TOF) *m/z* 999.6 ($M+H^+$).

5,10,15,20-Tetrakis(2,4,6-trimethylphenyl)-6',7'-dicarboxyquinoxalino[2,3-β]porphyrin (8b). To a solution of **7b** (123 mg, 0.12 mmol) in 2-propanol (90 mL) was added a solution of potassium hydroxide (1.53 g, 27.3 mmol) in water (23 mL). The solution was refluxed (80 °C) for 2h. After cooling to room temperature, the reaction mixture was treated with aqueous HCl (1M, 28mL) solution. The solution was washed with saturated aqueous sodium bicarbonate and water. Collected organic layer was dried over anhydrous sodium sulfate, and then the solvent was removed in vacuo. Reprecipitation from CH_2Cl_2/hexane gave **8b** as a deep violet solid (104 mg, 0.11 mmol, 89 %). Mp > 300 ^oC; ^1H NMR (400 MHz, acetone-d_6) δ 8.87 (d, *J*=4.9 Hz, 2H, β-pyrrolic H), 8.82 (d, *J*=4.9 Hz, 2H, β-pyrrolic H), 8.52 (s, 2H, β-pyrrolic H), 8.47 (s, 2H, quinoxaline H), 7.38 (s, 4H, phenyl H), 7.35 (s, 4H, phenyl H), 2.71 (s, 6H, methyl H), 2.61 (s, 6H, methyl H), 1.88 (s, 12H, methyl H), 1.78 (s, 12H, methyl H), -2.23 (s, 2H, inner H); FT-IR (KBr) ν_{max} 3350, 2917, 2860, 1716, 1611, 1441, 1343, 1211, 1139, 979, 852, 821, 802, 725 cm^{-1}; MS (MALDI-TOF) *m/z* 971.9 ($M+H^+$).

5,10,15,20-Tetrakis(2,4,6-trimethylphenyl)-6',7'-dicarboxyquinoxalino[2,3-β]porphyrinatozinc (II) (ZnQDA). To a solution of **8a** (90 mg, 0.092 mmol) in chloroform (150 mL) was added a solution of zinc acetate dihydrate (450 mg, 2.1 mmol) in methanol (30 mL). The solution was stirred at reflux (60 °C) for 18 h. The solvent was removed by using a rotary evaporator, and the residue dissolved in dichloromethane and passed through filter paper (ADVANTEC). The filtrate was washed with water, dried over anhydrous sodium sulfate, and then the solvent was removed in vacuo. Reprecipitation

from CH_2Cl_2/hexane gave **ZnQDA** as a deep purple solid (77 mg, 0.075 mmol, 81 % yield). ^{1}H NMR (400 MHz, acetone-d_6 + CD_3OD) δ 8.70 and 8.67 (ABq, *J*=4.4 Hz, 4H, β-pyrrolic H), 8.57 (s, 2H, β-pyrrolic H), 8.42 (s, 2H, quinoxaline H), 7.36 (s, 4H, phenyl H), 7.32 (s, 4H, phenyl H), 2.71 (s, 6H, methyl H), 2.61 (s, 6H, methyl H), 1.88 (s, 12H, methyl H), 1.77 (s, 12H, methyl H); UV-vis (MeOH) λ_{max} (nm) 424.5, 583.5, 627.5; MS (MALDI-TOF) *m/z* 1034.0 ($M+H^+$).

Optical Spectroscopy. UV-visible absorption spectra of the porphyrins in methanol and the porphyrin monolayers on the TiO_2 electrodes were recorded using a Perkin-Elmer Lambda 900 UV/vis/NIR Spectrometer. Steady-state fluorescence spectra were acquired by using a SPEX Fluoromax-3 Spectrofluorometer. Time-resolved fluorescence spectra were measured by a single-photon counting method using a second harmonic generation (SHG, 400 nm) of a Ti:sapphire laser (Spectra-Physics, Tsunami 3950-L2S, 150 fs fwhm) and a streakscope (Hamamatsu Photonics, C4334-01) equipped with a polychromator (Acton Research, SpectraPro 150) as an excitation source and a detector, respectively. Spectroscopy grade methanol was used for the measurements of UV-visible absorption spectra, fluorescence spectra, and fluorescence lifetimes.

Electrochemistry. Electrochemical measurements were made using a BAS 50W electrochemical analyzer. Redox potentials of the porphyrins in solution were determined by differential pulse voltammetry (DPV) as well as cyclic voltammery (CV) in dichloromethane containing 0.1 M tetrabutylammonium perchlorate (TBAP) as a supporting electrolyte. A glassy carbon working electrode (3 mm diameter), $Ag/AgNO_3$ (0.01M in acetonitrile) reference electrode, and Pt wire counter electrode were employed. Ferrocene/ferrocenium (+0.642 V vs NHE) was used as an internal standard for all measurements. For DPV measurements, scan rate of 50 mV s^{-1}, pulse amplitude of 50 mV, pulse width of 50 ms, and pulse period of 200 ms were employed. For CV measurements, scan rate of 100 mV s^{-1} was employed. The oxidation potentials for the adsorbed porphyrins on the TiO_2 films were measured by cyclic voltammetry in acetonitrile

containing 0.1 M tetrabutylammonium perchlorate (TBAP) at a scan rate of 100 mV s^{-1}. The porphyrin-modified TiO_2 electrode was employed as a working electrode along with the Ag/AgCl (saturated KCl) reference electrode (+0.197 V vs NHE) and Pt wire counter electrode. All of the measured potentials were converted to the NHE scale.

Density Functional Theory (DFT) Calculations. Geometry optimization and electronic structure calculations of the porphyrins were performed by using B3LYP functional and 3-21G (d) basis set implemented in the Gaussian 03 program package.[xli] Molecular orbitals were visualized by GaussView 3.0 software.

X-ray Photoelectron Spectroscopy (XPS) Measurements. The XPS data were acquired using an ULVAC-PHI 5500MT system equipped with Mg Kα X-ray source (1253.6 eV) and a hemispherical energy analyzer. The electron takeoff angle was set at 45 degree and the pressure of the main XPS chamber was maintained of less than 2.4×10^{-9} Torr during analysis. All of the XPS peak positions were referenced to the O1s peak of the TiO_2 substrate at 530.2 eV. Peaks of interests were deconvoluted by Gaussian/Lorentzian mixed functions with PeakFit 4.12 program. All of the samples for XPS measurements were made by the same method for preparing the porphyrin monolayers on the TiO_2 electrodes.

Preparation of Porphyrin-Modified TiO_2 Electrode and Photovoltaic Measurements. Preparation of mesoporous TiO_2 films, immobilization of the porphyrins on the TiO_2 surface, and characterization of the photovoltaic properties of porphyrin-modified TiO_2 were made by following the procedures reported previously.[23] Methanol was used as an immersing solvent in the present experiments instead of ethanol. The TiO_2 electrodes modified with ZnQMA and ZnQDA are denoted as TiO_2/ZnQMA and TiO_2/ZnQDA, respectively. The amounts of the porphyrins adsorbed on the TiO_2 films were determined by measuring the changes in the absorbance of the porphyrin solutions (4 mL) before and after immersing the TiO_2 films (0.25 cm^2 of projected area).

References and Notes

(i) Tanaka, M.; Hayashi, S.; Eu, S.; Umeyama, T.; Matano, Y.; Imahori, H. *Chem. Commun*. **2007**, 2069.

(ii) Chen, C.-T.; Yeh, H.-C.; Zhang, X.; Yu, J. *Org. Lett.* **1999**, *1*, 1767.

(iii) (a) Wang, Q.; Campbell, W. M.; Bonfantani, E. E.; Jolley, K. W.; Officer, D. L.; Walsh, P. J.; Gordon, K.; Humphry-Baker, R.; Nazeeruddin, Md. K.; Grätzel, M. *J. Phys. Chem. B* **2005**, *109*, 15397. (b) Campbell, W. M.; Jolley, K. W.; Wagner, P.; Wagner, K.; Walsh, P. J.; Gordon, K. C.; Schmidt-Mende, L.; Nazeeruddin, Md. K.; Wang, Q.; Grätzel, M.; Officer, D. L. *J. Phys. Chem. C* **2007**, *111*, 11760.

(iv) (a) Sendt, K.; Johnston, L. A.; Hough, W. A.; Crossley, M. J.; Hush, N. S.; Reimers, J. R. *J. Am. Chem. Soc.* **2002**, *124*, 9299. (b) Reimers, J. R.; Hall, L. E.; Crossley, M. J.; Hush, N. S. *J. Phys. Chem. A* **1999**, *103*, 4385. (c) Cai, Z.-L.; Crossley, M. J.; Reimers, J. R.; Kobayashi, R.; Amos, R. D. *J. Phys. Chem. B* **2006**, *110*, 15624. (d) Crossley, M. J.; McDonald. J. A. *J. Chem. Soc., Perkin Trans 1* **1999**, 2429. (e) Crossley, M. J.; Burn, P. L. *Chem. Commun*. **1991**, 1569.

(v) Kadish, K. M.; Wenbo. E.; Sintic, P. J.; Ou, Z.; Shao, J.; Ohkubo, K.; Fukuzumi, S.; Govenlock, L. J.; McDonald, J. A.; Try, A. C.; Cai, Z.-L.; Reimers, J. R.; Crossley, M. J. *J. Phys. Chem. B* **2007**, *111*, 8762.

(vi) Chng, L. L.; Chang, C. J.; Nocera, D. G. *J. Org. Chem.* **2003**, *68*, 4075.

(vii) (a) Crossley, M. J.; King, L. G. J. *Chem. Commun.* **1984**, 920. (b) Crossley, M. J.; King, L. G.; Newsom, I. A.; Sheehan, G. S. *J. Chem. Soc., Perkin Trans 1* **1996**, 2675. (c) Promarak, V.; Burn, P. L. *J. Chem. Soc., Perkin Trans. 1* **2001**, 14.

(viii) (a) Lindsey, J. S.; Wagner, R. W. *J. Org. Chem.* **1989**, *54*, 828. (b) Vannelli, T. A.; Karpishin, T. B. *Inorg. Chem.* **2000**, *39*, 340. (c) Lundin, N. J.; Walsh, P. J.; Howell, S. L.; McGarvey, J. J.; Blackman, A. G.; Gordon, K. C. *Inorg. Chem.* **2005**, *44*, 3551. (d) Williams, R. L.; Shalay, S. W. *J. Heterocycl. Chem.* **1973**, *10*, 891.

(ix) Giraudeau, A.; Callot, H. J.; Jorgan, J.; Ezhar, I.; Gross, M. *J. Am. Chem. Soc.* **1979**, *101*, 3857. Although the β nitration in the typical Crossley's protocol is accomplished by using gaseous nitrogen dioxide, the method was not employed because it is a rather inconvenient and expensive procedure.

(x) Catalano, M. M.; Crossley, M. J.; Harding, M. M.; King, L. G. *Chem. Commun*. **1984**, 1535. While the Ni (II) counterpart of copper porphyrin **2**, 5,10,15,20-tetrakis(2,4,6-trimethylphenyl)porphyrinatonickel (II), displayed the similar reactivity for the nitration, demetalation of the nickel porphyrin showed too low yield in these experiments.

(xi) Both 2,3-Dioxo-5,10,15,20-tetrakis(2,4,6-trimethylphenyl)chlorinatocopper (II) and 2,3-dioxo-5,10,15,20-tetrakis(2,4,6-trimethylphenyl)chlorinatonickel (II) showed higher stability than the free base one, and could be used for the Schiff base forming reaction with the diamine compounds, but demetalations of the resulting carboxyquinoxalino[2,3-β]porphyrins were practically impossible, at least in this experiment.

(xii) Initially, it was attempted in dichloromethane or ethanol solutions; however, neither of the trials were successful.

(xiii) Foresman, J. B.; Frisch, A. In *Exploring Chemistry with Electronic Structure Methods*; Gaussian Inc.: Pittsburgh, PA, 1995.

(xiv) Hagberg, D. P.; Edvinsson, T.; Marinado, T.; Boschloo, G.; Hagfeldt, A.; Sun, L. *Chem. Commun.* **2006**, 2245.

(xv) Piotrowiak, P.; Galoppini, E.; Wei, Q.; Meyer, G. J.; Wiewior, P. *J. Am. Chem. Soc.* **2003**, *125*, 5278.

(xvi) Gouterman, M. *J. Chem. Phys.* **1959**, *30*, 1139.

(xvii) Gierschner, J.; Cornil, J.; Egelhaaf, H.-J. *Adv. Mater.* **2007**, *19*, 173.

(xviii) (a) Rehm, J. M.; McLendon, G. L.; Nagasawa, Y.; Yoshihara, K.; Moser, J.; Grätzel, M. *J. Phys. Chem.***1996**, *100*, 9577. (b) Burfeindt, B.; Hannappel, T.; Storck, W.; Willig, F. *J. Phys. Chem.* **1996**, *100*, 16463. (c) Hilgendorff, M.; Sundström, V. *J. Phys. Chem. B.* **1998**, *102*, 10505. (d) Asbury, J. B.; Hao, E.; Wang, Y.; Ghosh, H. N.; Lian, T. *J. Phys. Chem. B* **2001**, *105*, 4545. (e) Tachibana, Y.; Haque, S. A.; Mercer, I. P.; Durrant, J. R.; Klug, D. R. *J. Phys. Chem. B* **2000**, *104*, 1198.

(xix) (a) Brett, C. M. A.; Brett, A. M. O. In *Electrochemistry-Principles, Methods, and Applications*; Oxford University Press: New York, 1993; p 185. (b) Bard, A. J.; Faulkner, L. R. In *Electrochemical Methods-Fundamentals and Applications,* 2nd

ed.; John Wiley & Sons: New York, 2001; p 590.

(xx) (a) Södergren, S.; Hagfeldt, A.; Olsson, J.; Lindquist, S.-E. *J. Phys. Chem.* **1994**, *98*, 5552. (b) Pichot, F.; Gregg, B. A. *J. Phys. Chem. B* **2000**, *104*, 6. (c) Lee, J.-J.; Coia, G. M.; Lewis, N. S. *J. Phys. Chem. B* **2004**, *108*, 5269.

(xxi) (a) Cass, M. J.; Walker, A. B.; Martinez, D.; Peter, L. M. *J. Phys. Chem. B* **2005**, *109*, 5100. (b) Frank, A, J.; Kopidakis, van de Lagemaat, J. *Coord. Chem. Rev.* **2004**, *248*, 1165. (c) Peter, L. M. *J. Phys. Chem. C* **2007**, *111*, 6601.

(xxii) Kamat, P. V.; Haria, M.; Hotchandani, S. *J. Phys. Chem. B* **2004**, *108*, 5166.

(xxiii) Eu, S.; Hayashi, S.; Umeyama, T.; Oguro, A.; Kawasaki, M.; Kadota, N.; Matano, Y.; Imahori, H. *J. Phys. Chem. C* **2007**, *111*, 3528.

(xxiv) (a) Fillinger, A.; Parkinson, B. A. *J. Electrochem. Soc.* **1999**, *146*, 4559. (b) Lu, Y.; Choi, D.; Nelson, J.; Yang, O.; Parkinson, B. A. *J. Electrochem. Soc*. **2006**, *153*, E131. (c) Vittadini, A.; Selloni, A.; Rotzinger, F. P.; Grätzel, M. *J. Phys. Chem. B* **2000**, *104*, 1300. (d) Finnie, K. S.; Bartlett, J. R.; Woolfrey, J. L. *Langmui*r **1998**, *14*, 2744.

(xxv) Johansson, E. M. J.; Hedlund, M.; Siegbahn, H.; Rensmo, H. *J. Phys. Chem. B* **2005**, *109*, 22256.

(xxvi) Patthey, L.; Rensmo, H.; Persson, P.; Westermark, K.; Vayssieres, L.; Stashans, A.; Petersson, Å.; Bruhwiler, P. A.; Siegbahn, H.; Lunell, S.; Martensson, N. *J. Chem. Phys*. **1999**, *110*, 5913.

(xxvii) We cannot rule out the probability of the carbonyl oxygen coordination to the TiO_2 surface. Readers who are interested in the possible adsorption modes of carboxylic acid group onto the TiO_2 surface should be referred to the reference. Vittadini, A.; Selloni, A.; Rotzinger, F. P.; Grätzel, M. *J. Phys. Chem. B* **2000**, *104*, 1300.

(xxviii) Ito, S.; Liska, P.; Comte, P.; Charvet, R. L.; Pechy, P.; Bach, U.; Schmidt-Mende, L.; Zakeeruddin, S. M.; Kay, A.; Nazeeruddin, Md. K.; Gratzel, M. *Chem. Commun.* **2005**, 4351.

(xxix) (a) Wang, Z.-S.; Kawauchi, H.; Kashima, T.; Arakawa, H. *Coord. Chem. Rev.* **2004**, *248*, 1381. (b) Wang, Z.-S.; Huang, C.-H.; Huang, Y.-Y.; Hou, Y.-J.; Xie,

P.-H.; Zhang, B.-W.; Cheng, H.-M. *Chem. Mater.* **2001**, *13*, 678. (c) Kusama, H.; Arakawa. H. *J. Photochem. Photobiol., A* **2003**, *160*, 171.

(xxx) Grätzel, M. *Inorg. Chem.* **2005**, *44*, 6841.

(xxxi) Kroeze, J. E.; Hirata, N.; Koops, S.; Nazeeruddin, Md. K.; Schmidt-Mende, L.; Grätzel, M.; Durrant, J. R. *J. Am. Chem. Soc.* **2006**, *128*, 16376.

(xxxii) (a) Hara, K.; Miyamoto, K.; Abe, Y.; Yanagida, M. *J. Phys. Chem. B* **2005**, *109*, 23776. (b) Chen, R.; Yang, X.; Tian, H.; Wang, X.; Hagfeldt, A.; Sun, L. *Chem. Mater.* **2007**, *19*, 4007.

(xxxiii) Nazeeruddin, Md. K.; Zakeeruddin, S. M.; Humphry-Baker, R.; Jirousek, M.; Liska, P.; Vlachopoulos, N.; Shklover, V.; Fischer, C.-H.; Grätzel, M. *Inorg. Chem.* **1999**, *38*, 6298.

(xxxiv) Rühle, S.; Greenshtein, M.; Chen, S.-G.; Merson, A.; Pizem, H.; Sukenik, C. S.; Cahen, D.; Zaban, A. *J. Phys. Chem. B* **2005**, *109*, 18907.

(xxxv) (a) Clark, C. C.; Meyer, G. J.; Wei, Q.; Galoppini, E. *J. Phys. Chem. B* **2006**, *110*, 11044. (b) Hodes, G. In *Electrochemistry of Nanomaterials*; Wiley-VCH: Weinheim, 2001; p 219.

(xxxvi) Nazeeruddin, Md. K.; Humphry-Baker, R.; Liska, P.; Grätzel, M. *J. Phys. Chem. B* **2003**, *107*, 8981.

(xxxvii) Carcel, C. M.; Laha, J. K.; Loewe, R. S.; Thamyongkit, P.; Schweikart, K. -H.; Misra, V.; Bocian, D. F.; Lindsey, J. S. *J. Org. Chem.* **2004**, *69*, 6739.

(xxxviii) Baldwin, J. E.; Crossley, M. J.; DeBernardis, J. *Tetrahedron* **1982**, *38*, 685.

(xxxix) Contrary to the present case, inner metallated ones (e.g., Cu (II) or Ni (II) porphyrin and chlorin) showed different colors and R_f values under the similar conditions.

(xl) Beavington, R.; Burn, P. L. *J. Chem. Soc., Perkin Trans. 1* **2000,** 1231.

(xli) Frisch, M. J. *et al. Gaussian 03*, revision C.02; Gaussian, Inc.: Wallingford, CT, 2004.

CHAPTER 3

Synthesis of Sterically Hindered Phthalocyanines and Their Applications to Dye-Sensitized Solar Cells

Introduction

The fundamental aspects of the DSSCs have been well documented based on widespread research efforts to disclose the nature of the devices including interfacial photoinduced electron transfer, role of mesoporous semiconductor electrode, and electrolyte.[i] From the practical and industrial point of view, however, the improvement in the performance has been rather stagnated during the last two decades. The main reason for this could be attributed to the limited light-harvesting capabilities of the existing dyes, especially for the near-infrared region.[ii] As such, to devise and develop novel photosensitizer dyes that can effectively harvest the red light is an urgent task to make the DSSCs practically viable.

Phathalocyanines are the proper choice for this objective due to their strong Q band light absorption properties at around 700 nm.[iii] Their extreme stabilities against thermal, chemical, and photochemical reactions are definitively desirable features for the long-term and outdoor robustness of DSSCs. Applications of phthalocyanines for DSSCs as photosensitizers, however, have not been successful.[iv] Notoriously poor solubility to common organic solvents and a high tendency to form aggregations have been attributed as the main reasons impeding the revelation of their potential as use for DSSCs. A recent study by Torres and Nazeeruddin et al. demonstrated the usefulness of phthalocyanines for red light-harvesting provided that the degree of aggregation is partially diminished by introducing three bulky *t*-butyl groups into the macrocycle plane.[v] The directionality in the excited state of the dye was also emphasized as an

important factor for efficient light-harvesting. However, the reported compound is a mixture of the regioisomers, and this may result in the formation of rather complex monolayer on the TiO_2 surface, making it difficult to disclose the relationship between the monolayer structure and the photovoltaic properties. More importantly, the cell performance is still aided with the co-adsorption of chenodeoxycholic acid which is well-known to suppress dye aggregation on the TiO_2 surface. Although the power conversion efficiency is the highest among the reported phthalocyanine-sensitized TiO_2 cell (η =3.5 %), it is much lower than those of Ru dye-based DSSCs (η =10-11 %).[2-4] Therefore, further studies are still needed to elucidate the close relationship between the molecular structure and the photovoltaic properties toward the improvement of cell performances.

In this chapter, the synthesis and photovoltaic properties of a novel highly substituted zinc phthalocyanine carboxylic acid (ZnPc) and its metal free counterpart (H_2Pc), as depicted in Figure 1, are reported. The compounds retain eight sterically hindered phenyl groups where the neighboring phenyl rings are rotated about each other

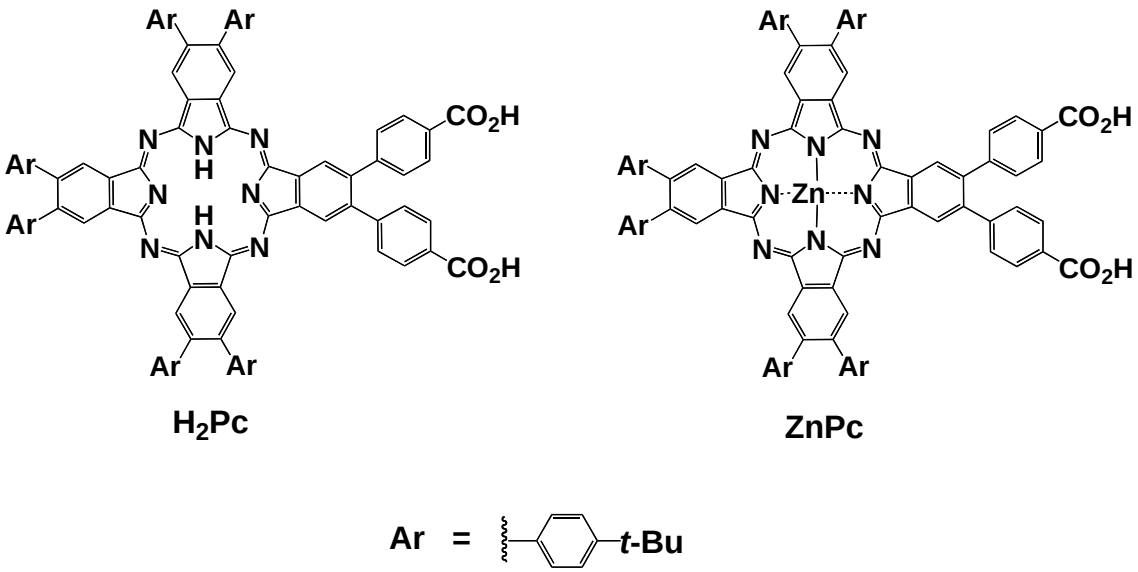

Figure 1. Structures of the phthalocyanines used in this study.

with respect to the phthalocyanine plane to avoid steric congestion around the *ortho*-protons. Moreover, the six phenyl groups also possess bulky *t*-butyl moieties. Therefore, ZnPc and H_2Pc are expected to show high solubility toward common organic solvents and a reduced tendency towards aggregation. Since the two neighboring β positions are occupied by the same functional groups, the target compound can be isolated free from the problem of regioisomeric mixtures. Two carboxylic acid binding groups could guarantee the stable immobilization of the phthalocyanine onto the TiO_2 surface. Additionally, intramolecular push-pull character afforded by electron-donating (*t*-butyl) and electron-withdrawing (carboxylic acid) groups would be anticipated to make the efficient electron transfer from the phthalocyanine excited singlet state to the conduction band (CB) of the TiO_2.

Results and Discussion

Synthesis. Syntheses of phthalocyanines used in this study were achieved by the statistical condensation method.[vi] A key step in this protocol is the preparation of the adequate phthalonitrile precursors. Synthetic routes to H_2Pc and ZnPc are displayed in Scheme 1. Precursor compound **1** was accomplished by the Suzuki-Miyaura cross-coupling reaction between the 4,5-dichlorophthalonitrile and 4-*t*-butylphenylboronic acid. Suzuki-Miyaura coupling is one of the most widely used reactions for C-C bond formation.[vii] However, it is well known that the coupling reactions for substrates with high steric hindrance or for the arylchlorides are ineffective, as for the substrate in this study. To attain the desired compound, we have employed electron-rich and sterically hindered ligand, 2-(2',6'-dimethoxybiphenyl)dicyclohexylphosphine (S-Phos). [viii] Because the electron-rich ligand with high steric hindrance such as S-Phos or P(*t*-Bu)$_3$ makes the palladium (0) coordinatively unsaturated, the cross-coupling reactions even for the difficult substrates proceeded smoothly with moderate to good yield.[ix]

SCHEME 1

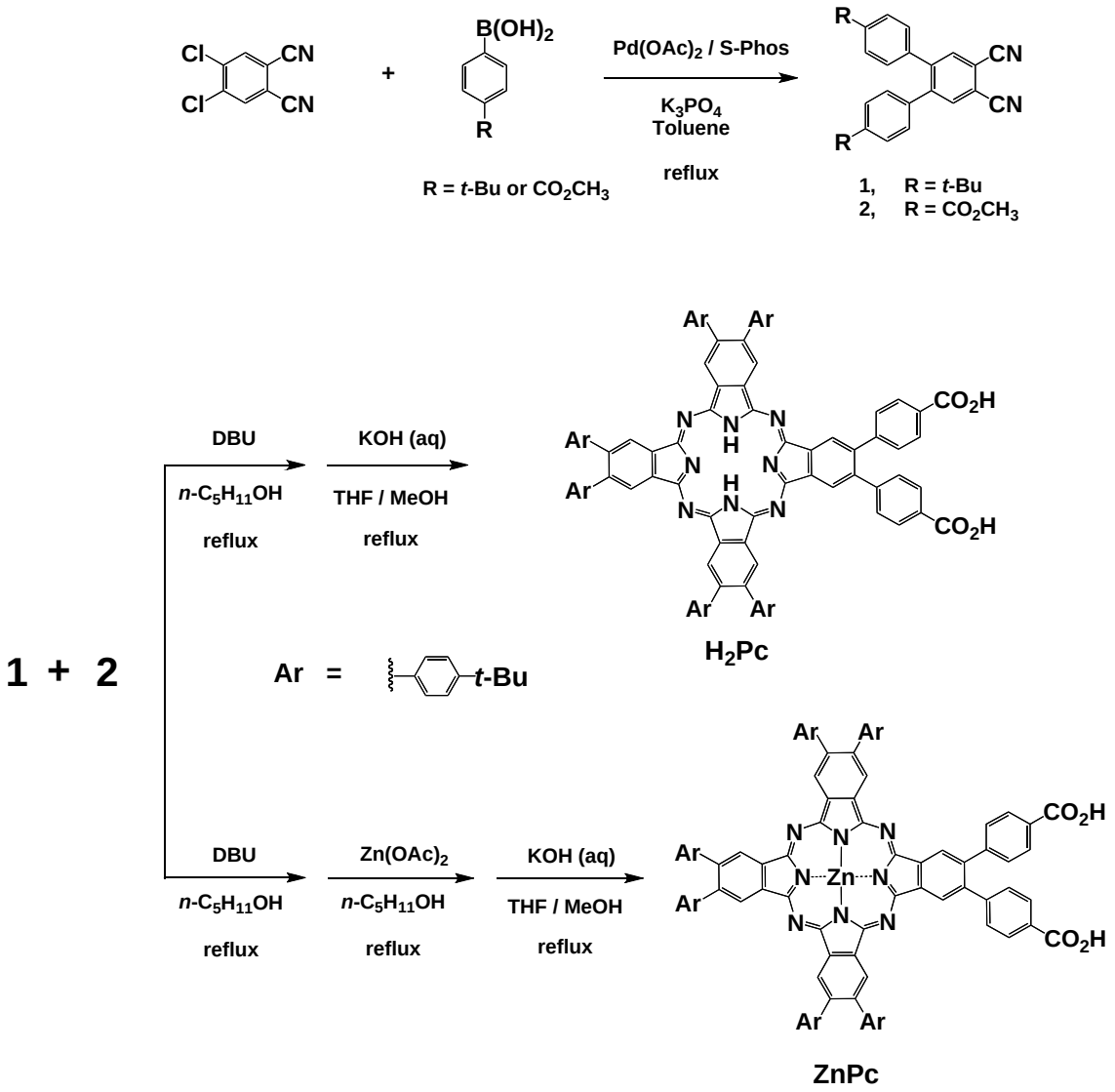

Precursor compound **2** was also achieved through Suzuki-Miyaura cross-coupling between 4,5-dichlorophthalonitrile and 4-(methoxycarbonylphenyl)boronic acid, but it needed longer reaction time compared with that of **1**. Owing to the presence of ester group, the boronic acid would be an inferior nucleophile compared with 4-*t*-butylphenylboronic acid, and this could be the reason of the longer reaction time. After obtaining the precursor compounds, it was tried to obtain the desired cyclo-tetramer by statistical condensation of **1** and **2** in 1-pentanol in the presence of

DBU (1,8-diazabicyclo[5.4.0]undec-7-ene). Although we have expected to prepare 2,3,9,10,16,17-hexakis(4-*t*-butylphenyl)-23,24-bis(4-methoxycarbonylphenyl)phthalocyanine, we obtained a mixture of two phthalocyanine compounds. The compounds showed two molecular ion peaks at 1630.7 and 1686.8 with an intensity ratio of 1:3 in the mass spectrometrum (MALDI-TOF). The peaks correspond to 2,3,9,10,16,17-hexakis(4-*t*-butyl-phenyl)-23-(4-methoxycarbonylphenyl)-24-(4-pentoxycarbonylphenyl)phthalocyanine, and 2,3,9,10,16,17-hexakis(4-*t*-butylphenyl)-23,24-bis(4-pentoxycarbonylphenyl)-phthalocyanine, respectively. It is believed that the exchange reaction between the methoxide and pentoxide was occurred during the cyclo-condensation reaction, as already reported.[6(g),(h)] Because both of the compounds would afford the same target compound (i.e., H_2Pc) by hydrolysis, the mixture was directly employed for the next reaction without further purification. The basic hydrolysis of the compounds in THF/methanol containing aqueous potassium hydroxide solution afforded the corresponding phthalocyanine carboxylic acid, H_2Pc. To achieve the zinc phthalocyanine carboxylic acid (ZnPc), zinc (II) was inserted into the core of the phthalocyanine esters by treatment with zinc acetate. The resulting compounds displayed the molecular ion peaks at 1692.5 and 1748.6 in the mass spectrum (MALDI-TOF). The peaks correspond to 2,3,9,10,16,17-hexakis(4-*t*-butylphenyl)-23-(4-methoxycarbonylphenyl)-24-(4-pentoxycarbonylphenyl)phthalocyanatozinc (II) and 2,3,9,10,16,17-hexakis-(4-*t*-butylphenyl)-23,24-bis(4-pentoxycarbonylphenyl)phthalocyanatozinc (II), respectively. The basic hydrolysis of the compounds in THF/methanol containing aqueous potassium hydroxide solution afforded the corresponding zinc phthalocyanine carboxylic acid, ZnPc. Structures of all the new compounds were verified by spectroscopic analyses including ^{1}H NMR, ^{13}C NMR, FT-IR, mass spectra, and elemental analyses.

Optical and Electrochemical Properties. UV-visible absorption spectra for H_2PC and ZnPc in THF are displayed in Figure 2. Each of the compounds showed characteristic optical features of zinc and metal free phthalocyanine, respectively. The peak positions in the B and Q bands regions are summarized in Table 1. The steady state fluorescence spectra of the phthalocyanines were also measured in THF and the wavelengths for emission maxima are listed in Table 1. The Stokes shifts are determined to be 68.2 cm^{-1} for H_2Pc and 165.6 cm^{-1} for ZnPc. This fairly small value suggests that the variations in the atomic coordinates during the electronic transitions are small for both of the compounds. From the intersection of the normalized absorption and emission spectra, the zero-zero excitation energies ($E_{0\text{-}0}$) are determined to be 1.73 eV for H_2Pc and 1.78 eV for ZnPc in THF.[x]

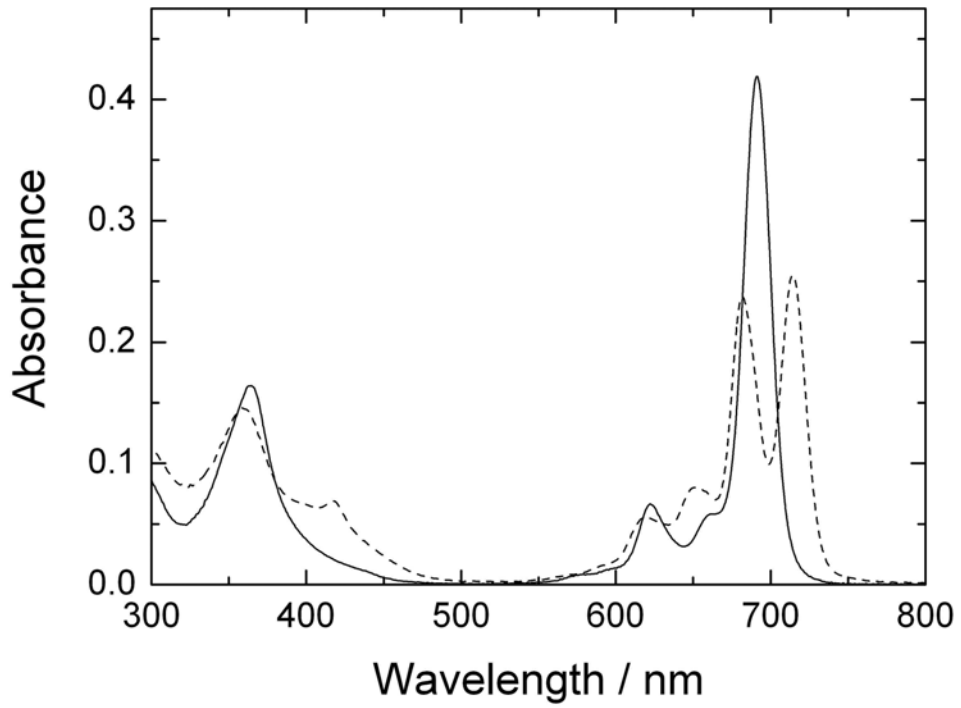

Figure 2. UV-visible absorption spectra of ZnPc (solid) and H_2Pc (dashed) measured in 2×10^{-6} M of THF solution. Optical length = 1 cm.

TABLE 1: Optical and Electrochemical Data for the Phthalocyanines and Driving Forces for Electron Transfer Processes on TiO_2.

	λ^{a}_{abs} / nm	λ^{b}_{em} / nm	$E_{ox}{}^{c}$ / V	$E_{0\text{-}0}{}^{d}$ / eV	$E_{ox}{}^{*e}$ / V	$\Delta G_{inj}{}^{f}$ / eV	$\Delta G_{reg}{}^{g}$ / eV
ZnPc	364.5 622.0 691.0	699 730	+ 0.94	1.78	- 0.84	- 0.34	- 0.44
H_2Pc	357.9, 416.3 619.4, 651.1 681.0, 714.5	718 747	+ 1.27	1.73	- 0.46	+ 0.04	- 0.77

[a] Wavelengths for B and Q bands maxima in THF. [b] Wavelengths for emission maxima in THF by exciting at the B band maxima. [c] Ground state oxidation potentials (vs NHE). [d] The zero-zero excitation energy estimated from the intersection of the normalized absorption and emission spectra. [e] Excited-state oxidation potentials approximated from E_{ox} and $E_{0\text{-}0}$ (vs NHE). [f] Driving forces for electron injection from the phthalocyanine excited singlet state (E_{ox}*) to the conduction band of the TiO_2 (-0.5 V vs NHE). [g] Driving forces for the regeneration of phthalocyanine radical cation (E_{ox}) by I^-/I_3^- redox couple (+0.5 V vs NHE).

To determine the first oxidation potential (E_{ox}) of the phthalocyanines, differential pulse voltammetry (DPV)[xi] measurements were performed in DMF containing 0.1M tetrabutylammonium hexafluorophosphate (TBAP) as a supporting electrolyte and the results are summarized in Table 1. Both H_2Pc and ZnPc display one oxidation peak corresponding to the phthalocyanine radical cation under the same sweep conditions (-0.1 V to +0.8 V vs $Ag/AgNO_3$). The oxidation potential of H_2Pc appears at +1.27 V (vs NHE), whereas that of ZnPc is determined to be +0.94 V (vs NHE). This indicates that the phthalocyanine is easier to oxidize upon zinc (II) metalation, as reported for other phthalocyanine compounds.[xii] This variation results in the important consequence of electron injection from the excited state dye (LUMO)

to the CB of the TiO_2 (*vide infra*). On the basis of the spectroscopic and electrochemical measurements, driving forces for electron injection from the LUMO of the dye to the CB of the TiO_2 (-0.5 V vs NHE) (ΔG_{inj})[xiii] and the regeneration of the dye radical cation by the I^-/I_3^- redox couple (+0.5V vs NHE) (ΔG_{reg})[15] for the phthalocyanine-sensitized solar cells are evaluated (Table 1). Both of the processes for ZnPc-sensitized TiO_2 cell are thermodynamically feasible, whereas the electron injection from the excited H_2Pc to the CB of the TiO_2 is thermodynamically uphill.

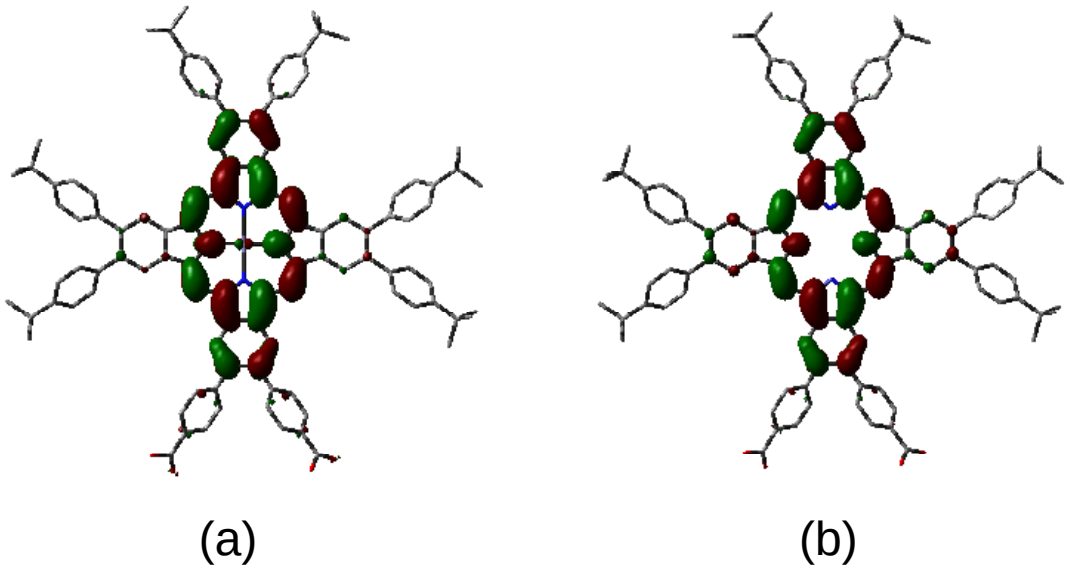

Figure 3. LUMOs of (a) ZnPc and (b) H_2Pc calculated by DFT methods with B3LYP/3-21G(d). The protons are omitted for clarity.

DFT Calculations. DFT calculations were employed to gain insight into the equilibrium geometry and electronic structures for the molecular orbitals of the phthalocyanines. The calculated structures do not show negative frequencies, implying that the optimized geometries are in the global energy minima.[xiv] Figure 3

illustrates the electron density distributions of H_2Pc and ZnPc in their respective LUMOs. Sufficient electron densities around the carboxylic acid binding group on the LUMO of dye are required for the good electronic coupling between the excited state of dye and 3d orbital of TiO_2.[xv] However, there exists little electron density distribution on and near the carboxylic acid binding groups of the phthalocyanines.

Photovoltaic and Photoelectrochemical Properties of Phthalocyanine-Sensitized TiO_2 Cells. Mesoporous TiO_2 films (10-μm-thick) were prepared from a colloidal suspension of TiO_2 nanoparticles (P25) (see Experimental Section). The TiO_2 electrodes were immersed into THF containing 0.05 mM phthalocyanine at room temperature to give the phthalocyanine-modified TiO_2 electrodes. Since the light-harvesting ability and consequently the cell performance are, to a large extent, controlled by the surface coverage (Γ) of the dye on the TiO_2 surface, first we examined the immersing time dependency of the Γ value for the phthalocyanines. Both of the dyes showed similar and rather slow adsorption rates, and reached saturated coverage (Γ) on the surface for about 10h of immersing time (Figure 4). Total amounts of the dyes adsorbed on the TiO_2 surface were determined by measuring the changes in the absorbance of the dye solutions before and after immersing the TiO_2 films. Dye concentrations on the TiO_2 films (0.25 cm^2 of area with thickness of 10

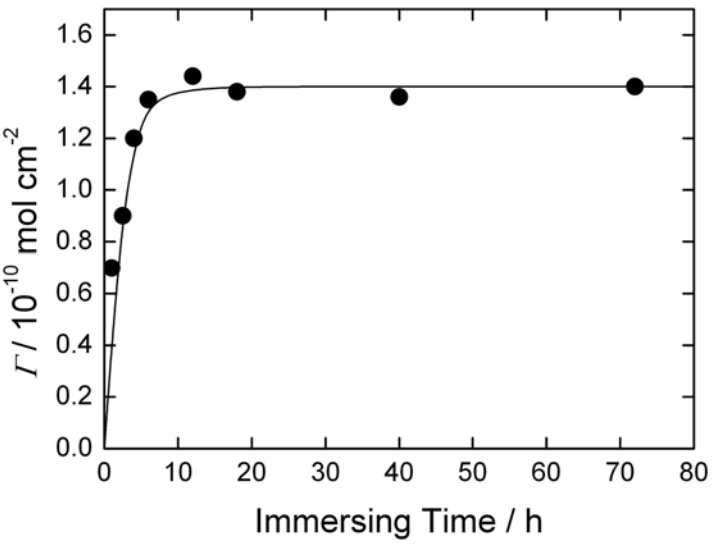

Figure 4. Profile of the surface coverage (Γ) of ZnPc on the TiO_2 electrode depending on the immersing time of the TiO_2 electrode into a THF solution of ZnPc (0.05 mM).

μm) are determined to be about 1.4×10^{-10} mol cm^{-2}. Assuming that (i) the phthalocyanine molecule is a rectangular hexahedron and (ii) the phthalocyanine molecules are densely packed onto the TiO_2 surface with a perpendicular orientation, the occupied area of one molecule on the TiO_2 surface is calculated to be ca. 103 $Å^2$ (4.3 × 24.0 $Å^2$). Accordingly, the Γ□□ value is estimated to be 1.6×10^{-10} mol cm^{-2}, which is close to the experimental value. The TiO_2 electrodes modified with H_2Pc and ZnPc are denoted as TiO_2/H_2Pc and TiO_2/ZnPc, respectively.

To judge the potential of H_2Pc and ZnPc as a photosensitizer for DSSC, we evaluated their cell performances using P25 TiO_2 film. A 10-μm-thick TiO_2 electrode was modified with H_2Pc (0.05 mM) which was dissolved in THF for an immersing time of 1-72 h. The H_2Pc-sensitized TiO_2 cell showed no power conversion due to the lower energy level of the H_2Pc excited singlet state (-0.46 V vs NHE) than that of the CB of the TiO_2 (-0.5 V vs NHE).[15] In contrast, the η values of the ZnPc-sensitized cell gradually increased with increasing the immersing time to reach maximum η values (η_{max}) of ca. 0.6 % for 12 h. The power conversion efficiency (η) is derived from the equation: $\eta = J_{SC} \times V_{OC} \times ff$, where J_{SC} is the short circuit current, V_{OC} is the open circuit potential, and ff is the fill factor. Further increase of the immersing time of

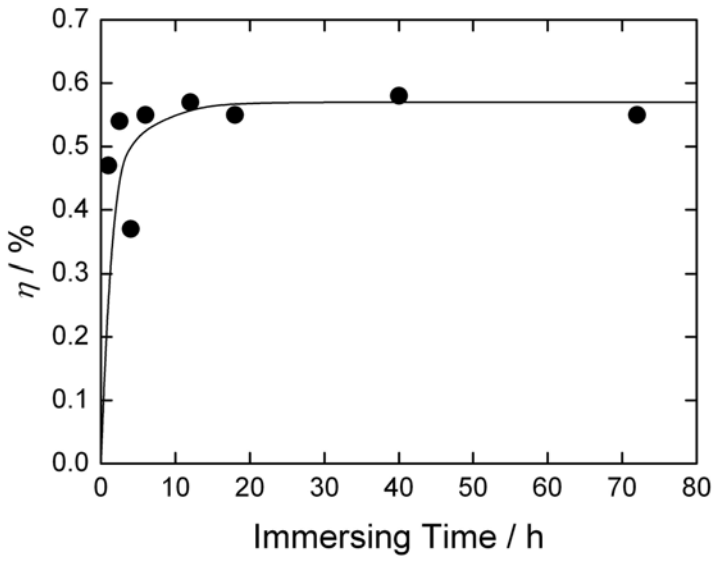

Figure 5. Profile of the power conversion efficiency (η) of a ZnPc-sensitized TiO_2 cell depending on the immersing time of the TiO_2 electrode in ZnPc-THF solution (0.05 mM).

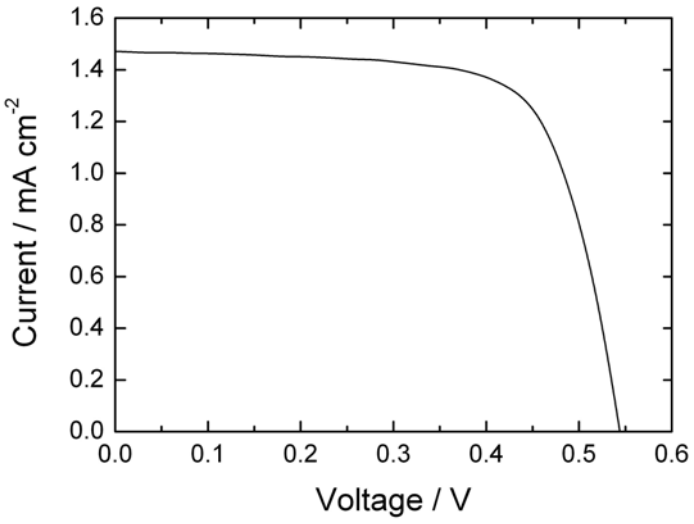

Figure 6. Photocurrent-voltage characteristics of a ZnPc-sensitized TiO_2 cell (η = 0.57 %, J_{sc} = 1.47 mA cm^{-2}, V_{oc} = 0.54 V, *ff* = 0.71). Conditions: electrolyte 0.1 M LiI, 0.05 M I_2, 0.6 M 2,3-dimethyl-1-propyl imidazolium iodide, and 0.5 M 4-*t*-butylpyridine in CH_3CN; input power: AM 1.5 under simulated solar light (100 mW cm^{-2}). $\eta = J_{sc} \times V_{oc} \times ff$.

up to 72 h exhibited no noticeable changes in the η values. The time profiles of the η values (Figure 5) correlate well with those of the Γ values (*vide supra*). This is in sharp contrast with the porphyrin-sensitized TiO_2 cells in which at first the η values are increased and then decreased significantly with increasing the immersing time.[4b, xvi] The representative photocurrent-voltage characteristics of ZnPc-sensitized TiO_2 cells with the immersing time of 12 h is depicted in Figure 6; η=0.57 ± 0.03 % with J_{SC}=1.47 ± 0.05 mA cm^{-2}, V_{OC}=0.54 ± 0.02 V, and *ff* =0.71 ± 0.03.

For the phthalocyanine-sensitized TiO_2 cell, co-adsorbates such as chenodeoxycholic acid have been employed to reduce the tendency of dye aggregations on the TiO_2 surface.[6,7] For instance, in a previous report Sundström et al. manufactured the double enhanced performance by introducing the co-adsorbates into the immersing bath (η=0.29% in the absence of the co-adsorbates and η=0.54 % in the presence of the co-adsorbates).[xvii] To further improve the performance of the present cell, we also introduced the chenodeoxychloic acid (2.5 mM) to the ZnPc-THF solution (0.05 mM), and prepared the phthalocyanine-sensitized TiO_2 cell. The cell, however,

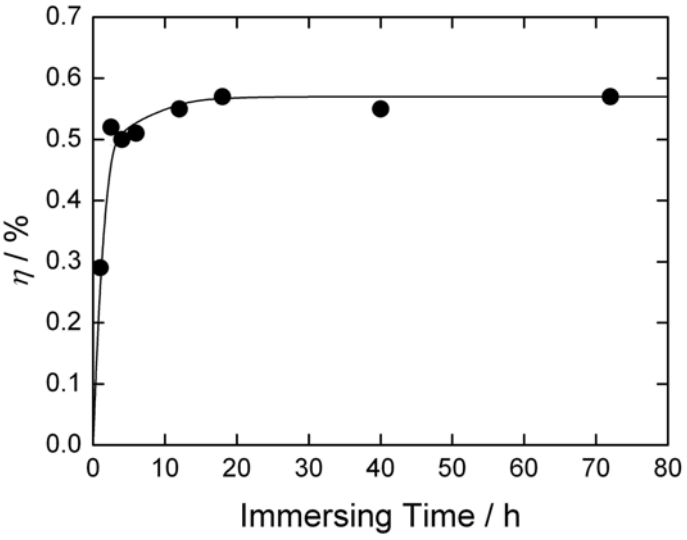

Figure 7. Profile of the power conversion efficiency (η) of a ZnPc-sensitized TiO_2 cell depending on the immersing time of the TiO_2 electrode in ZnPc-THF solution (0.05 mM) in the presence of chenodeoxycholic acid (2.5 mM).

exhibited no apparent difference in the η values with the cell prepared in the absence of chenodeoxycholic acid under the same conditions (Figure 7); η = 0.54 ± 0.03 %, J_{sc} = 1.44 ± 0.06 mA cm^{-2}, V_{oc} = 0.54 ± 0.03 V, and *ff* = 0.70 ± 0.03 for the cell with chenodeoxycholic acid. If there exist significant aggregations of ZnPc on the TiO_2 surface, the electron injection yield would be considerably diminished by the accelerated decay of the ZnPc excited singlet state, leading to a fair decrease in the cell performance, especially in the short circuit current. No apparent difference between the two cells with and without the presence of chenodeoxycholic acid reveals that the performance of our present cell is not perturbed by the well-known tendency of phthalocyanine aggregation. We understood this phenomenon to originate from the high steric hindrance of the ZnPc. Considering that the degree of dye aggregation on the TiO_2 surface is generally increased along with prolonged immersion, this interpretation is consistent with the parallel correlation between the time profiles of the η values and the Γ values (*vide supra*).

To investigate the photovoltaic response of the present cell in more detail, we measured the photocurrent action spectra of ZnPc-sensitized TiO_2 cell under the same conditions for the photocurrent-voltage characteristic measurements (Figure 8a).[xviii]

To

a large extent, the photocurrent response follows the general trend of the absorption feature of the ZnPc/TiO_2 (Figure 8b), indicating that the phthalocyanine is the main source for the photocurrent generation. The maximal IPCE value at the near-infrared region is measured to be 4.9 %.

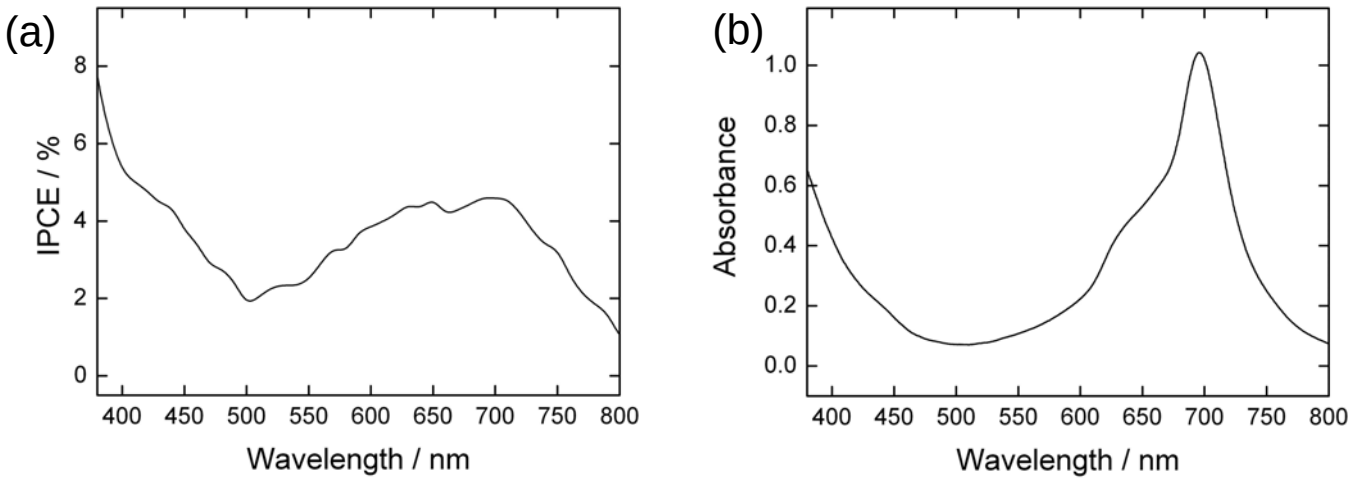

Figure 8. (a) Photocurrent action spectra of a ZnPc-sensitized TiO_2 cell. The phthalocyanine-modified TiO_2 electrode was prepared under the same conditions for the power conversion efficiency (η) measurements. Conditions: electrolyte 0.1 M LiI, 0.05 M I_2, 0.6 M 2,3-dimethyl-1-propyl imidazolium iodide, and 0.5 M 4-*t*-butylpyridine in CH_3CN; input power: AM 1.5 under simulated solar light (100 mW cm^{-2}). (b) UV-visible absorption spectra of TiO_2/ZnPc. The thickness of the TiO_2 was adjusted to be 700 – 1000 nm to obtain the shape and peak position of the spectra accurately.

Considering the full coverage on the TiO_2 surface and the high molar extinction coefficient at around 700 nm region of ZnPc, the low IPCE value of the ZnPc-sensitized TiO_2 cell cannot be explained by light-harvesting efficiency. The remaining two factors are the quantum yield of electron injection from the ZnPc excited singlet state to the CB of the TiO_2 electrode, and the efficiency of charge collection.[xix] The charge

collection efficiency is determined primarily by the relative rate of charge transport and charge recombination. In DSSCs, the injected electron can be recombined by the resulting dye cation and I^-/I_3^- redox couple before going to the outer circuit.[xx] The charge transport is reported to be occurred on the timescale of 10^{-7} ~ 10^{-5} s, whereas the recombination between the electron and I^-/I_3^- happens on the timescale of 10^{-3} ~ 1 s.[xxi,xxii] Although the time scale of the charge recombination with the resulting dye cation is known to vary depending on the electron density on TiO_2, a typical range is from 10^{-5} to 10^{-3} s.[23,xxiii] Therefore, the charge collection efficiency may not be the limiting factor for the low photocurrent generation. The quantum yield of electron injection is controlled by the competing processes against electron injection such as intersystem crossing, nonradiative decay, emission, and excited-state quenching; the most important factor is, however, the driving force for electron injection (ΔG_{inj}) from the excited state dye to the CB of the TiO_2.[3c] From the solution electrochemistry and spectroscopy, the ΔG_{inj} for ZnPc-sensitized TiO_2 cell is determined to be -0.34 eV. Apparently, it indicates that the electron injection is a thermodynamically feasible process. The energy level of the CB is, however, not laid at a fixed point but is subject to change depending on the operating conditions of the DSSCs. Mesoporous TiO_2 films have been known to show Nernstian shifts in their CB level depending on the degree of surface protonations.[xxiv] The shift of the CB of about 0.3 eV related with the changes in the electrolyte compositions is also reported.[22] Besides, the level of the CB would be raised to some degree due to the electron injection itself. The oxidation potential of the dye, in addition, is to be positively shifted by the chemical adsorption on the TiO_2.[18c,xxv] Thus, the actual driving force for the ZnPc-sensitized cell is estimated to be smaller than the above-mentioned value. In such a case, the electron injection from the excited ZnPc to the CB of the TiO_2 may occur mainly or only through surface states because there exist little available acceptor states for efficient electron injection.[xxvi] Besides, the electronic coupling between the LUMO of the ZnPc and the 3d orbital of

the TiO_2 cannot be anticipated to be large enough due to no apparent electron density on the carboxylic acid binding groups together with the intervening phenyl moieties between the ZnPc core and the carboxylic acid (*vide supra*). Thus, both of the small driving force and the weak electronic coupling would make the ZnPc an inefficient photosensitizer for DSSCs.

Certainly, the performance of our present cell is not good and is far from our expectations. From this study, however, we can detect invaluable clues for devising effective phthalocyanine photosensitizers for DSSCs applications.

Conclusions

Sterically hindered zinc phthalocyanine carboxylic acid (ZnPc) and its metal free counterpart (H_2Pc) were synthesized and evaluated for photosensitizers for DSSCs applications. The H_2Pc-sensitized TiO_2 cell showed no photocurrent response due to its low excited singlet state compared with the CB of TiO_2. The ZnPc-sensitized TiO_2 cell displayed 0.57 % of power conversion efficiency (η) and 4.9 % of maximal IPCE value in the near-infrared region. Introduction of the chenodeoxycholic acid revealed no noticeable change in the cell performance, showing that the aggregation of ZnPc is effectively suppressed by steric hindrance. The moderate cell performance can be rationalized by the small driving force for electron injection from the excited-state ZnPc to the TiO_2, and the poor electronic coupling between the LUMO of the ZnPc and the CB of the TiO_2. Even though the performance of the present cell is not impressive, this study affords an important clue for devising novel phthalocyanines for DSSCs applications.

Experimental

General

All solvents and chemicals were of reagent grade quality, purchased, and used without

further purification unless otherwise noted. Column chromatography and thin-layer chromatography (TLC) were performed with UltraPure Silica Gel (230-400 mesh, SiliCycle) and Silica gel 60 F_{254} (Merck), respectively. ^{1}H NMR spectra were measured on a JEOL EX-400 (400 MHz) or a Varian Unity 500 (500 MHz) spectrometer. ^{13}C NMR spectra were measured on a JEOL EX-400 (100 MHz) spectrometer. High-resolution mass spectra (HRMS) were recorded on a JEOL JMS-HX 110A spectrometer (FAB) using 3-nitrobenzylic alcohol as a matrix or a JEOL JMS-700 MStation spectrometer (EI). Matrix assisted laser desorption/ionization time-of-flight (MALDI-TOF) mass spectra were made on a BRUKER Autoflex III using CHCA as a matrix. UV-vis absorption spectra were measured using a Perkin-Elmer Lambda 900 UV/vis/NIR Spectrometer. Steady-state fluorescence spectra were acquired with a SPEX Fluoromax-3 Spectrofluorometer. Spectroscopy grade tetrahydrofuran was used for the measurements of UV-visible absorption and fluorescence spectra. FT-IR spectra were acquired using by a JASCO FT/IR-470 plus or a FT/IR-4200 spectrometer with a KBr pellet. Melting points were recorded on a Yanagimoto micro-melting point apparatus and were not corrected. Electrochemical measurements were made using a BAS 50W electrochemical workstation. Oxidation potentials in solution were determined by differential pulse voltammetry (DPV) with the pulse amplitude of 50 mV in Ar saturated *N, N'*-dimethylformamide containing 0.1M tetrabutylammonium perchlorate (TBAP) as supporting electrolyte. A glassy carbon working electrode (3 mm diameter), $Ag/AgNO_3$ reference electrode, and Pt wire counter electrode were employed. Ferrocene/ferrocenium (+0.642 V vs NHE) was used as an internal standard for all measurements. The measured potentials were quoted with reference to NHE.

Synthesis

4,5-Bis(4-*t*-butylphenyl)phthalonitrile (1). Although this compound has been already reported, the previous characterization is not complete.[xxvii] A 100 mL ~~of~~

round-bottomed flask was charged with 4,5-dichlorophthalonitrile (1.87 g, 9.5 mmol), 4-*t*-butylphenylboronic acid (5.0 g, 28.1 mmol), palladium (II) acetate (44 mg, 0.2 mmol), 2-(2',6'-dimethoxybiphenyl)dicyclohexylphosphine (200 mg, 0.49 mmol), K_3PO_4 (8.48 g, 40 mmol), and anhydrous toluene (25 mL). The solution was stirred at 90 ^oC for 2 h. After cooling to room temperature, the reaction mixture was washed twice with water. The combined organic layers were washed once with water, subsequently dried over anhydrous magnesium sulfate, and then concentrated in vacuo. The residue was dissolved in hexane, and the solid material was obtained by precipitation. Dissolution in and reprecipitation with cold hexane was repeated until no solid material appeared. Reprecipitation of the combined crude product with ethyl acetate/hexane afforded **1** as needle-like off-white crystals (2.44 g, 6.22 mmol, 66 % yield). Mp. 165.2-166.9 ^oC; ^1H NMR (400 MHz, $CDCl_3$) δ 7.82 (s, 2H, phenyl H), 7.28 (d, *J*=8.3 Hz, 4H, phenyl H), 7.03 (d, *J*=8.3 Hz, 4H, phenyl H), 1.29 (s, 18H, *t*-butyl H); ^{13}C NMR (100 MHz, $CDCl_3$) 151.77, 145.81, 135.54, 134.80, 129.01, 125.46, 115.56, 113.97, 34.64, 31.20; FT-IR (KBr) ν_{max} 2964, 2905, 2869, 2233 (CN), 1735, 1608, 1589, 1484, 1462, 1363, 1268, 1113, 1015, 915, 835, 594, 569 cm^{-1}; HRMS (EI positive) *m/z* calcd for 392.2252 ($C_{28}H_{28}N_2$), found 392.2249; elemental analysis (% calcd, % found for $C_{28}H_{28}N_2$) : C (85.67, 85.37), H (7.19, 7.30), N (7.14, 6.87).

4,5-Bis(4-methoxycarbonylphenyl)phthalonitrile (2). A 100 mL round-bottomed flask was charged with 4,5-dichlorophthalonitrile (1.0 g, 5.1 mmol), 4-(methoxycarbonylphenyl)boronic acid (2.7 g, 15.0 mmol), palladium (II) acetate (22 mg, 0.1 mmol), 2-(2',6'-dimethoxybiphenyl)dicyclohexylphosphine (100 mg, 0.25 mmol), K_3PO_4 (4.24 g, 20 mmol), and anhydrous toluene (20 mL). The solution was stirred at 90 ^oC for 15 h. After cooling to room temperature, the reaction mixture was washed twice with water. The combined organic layers were washed once with water, subsequently dried over anhydrous magnesium sulfate, and then concentrated in vacuo. Reprecipitation of the crude product from ethyl acetate twice afforded **2** as plate-like

off-white crystals (1.20 g, 2.62 mmol, 60.6 % yield). Mp. 225.6-227.1 ^{o}C; ^{1}H NMR (300 MHz, $CDCl_3$) δ 7.96 (d, *J*=8.4 Hz, 4H, phenyl H), 7.89 (s, 2H, phenyl H), 7.17 (d, *J*=8.4 Hz, 4H, phenyl H), 3.92 (s, 6H, ester H); ^{13}C NMR (75 MHz, $CDCl_3$) 166.20, 144.86, 141.58, 135.39, 130.50, 130.00, 129.39, 115.31, 114.97, 52.38; FT-IR (KBr) ν_{max} 3437, 2236 (CN), 1725, 1609, 1436, 1314, 1282, 1188, 1115, 1105, 1018, 861, 777, 713, 523 cm^{-1}; HRMS (EI positive) *m/z* calcd for 396.1110 ($C_{26}H_{16}N_2O_4$), found 396.1114; elemental analysis (% calcd, % found for $C_{26}H_{16}N_2O_4$) : C (72.72, 72.79), H (4.07, 4.05), O (16.14, 16.29), N (7.07, 6.87).

2,3,9,10,16,17-Hexakis(4-*t*-butylphenyl)-23,24-bis(4-carboxyphenyl)phthalocyanine (H_2Pc). A 200 mL round-bottomed flask was charged with **1** (4.24 g, 10.8 mmol), **2** (1.43 g, 3.60 mmol), 1,8-diazabicyclo[5.4.0]undec-7-ene (DBU) (0.3 g, 1.97 mmol), and 1-pentanol (60 mL). The solution was stirred at reflux for 20 h and cooled to room temperature. The solvent was then removed under reduced pressure. The solid material was obtained from methanol, and subjected to silica gel column chromatography (chloroform/hexane = 3:1). The second fraction was collected and reprecipitated from methanol. Silica gel column chromatography (chloroform/hexane = 1:5) of the previously collected material afforded a dark green solid (1.02 g). The solid showed two molecular ion peaks at 1630.7 and 1686.8 with an intensity ratio of 1:3 in the mass spectrum (MALDI-TOF). The peaks correspond to 2,3,9,10,16,17-hexakis(4-*t*-butylphenyl)-23-(4-methoxycarbonylphenyl)-24-(4-pentoxycarbonylphenyl)phthalocyanine, and 2,3,9,10,16,17-hexakis(4-*t*-butylphenyl)-23,24-bis(4-pentoxycarbonylphenyl)phthalocyanine, respectively. The mixture was directly employed for the next reaction without further purification.

To a solution of the previously collected dark green solid (1.03 g) in THF/methanol (2:1(v/v), 280 mL) in a 500 mL round-bottomed flask was added a 40 % aqueous KOH solution (40 mL). The solution was stirred at reflux for 8 h, cooled to

room temperature, and the organic solvent was removed under reduced pressure. The pH of the reaction mixture was set to 2 by adding HCl solution (6M), and a precipitate was formed. The precipitate was collected and washed with copious amounts of water and dried. The collected solid material was suspended in chloroform (100 mL), and stirred at reflux for 1 h. Filtering, and subsequent drying under reduced pressure of the solid was afforded **H_2Pc** as a dark green solid (336 mg, 6.0 % overall yield for 2 steps with reference to **2** used). Mp. > 300 ^oC; ^1H NMR (400 MHz, THF-d_8) δ 10.83 (s, 1H, carboxy H), 9.18 (s, 6H, phenyl H (2,3,9,10,16,17)), 9.15 (s, 2H, phenyl H (23,24)), 8.08 (d, 4H, *J*=8.3 Hz, carboxyphenyl H), 7.63 (d, 4H, *J*=8.3 Hz, carboxyphenyl H), 7.49 (d, 4H, *J*=8.3 Hz, carboxyphenyl H), 7.43 (s, 20H, carboxyphenyl H), 1.43 (s, 36H, *t*-Bu H), 1.41 (s, 18H, *t*-Bu H), -1.55 (br s, 2H, inner H); FT-IR (KBr) ν_{max} 3431, 3296, 2962, 2903, 1716, 1698, 1609, 1506, 1499, 1446, 1435, 1395, 1363, 1315, 1292, 1269, 1105, 1011, 925, 835, 764, 727, 719 cm^{-1}; HRMS (FAB positive) *m/z* calcd for 1547.7745 ($C_{106}H_{98}N_8O_4$), found 1547.7822 $(M+H)^+$.

2,3,9,10,16,17-Hexakis(4-*t*-butylphenyl)-23,24-bis(4-carboxyphenyl)phthalocyanato zinc (II) (ZnPc). To a solution of the previously collected dark green solid (500 mg, mixture of the 2,3,9,10,16,17-hexakis(4-*t*-butylphenyl)-23-(4-methoxycarbonyl-phenyl)-24-(4-pentoxycarbonylphenyl)phthalocyanine and 2,3,9,10,16,17-hexakis-(4-*t*-butylphenyl)-23,24-bis(4-pentoxycarbonylphenyl)phthalocyanine) in 1-pentanol (100 mL) in a 300 mL round-bottomed flask was added anhydrous zinc acetate (500 mg, 3.0 mmol). The solution was stirred at 130 ^oC for 3 h under a nitrogen atmosphere. After cooling to room temperature, the solvent was removed under reduced pressure. Silica gel column chromatography (chloroform) of the crude product afforded a green solid (103 mg). The solid showed the two molecular ion peaks at 1692.5 and 1748.6 with an intensity ratio of 1:3 in the mass spectrum (MALDI-TOF). The peaks correspond to 2,3,9,10,16,17-hexakis(4-*t*-butylphenyl)-23-(4-methoxycarbonyl-phenyl)-24-(4-pentoxy

carbonylphenyl)phthalocyanatozinc (II), and 2,3,9,10,16,17-hexakis(4-*t*-butylphenyl)-23,24-bis(4-pentoxycarbonylphenyl)phthalocyanatozinc (II), respectively. The mixture was directly employed for the next reaction without further purification.

To a solution of the previously collected green solid (103 mg) in THF/methanol (2:1(v/v), 30 mL) in a 100 mL round-bottomed flask was added a 40 % aqueous KOH solution (30 mL). The solution was stirred at reflux for 5 h, cooled to room temperature, and the organic solvent was removed under reduced pressure. The pH of the reaction mixture was set to 4 by adding 6M HCl solution, and a precipitate was formed. The precipitate was collected and washed with copious amounts of water and dried. The collected solid material was suspended in chloroform (100mL), and stirred at reflux for 1h. Filtering, and subsequent drying under reduced pressure of the solid was afforded **ZnPc** as a dark green solid (52.6 mg, 4.6 % overall yield for 3 steps with reference to **2** used). Mp. > 300 ^{o}C; ^{1}H NMR (400 MHz, THF-d_8) δ 10.72 (s, 1H, carboxy H), 9.47 (s, 2H, phenyl H (23,24)), 9.40 (s, 2H, phenyl H (9,10)), 9.39 (s, 4H, phenyl H (2,3,16,17)), 8.10 (d, 4H, *J*=8.3 Hz, carboxyphenyl H), 7.72 (d, 4H, *J*=8.3 Hz, carboxyphenyl H), 7.53 (skewed d, *J*=8.3 Hz, 12H, carboxyphenyl H), 7.46 (skewed d, *J*=8.3 Hz, 12H, carboxyphenyl H), 1.41 (s, 36H, *t*-Bu H), 1.40 (s, 18H, *t*-Bu H); HRMS (FAB positive) *m/z* calcd for 1608.6846 ($C_{106}H_{96}N_8O_4Zn$), found 1608.6816 $(M+H)^+$.

Density Functional Theory (DFT) Calculations. Geometry optimization and electronic structure calculations of the phthalocyanines were performed by using B3LYP functional and 3-21G (d) basis set implemented in the Gaussian 03 program package.[xxviii] Molecular orbitals were visualized by GaussView 3.0 software.

Preparation of Phthalocyanine-Modified TiO_2 Electrode and Photovoltaic Measurements. Preparation of mesoporous TiO_2 films and immobilization of the phthalocyanine on the TiO_2 surface, and characterization of the photovoltaic properties of phthalocyanine-modified TiO_2 were made by following the procedures reported

previously.[18] Tetrahydrofuran was used as an immersing solvent in the present experiments instead of ethanol or methanol. The TiO_2 electrodes modified with H_2Pc and ZnPc are denoted as TiO_2/H_2Pc and TiO_2/ ZnPc, respectively. The amounts of the phthalocyanines adsorbed on the TiO_2 films were determined by measuring the changes in the absorbance of the phthalocyanine solutions (4 mL) before and after immersion of the TiO_2 films (0.25 cm^2 of projected area). All the experimental values were given as an average from six independent measurements.

Notes and references

(i) (a) Special Issue on Dye-Sensitized Solar Cells: *Coord. Chem. Rev.,* **2004**, *248*, 1161. (b) Forum on Solar and Renewable Energy: *Inorg. Chem*., **2005**, *44*, 6799. (c) Watson, D. F.; Meyer, G. J. *Ann. Rev. Phys. Chem.* **2005**, *56*, 119. (d) Anderson, N. A.; Lian, T. *Ann. Rev. Phys. Chem*. **2005**, *56*, 491. (e) Duncan, W. R.; Prezhdo, O. V. *Ann. Rev. Phys. Chem.* **2007**, *58*, 143. (f) Robertson, N. *Angew. Chem., Int. Ed*. **2006**, *45*, 2338.

(ii) (a) Robertson, N. *Angew. Chem., Int. Ed*. **2008**, *47*, 1012. (b) Tanaka, T.; Hayashi, S.; Eu, S.; Umeyama, T.; Matano, Y.; Imahori, H. *Chem. Commun.* **2007**, 2069. (c) Shibano, Y.; Umeyama, T.; Matano, Y.; Imahori, H. *Org. Lett.* **2007**, *9*, 1971.

(iii) de la Torre, G.; Claessens, C. G.; Torres, T. *Chem. Commun*. **2007**, 2000.

(iv) (a) Nazeeruddin, Md. K.; Humphry-Baker, R.; Grätzel, M.; Wöhrle, D.; Schnurpfeil, S.; Schneider, G.; Hirth, A.; Trombach, N. *J. Porphyrins Phthalocyanines* **1999**, *3*, 230. (b) Aranyos, V.; Hjelm, J.; Hagfeldt, A; Grennberg, H. *J. Porphyrins Phthalocyanines* **2001**, *5*, 609. (c) He, J.; Hagfeldt, A.; Lindquist, S.-E.; Grennberg, H.; Korodi, F.; Sun, L.; Åkermark, B. *Langmuir* **2001**, *17*, 2743. (d) Amao, Y.; Komori, T. *Langmuir* **2003**, *19*, 8872. (e) Palomares, E.; Martinez-Diaz, M. V.; Haque, S. A.; Torres, T.; Durrant, J. R. *Chem. Commun.*

2004, 2112. (f) Giribabu, L.; Kumar, C. H. V.; Reddy, V. G.; Reddy, P. Y.; Rao, Ch. S.; Jang, S.-R.; Yum, J.-H.; Nazeeruddin, Md. K.; Grätzel, M. *Solar Energy Mater. Solar Cells* **2007**, *91*, 1611. (g) Yanagisawa, M.; Korodi, F.; He, J.; Sun, L.; Sundström, V.; Åkermark, B. *J. Porphyrins Phthalocyanines* **2002**, *6*, 217. (h) Yanagisawa, M.; Korodi, F.; Bergquist, J.; Holmberg, A.; Hagfeldt, A.; Åkermark, B.; Sun, L. *J. Porphyrins Phthalocyanines* **2004**, *8*, 1228. (i) Morandeira, A.; Lopez-Duarte, I.; Martínez-Díaz, M. V.; O'Regan, B.; Shuttle, C.; Haji-Zainulabidin, N. A.; Torres, T.; Palomares, E.; Durrant, J. R. *J. Am. Chem. Soc.* **2007**, *129*, 9250. (j) O'Regan, B.; Lopez-Duarte, I.; Martínez-Díaz, M. V.; Forneli, A.; Albero, J.; Morandeira, A.; Palomares, E.; Torres, T.; Durrant, J. R. *J. Am. Chem. Soc.* **2008**, *130*, 2906.

(v) (a) Reddy, P. Y.; Giribabu, L.; Lyness, C.; Snaith, H. J.; Vijaykumar, C.; Chandrasekharam, M.; Lakshmikantam, M.; Yum, J.-H.; Kalyanasundaram, K.; Grätzel, M.; Nazeeruddin, Md. K. *Angew. Chem., Int. Ed*. **2007**, *46*, 373. (b) Cíd, J.-J.; Yum, J.-H.; Jang, S.-R.; Nazeeruddin, Md. K.; Martínez-Ferrero, E.; Palomares, E.; Ko, J.; Grätzel, M.; Torres, T. *Angew. Chem., Int. Ed*. **2007**, *46*, 8358.

(vi) Rodríguez-Morgade, M. S.; de la Torre, G.; Torres, T. In *The Porphyrin Handbook*; Kadish, K. M., Smith, K. M., Guilard, R., Eds.; Academic Press: New York, 2000; Vol. 15, Ch. 99, pp 125-160.

(vii) (a) Miyaura, N.; Suzuki, A. *Chem. Rev.* **1995**, *95*, 2457. (b) Suzuki, A. *J. Organomet. Chem*. **1999**, *576*, 147. (c) Corbet, J-P.; Mignani, G. *Chem. Rev*. **2006**, *106*, 2651.

(viii) Yin, J.; Rainka, M. P.; Zhang, X-.X.; Buchwald, S. L. *J. Am. Chem. Soc*. **2002**, *124*, 1162.

(ix) (a) Littke, A. F.; Dai, C.; Fu, G. C. *J. Am. Chem. Soc*. **2000**, *122*, 4020. (b) Littke,

A. F.; Dai, C.; Fu, G. C. *J. Am. Chem. Soc*. **2002**, *124*, 1162. (c) Nolan, S. P.; Navarro, O. In *Comprehensive Organometallic Chemistry III*; Crabtree R. H., Mingos, D. M. P., Eds.; Elsevier: Oxford, 2007; Vol. 11, Ch. 11.01, p 7.

(x) Gierschner, J.; Cornil, J.; Egelhaaf, H.-J. *Adv. Mater.* **2007***, 19*, 173.

(xi) The oxidation potential (E_0) was determined by the following equation; $E_0 = E_{peak} + \Delta E/2$, where E_{peak} is the potential of peak maximum and ΔE is the pulse amplitude. Bard, A. J.; Faulkner, L. R. In *Electrochemical Methods–Fundamentals and Applications*, 2nd ed.; John Wiley & Sons: New York, 2001; p 290.

(xii) Wang, X.; Zhang, Y.; Sun, X.; Bian, Y.; Ma, C.; Jiang, J. *Inorg. Chem*. **2007**, *46*, 7136.

(xiii) Kamat, P. V.; Haria, M.; Hotchandani, S. *J. Phys. Chem. B* **2004**, *108*, 5166.

(xiv) Foresman, J. B.; Frisch, A. In *Exploring Chemistry with Electronic Structure Methods*; Gaussian Inc.: Pittsburgh, 1995; p 62.

(xv) Hagberg, D. P.; Edvinsson, T.; Marinado, T.; Boschloo, G.; Hagfeldt, A.; Sun, L. *Chem. Commun.* **2006**, 2245.

(xvi) (a) Imahori, H.; Hayashi, S.; Umeyama, T.; Eu, S.; Oguro, A.; Kang, S.; Matano, Y.; Shishido, T.; Ngamsinlapasathian, S.; Yoshikawa, S. *Langmuir* **2006**, *22*, 11405. (b) Eu, S.; Hayashi, S.; Umeyama, T.; Oguro, A.; Kawasaki, M.; Kadota, N.; Matano, Y.; Imahori, H. *J. Phys. Chem. C* **2007***, 111*, 3528. (c) Eu, S.; Hayashi, S.; Umeyama, T.; Araki, Y.; Matano, Y.; Imahori, H. *J. Phys. Chem. C* **2008***, 112*, 4396.

(xvii) He, J.; Benkö, G.; Korodi, F.; Polívka, T.; Lomoth, R.; Åkermark, B.; Sun, L.; Hagfeldt, A.; Sundström, V. *J. Am. Chem. Soc.* **2002**, *124*, 4922.

(xviii) H_2Pc-sensitized TiO_2 cell displayed no photocurrent response, as predicted.

(xix) IPCE = LHE × ϕ_{inj} × η_{col}, where LHE is the light harvesting efficiency, ϕ_{inj} is the quantum of yield of electron injection, and η_{col} is the efficiency of charge

collection.

(xx) Haque, S. A.; Palomares, E.; Cho, B. M.; Green, A. N. M.; Hirata, N.; Klug, D. R.; Durrant, J. R. *J. Am. Chem. Soc*. **2005**, *127*, 3456.

(xxi) Mori, S. N.; Kubo, W.; Kanzaki, T.; Masaki, N.; Wada, Y.; Yanagida, S. *J. Phys. Chem. C* **2007**, *111*, 3522.

(xxii) (a) Green, A. N. M.; Palomares, E.; Haque, S. A.; Kroon, J. M.; Durrant, J. R. *J. Phys. Chem. B* **2005**, *109*, 12525. (b) Haque, S. A.; Handa, S.; Peter, K.; Palomares, E.; Thelakkat, M.; Durrant, J. R. *Ang. Chem., Int. Ed*. **2005**, *44*, 5740.

(xxiii) (a) O'Regan, B.; Moser, J. E.; Anderson, M.; Grätzel, M. *J. Phys. Chem* **1990**, *94*, 8720. (b) Haque, S. A.; Tachibana, Y.; Klug, D. R.; Durrant, J. R. *J. Phys. Chem. B* **1998**, *102*, 1745. (c) Heimer, T. A.; Heilweil, E. J.; Bignozzi, C. A.; Meyer, G. J. *J. Phys. Chem. A* **2000**, *104*, 4256. (d) Clifford, J. N.; Palomares, E.; Nazeeruddin, Md. K.; Grätzel, M.; Nelson, J.; Li, X.; Long, N. J.; Durrant, J. R. *J. Am. Chem. Soc*. **2004**, *126*, 5225.

(xxiv) (a) Rothenberger, G.; Fitzmaurice, D.; Grätzel, M. *J. Phys. Chem. B* **1992**, *96*, 5983. (b) Watson, D. F.; Marton, A.; Stux, A. M.; Meyer, G. J. *J. Phys. Chem. B* **2003**, *107*, 10971. (c) Watson, D. F.; Marton, A.; Stux, A. M.; Meyer, G. *J. Phys. Chem. B* **2004**, *108*, 11680.

(xxv) (a) Wang, P.; Zakeeruddin, S. M.; Moser, J. E.; Humphry-Baker, R.; Comte, P.; Aranyos, V.; Hagfeldt, A.; Nazeeruddin, Md. K.; Grätzel, M. *Adv. Mater.* **2004**, *16*, 1806. (b) Zaban, A.; Ferrere, S.; Sprague, J.; Gregg, B. *J. Phys. Chem. B* **1997**, *101*, 55. (c) Zaban, A.; Ferrere, S.; Gregg, B. *J. Phys. Chem. B* **1998**, *102*, 452.

(xxvi) (a) Grätzel, M. *Pure Appl. Chem.* **2001**, *73*, 459. (b) Tachibana, Y.; Nazeeruddin, Md. K.; Grätzel, M.; Klug, D. R.; Durrant, J. R. *Chem. Phys*. **2002**, *285*, 127.

(xxvii) Sugimori, T.; Torikata, M.; Nojima, J.; Tominaka, S.; Tobikawa, K.; Handa, M.; Kasuga, K. *Inorg. Chem. Comm.* **2002**, *5*, 1031.

(xxviii) Frisch, M. J. *et al. Gaussian 03, revision C.02*, Gaussian Inc., Wallingford, CT, 2004.

CONCLUDING REMARKS

This dissertation details the molecular design tactics for achieving high performance dye sensitizers, syntheses of novel compounds based on the tactics, and evaluations of the compounds for dye-sensitized solar cells applications. The results and findings can be summarized as follows.

In the Chapter 1, the syntheses, structures of porphyrin films on TiO_2, and photovoltaic properties of porphyrins with different 5-membered heteroaromatic spacers (Zn5S, Zn5O, and Zn4S) are described. Modifications in spacers including switching one element (i.e., sulfur vs oxygen) in the bridge or changing the position of the anchoring group (i.e., carboxylic acid) are found to have significant effects on the dye coverage on the TiO_2 surface, and photovoltaic properties of the porphyrin-sensitized TiO_2 cells. The high photovoltaic properties of Zn5S-sensitized cell relative to the other cells are rationalized by the additional electron transfer pathway through specific interaction between the sulfur atom inherent in the bridge and the TiO_2 surface.

In the Chapter 2, the synthesis and the optical, electrochemical, and photovoltaic properties of mono- and dicarboxyquinoxalino[2,3-β]porphyrins (ZnQMA and ZnQDA) for dye-sensitized solar cells are described. Both of the compounds show broadened, red-shifted, and amplified light absorption with the aid of π-extensions. Electrochemistry along with DFT calculations reveals that the low-lying LUMO by the substitutions is the main reason for the narrowed HOMO-LUMO gaps. From the X-ray photoelectron spectroscopy and cyclic voltammetry study for the adsorbed porphyrins, difference in the binding mode between the two compounds are clarified; one carboxylic acid employs bidentate binding mode to anchor ZnQMA onto the TiO_2 surface, whereas the two binding groups in ZnQDA utilize one bidentate and one monodentate binding modes. Photovoltaic measurements of ZnQMA- and ZnQDA-sensitized TiO_2 cells with

P25 revealed power conversion efficiencies of 5.2 % and 4.0 %, respectively. Since the light absorption capabilities of the two porphyrins are more or less similar, the number and the position of binding groups in the porphyrins are attributed to have a large impact on the photovoltaic and photoelectrochemical performances.

In the Chapter 3, the synthesis of phthalocyanines with high peripheral substitutions and free from potential contamination by regioisomers, and evaluation of the compounds as photosensitizers for dye-sensitized solar cell applications are described. Metal free phthalocyanine-sensitized solar cell showed no photocurrent generation due to its low excited singlet state compared with the conduction band of the TiO_2. Upon zinc metalation, the excited singlet state of the phthalocyanine was pushed up, and this variation afforded an exergonic free energy change for the operation of the device. More importantly, the zinc phthalocyanine-sensitized solar cell prepared with and without the presence of co-adsorbate revealed no difference in the power conversion efficiency (η). This shows that the well-known aggregation tendency of phthalocyanines that is considered to enhance the self-quenching of the phthalocyanine excited singlet state is effectively suppressed by our design concept for the novel compound. The significance of the driving force for the electron injection and the distance between the dye core and the TiO_2 surface is also discussed and highlighted for devising high performance phthalocyanine photosensitizers.

List of Publications

This dissertation is based on the following papers.

1) Eu, S.; Hayashi, S.; Umeyama, T.; Oguro, A.; Kawasaki, M.; Kadota, N.; Matano, Y.; Imahori, H. *Effects of 5-membered heteroaromatic spacers on structures of porphyrin films and photovoltaic properties of porphyrin-sensitized TiO_2 cells. J. Phys. Chem. C* **2007**, *111*, 3528.
2) Eu, S.; Hayashi, S.; Umeyama, T.; Matano, Y.; Araki, Y.; Imahori, *H. Quinoxaline-fused porphyrins for dye-sensitized solar cells. J. Phys. Chem. C* **2008**, *112*, 4396.
3) Eu, S.; Katoh, T.; Umeyama, T.; Matano,Y.; Imahori, H. *Synthesis of sterically hindered phthalocyanines and their applications to dye-sensitized solar cells*. *Dalton. Trans*. **2008**, *in press*.

Other publications

4) Eu, S.; Paik, W. K. *Self-assembly process of organosulfur molecular layers on gold electrode: An in situ ellipsometric and electrochemical study. Chem. Lett*. **1998**, 405.
5) Eu, S.; Paik, W. K. *Self-assembly process of organosulfur molecular layers on gold: Electrochemical mechanisms*. *Mol. Cryst. Liq. Cryst*. **1999**, *337*, 49.
6) Paik, W. K.; Eu, S.; Lee, K.; Chon, S.; Kim, M. *Electrochemical reactions in adsorption of organosulfur molecules on gold and silver: Potential dependent adsorption*. *Langmuir* **2000**, *16*, 10198.
7) Imahori, H; Hayashi, S.; Umeyama, T.; Eu, S.; Oguro, A.; Kang, S.; Matano, Y.; Shishido, T.; Ngamsinlapasathian, S.; Yoshikawa, S. *Comparison of electrode structure and photovoltaic properties of porphyrin-sensitized solar cells with TiO_2 and Nb, Ge, Zr-added TiO_2 composite electrodes. Langmuir* **2006**, *22*, 11405.
8) Tanaka, M.; Hayashi, S.; Eu, S.; Umeyama, T.; Matano, Y.; Imahori, H. *Novel unsymmetrically π-elongated porphyrin for dye-sensitized TiO_2 cells. Chem.*

Commun. **2007**, 2069.

9) Hayashi, S.; Matsubara, Y.; Eu. S.; Hayashi, H.; Umeyama, T.; Matano, Y.; Imahori, H. *Fused fived-membered porphyrins for dye-sensitized solar cells. Chem.Lett. in press*.

10) Hayashi, S.; Tanaka, M.; Hayashi, H.; Eu. S.; Umeyama, T.; Matano, Y.; Araki, Y.; Imahori, H. *Naphthyl-fused π-elongated porphyrins for dye-sensitized TiO_2 cells. submitted for publication.*

Patents

1) Eu, S.; Lee, J. *Catalyst precursor resin composition for electroless plating, and preparation method of light-penetrating electromagnetic interference shielding material using the same*, KR2005013842; JP2006510809; US20050022692; TW267531; CN1701135; EP1649077; WO2005010234.

2) Eu, S.; Kim, D. *UV curable resin composition*, KR 2006026771.

ACKNOWLEDGEMENT

The allotted time has nearly been passed, and finally I arrived here at this exciting moment to express my gratitude for every person who deserves it. Professor Hiroshi Imahori has been made me know how to envisage, shape, and execute the research and moreover good research. I cannot imagine the existence of this dissertation without his invaluable guidance, suggestion, and encouragement. The insightful comments and assistance for this study by Professor Yoshihiro Matano and Professor Tomokazu Umeyama are acknowledged. All of the members in the Imahori group should be appreciated for their kindness and help.

Professor Susumu Yoshikawa (Kyoto University), Professor Mitsuo Kawasaki (Kyoto University), Professor Kenji Wada (Kyoto University), Professor Shozo Yanagida (Osaka University), Dr. Naruhiko Masaki (Osaka University), Professor Yasuyuki Araki (Tohoku University), Mr. Nara Akishi and Mr. Rika Harui (Thermo Electron Corporation) should also be acknowledged for their help during this study.

I also thank the International Doctoral Program in Engineering, Graduate School of Engineering, Kyoto University, for financial support.

Finally, I would like to express deep gratitude and affection to my wife and other family members.

Seunghun Eu

Kyoto, Japan

July 2008